# Operational strategies for hydrogen production powered by offshore wind

## Evaluating multi-stack PEM electrolyser systems for optimised hydrogen production and minimised stack degradation

Author: T. van Breemen
Date: 05-09-2025

TU Delft

This page is left blank intentionally

# Operational strategies for hydrogen production powered by offshore wind

## Evaluating multi-stack PEM electrolyser systems for optimised hydrogen production and minimised stack degradation

By

Thomas van Breemen

In partial fulfilment of the requirements for the degree of:

**Master of Science**
in Offshore & Dredging Engineering

at the Delft University of Technology,
to be defended publicly on Friday September 5, 2025 at 13:45.

| | | |
|---|---|---|
| Supervisors: | Dr.ir. J.S. Hoving | TU Delft |
| | Prof.dr.ir. J.R. van Ommen | TU Delft |
| | Ir. Timothée Macquart | Guidehouse |
| | Dr.ir. Carmen Wouters | Guidehouse |
| Thesis committee: | Dr.ir. J.S. Hoving | TU Delft |
| | Prof.dr.ir. J.R. van Ommen | TU Delft |

*“Stay hungry, Stay foolish”*

*Steve Jobs*

# Abstract

This thesis investigates how operational strategies influence the performance of offshore PEM electrolyser systems powered by intermittent offshore wind power. The central research question is:

*“How does the operational strategy for managing intermittent offshore wind power supply in an offshore PEM electrolyser system affect hydrogen production, stack degradation and the LCOH?”*

The study follows three phases. A literature review establishes PEM electrolysis as the most suitable technology for offshore hydrogen production, identifies degradation mechanisms under intermittent power operation, and derives a degradation relation. A dynamic Simulink model is then developed to simulate stack performance under variable power inputs. Finally, a techno-economic model in Python integrates the Simulink results with degradation data to evaluate operational strategies.

The analysis compares three strategies: equal-, serial-, and optimal efficiency power distribution over the stacks. Results show that operational strategy is a decisive factor. Equal distribution achieves the lowest LCOH of 12.17 $/kg with 68 stack replacements over a 15 year horizon, while serial distribution results in a 30% higher LCOH of 15.83 $/kg and requires 90 replacements. Hydrogen output differences between strategies are minimal. Strategy performance is best when operation under high current density is avoided, as this is a driving factor for degradation. The LCOH values remain significantly higher than those of fossil fuel based hydrogen.

The findings of this thesis also expose a critical knowledge gap: PEM electrolyser degradation under intermittent operation is poorly understood. Testing protocols are inconsistent, datasets fragmented, and long-term field data scarce. This complicates the viability assessment of future offshore hydrogen projects.

This research contributes by (1) highlighting the urgent need for standardized degradation testing and long-term datasets, (2) introducing a simulation framework that combines time-resolved dynamic modelling with techno-economic analysis, and (3) establishing operational strategy as a critical design factor for offshore hydrogen systems.

Future research should focus on (i) long-term degradation testing under realistic renewable power profiles, (ii) advanced time-resolved modelling with higher time resolution and incorporation of transient effects, (iii) development of optimization-based operational strategies, and (iv) integrated techno-economic analysis that includes dynamic electricity prices, offshore infrastructure, and possible integration of batteries.

To answer the research question: the operational strategy for managing intermittent offshore wind power supply has a significant impact on the performance of offshore PEM electrolyser systems, as strategies that avoid high current density operation substantially reduce degradation and lower the LCOH by up to 30%, while having only a limited effect on hydrogen production.

# Acknowledgements

This report represents the conclusion of my master thesis and thereby the end of my time as a student in Delft. I would like to express my gratitude to everyone who has supported me throughout this journey.

I would like to thank my supervisors, Jeroen and Ruud, for their guidance and for making it possible to investigate this topic, which has been of great interest to me. Their support and feedback have been valuable throughout the process and have greatly shaped the outcome of this thesis.

I would like to thank my supervisors Timo and Carmen from Guidehouse for the great weekly meetings and the sessions where, through open conversation, we arrived at new insights from which I learned a lot. They created a pleasant and supportive working environment, gave me an insight of how things work in the professional world, and offered me the opportunity to be part of the team and contribute to projects. I am also really grateful for the good coffee, the games of ping pong, the ski-trip and the ‘gezelligheid’, which made my time at Guidehouse both valuable and enjoyable.”

I would also like to thank my family and friends for creating an environment in which I was able to focus fully on my thesis and for always supporting me along the way. A special thanks goes to my dad for thinking along with me, helping me brainstorm at difficult moments, and giving me that extra push when I needed it.

I am grateful for what I have learned during this thesis and for the opportunity to dive deeper into offshore hydrogen production. I hope that my work contributes in to the energy transition, and I value the lessons and insights this thesis has given me. It has motivated me to continue supporting the (offshore) energy transition in the future and to work towards making a positive impact.

# Contents


Abstract v

Acknowledgements vi

1 Introduction 1
- 1.1 Motivation 1
- 1.2 Limitations in the Current Literature 2
- 1.3 Research Questions, Scope and Objectives 3
- 1.4 Research Methodology 4
  - 1.4.1 Literature Research Phase 4
  - 1.4.2 Simulation Modelling Phase 5
- 1.5 Thesis structure 6

2 State-Of-The-Art of Electrolysers for Hydrogen Production 7
- 2.1 What is Electrolysis? 7
  - 2.1.1 Basic Principles of Electrolysis 7
  - 2.1.2 Water electrolysis 8
- 2.2 Electrolyser Technologies: An Overview 11
  - 2.2.1 Introduction to The Different Types of Electrolysers 11
  - 2.2.2 Alkaline, AEM and SOEC Electrolysers 12
  - 2.2.3 PEM Electrolysers 16
  - 2.2.4 Technology Comparison and PEM Justification for Offshore Renewable Applications 21
- 2.3 Degradation Mechanisms in PEM Electrolysers 24
  - 2.3.1 PEM Electrolyser Degradation in General 24
  - 2.3.2 Detailed Components of a PEM Cell 25
  - 2.3.3 Overview of PEM Degradation Mechanisms 26
  - 2.3.4 PEM Electrolyser Degradation Classification, Probabilities and Effects on Overpotentials. 28
  - 2.3.5 Overview of The Influence of Operating Conditions on Degradation Mechanisms 29
  - 2.3.6 Conclusion of PEM Electrolyser Degradation Mechanisms 31
- 2.4 PEM Electrolyser Models 32
  - 2.4.1 PEM Electrolyser Modelling in General 32
  - 2.4.2 Different Types of PEM Electrolyser Models 33
  - 2.4.3 Status of PEM Electrolyser Modelling 34
- 2.5 CAPEX and OPEX of PEM Electrolyser Systems 35
  - 2.5.1 Introduction to PEM Electrolysers CAPEX and OPEX 35
  - 2.5.2 CAPEX of PEM Electrolysers Systems 36
  - 2.5.3 OPEX of PEM Electrolyser Systems 37
- 2.6 Conclusion and Discussion of PEM Electrolyser State-of-the-Art 38

3 PEM Electrolyser Simulink Model 41
- 3.1 Model Characteristics 41

3.2 Model Boundaries 42
3.3 Governing Equations 42
3.3.1 Power input 42
3.3.2 Voltage 43
3.3.3 Mass Flows 44
3.3.4 Pressure and Temperature 44
3.3.5 Efficiency 45
3.4 Model Parameters 46
3.5 Model Output, Verification and Validation 47
3.5.1 Simulated Polarization Curve 48
3.5.2 Simulated Hydrogen Production 50
3.5.3 Simulated Efficiency 51
3.6 Model Assumptions and Limitations 54
3.6.1 Electrochemical Dynamics 54
3.6.2 Dimensionality and Spatial Resolution 55
3.6.3 Parameter Scaling 55
3.6.4 Governing Equations Simplifications 55
3.6.5 Species and Phase Behaviour 56
3.6.6 Balance of Plant Efficiency 56
3.6.7 Simulink Component Constraints 56
3.6.8 Degradation Modelling 56

4 PEM Electrolyser Degradation Data Analysis 58
4.1 Introduction to PEM Electrolyser Degradation Data 58
4.2 Approach for PEM Electrolyser Degradation Data Collection and Analysis 59
4.3 Results of PEM Electrolyser Degradation Data Collection and Analysis 60
4.3.1 Overview of PEM degradation Data Collection 60
4.3.2 PEM Electrolyser Degradation Data Analysis 62
4.4 Conclusion and Selection of PEM Electrolyser Degradation Dataset 63

5 PEM Electrolyser Operational Strategy Model and Results 65
5.1 Operational Strategy Model Characteristics 65
5.1.1 The Operational Strategy Model - inputs 65
5.1.2 The Operational Strategy Model - Working Principles 66
5.1.3 The Operational Strategy Model - Assumptions 67
5.2 Operational Strategy Simulations and Results 68
5.2.1 Strategy 1 – Equal distribution 68
5.2.2 Strategy 2 – Serial distribution 69
5.2.3 Strategy 3 - Efficiency distribution 70
5.3 Operational Strategy Model Validation 71
5.4 Operational Strategy Simulations Conclusion 72
5.5 Sensitivity analysis 73
5.5.1 Degradation Sensitivity Analysis 73
5.5.2 Cost Sensitivity Analysis 75
5.5.3 Setup Sensitivity Analysis 77
5.6 Model Discussions and Limitations 78

6 Conclusion 80

7 Discussion and Recommendations 82

Bibliography 85

List of Figures 93

List of Tables 94

Appendix A – Alkaline Electrolysers 95

Appendix B – AEM Electrolysers 100

Appendix C – SOEC Electrolysers 105

Appendix D – Detailed PEM Components 110

Appendix E – PEM Degradation Mechanisms 111
E.1 Membrane degradation and inhibition 111
E.2 Anode catalyst degradation (iridium) 114
E.3 Cathode catalyst degradation (platinum) 116
E.4 Carbon porous transport layer degradation 117
E.5 Bipolar plate degradation 118
E.6 Titanium porous transport layer degradation 119
E.7 Degradation of gaskets and sealants. 119

Appendix F – PEM Electrolyser Model Classifications 121

Appendix G – SIMULINK Mode Equations 124

Appendix H – Additional Simulink model output 125

Appendix I – PEM Electrolyser Degradation Dataset 128

Appendix J – Correspondence on PEM Electrolyser Degradation 129

Appendix K – Degradation Data sample plots 131

Appendix L – North Sea Wind Data 133

Appendix M – Operational strategy Excel outputs. 134

Appendix N – Operational strategy Model Codes 136

This page is left blank intentionally

# 1 Introduction

The intermittent nature of renewable energy sources as a power input for electrolysers challenges hydrogen production, electrolyser degradation and ultimately the Levelized Cost of Hydrogen (LCOH[1]). These challenges threaten the technical and economic viability of renewable hydrogen projects. This thesis investigates the influence of operational strategies on Proton Exchange Membrane (PEM) electrolysers specifically, powered by offshore wind, to mitigate these challenges.

The introduction presents the motivation for the research, identifies key gaps in the current literature, formulates the research question, defines the scope and objectives, outlines the methodology, and provides an overview of the thesis structure.

## 1.1 Motivation

For over 150 years, fossil fuels, such as coal, oil, and natural gas have powered global economic growth. Today, they still account for roughly 80% of the world's energy supply (Environmental and Energy Study Institute, 2021). The widespread use of fossil fuels is the primary driver of greenhouse gas emissions, such as carbon dioxide, contributing to earth's average temperature rise by more than 1.1°C over the past century (World of Change: Global Temperatures, 2022). As a result, glaciers are melting, sea levels are rising, and extreme weather events occur more frequently. These changes disrupt ecosystems and threaten communities and economies. The world needs to decarbonize, replace fossil fuels by green alternatives, and reduce the greenhouse gas emissions to protect these ecosystems, communities and economies.

One of the trends to reduce emissions is trough electrifying industries and producing renewable electricity with for example, Offshore Wind Farms (OWF). The OWF capacity is growing rapidly but storage, grid constraints and hard-to-electrify sectors form a challenge. Hydrogen offers a solution: it produces no emissions at the point of use, reduces stress on the grid, can be stored more easily, and is suited for sectors where direct electrification is impractical (IEA, 2021)(NortH2, n.d.). If produced by renewable energy, hydrogen is labelled as 'green hydrogen'.

The global demand for green hydrogen is expected to rise, potentially reaching 500–800 million tonnes by 2050 and supplying up to 20% of global final energy consumption (Hydrogen Council & McKinsey & Company, 2024). Electrolysers, which convert electricity and water into hydrogen, are key in this transition (Glenk & Reichelstein, 2019). This thesis focuses specifically on PEM electrolysers for offshore hydrogen production as PEM technologies are widely regarded as the most suitable for coupling with intermittent renewable energy sources (Wang et al., 2022). Offshore hydrogen production, located directly at OWFs, offers advantages such as vast wind potential, reduced reliance on long-distance electricity transmission, and opportunities for offshore hydrogen storage (Gasunie, 2025).

In the Netherlands, projects like NortH2 aim to install 4 GW of offshore electrolyser capacity by 2030, scaling to 10 GW by 2040 (NortH2, n.d.). Similarly, the PosHYdon pilot, which is already operational, uses a 1.25 MW PEM electrolyser on a repurposed North Sea gas platform, powered by an OWF. (PosHYdon, 2024). These projects demonstrate the fast development of this sector. However, unlike

[1]The Levelized Cost of Hydrogen (LCOH) is a metric that represents the average cost of producing one unit of hydrogen, typically expressed in dollars per kilogram ($/kg), over the entire lifetime of a hydrogen production system.

conventional electrolyser systems powered by the stable grid, these offshore renewable systems must operate under highly variable wind power conditions. This introduces new challenges in terms of hydrogen production, degradation, and the LCOH (Schofield et al., 2024). Most electrolysers were designed for onshore steady-state operation with a constant power supply. The long-term impacts of intermittent power inputs on their performance remains poorly understood (Carmo et al., 2013). Currently, no standardized operational strategy exists for managing these variable conditions, and limited data is available to evaluate how different approaches affect both technical performance and economic viability.

This thesis is motivated by the urgent need to fill the critical gap in both academic research and engineering practice. It aims to explore how PEM electrolysers can be operated more effectively under offshore wind conditions, balancing efficiency[2], degradation, and hydrogen production in order to reduce the LCOH. By addressing this, the thesis aims to support the development of reliable and scalable offshore hydrogen production as a key component of our future energy system.

## 1.2 Limitations in the Current Literature

The previous section highlighted a core challenge: Offshore wind power intermittency impacts PEM electrolyser performance by accelerating degradation, lowering efficiency, and affecting hydrogen production (Weiß et al., 2019).

Although awareness of these issues is growing (Harrison et al., 2010)(Millet & Grigoriev, 2013)(Salehmin et al., 2022), the current literature remains limited. Several experimental studies confirm that PEM electrolysers degrade faster under intermittent power (Harrison et al., 2010)(Carmo et al., 2013)(Buttler & Spliethoff, 2018)(Shaun et al., 2019)(Siracusano et al., 2018), but most are small-scale and conducted under controlled laboratory conditions. These studies rarely use real offshore wind profiles or simulate multi-stack systems. Moreover, the number of published research quantifying PEM electrolyser degradation is scarce and there is no consensus on test protocols, making it difficult to compare degradation data (Millet & Grigoriev, 2013)(Salehmin et al., 2022).

Modelling efforts are also fragmented. Many studies focus on static performance or simplified single-stack dynamics (Rakousky et al., 2017)(Dong et al., 2023). Others address the techno-economic feasibility of hydrogen production but ignore degradation and omit operational control strategies (Solmaz Shanian & Oumarou Savadogo, 2024). Crucially, very few models integrate all relevant dimensions: intermittent power input, degradation behaviour, multi-stack operational strategies and their combined impact on the LCOH.

This exposes a clear research gap: there is no validated, system-level model that captures degradation effects under realistic offshore wind conditions and evaluates operational strategies at stack level. If this gap remains unaddressed, offshore hydrogen systems risk being less economically viable than expected.

[2]The efficiency (%), is defined as the amount of energy (kWh) required to produce one kg of $H_2$ , relative to a specific energy of 33kWh/$kg_{H2}$ (Idealhy, n.d.).

## 1.3 Research Questions, Scope and Objectives

As mentioned, the scope of this thesis focuses specifically on PEM electrolysers for offshore hydrogen production. Based on the research gap identified in the previous section, this thesis aims to answer the following research question:

*"How does the operational strategy for managing intermittent offshore wind power supply in an offshore PEM electrolyser system affect hydrogen production, stack degradation and the LCOH?"*

The study assumes a direct coupling between the OWF and the PEM electrolyser system, meaning that the wind farm is not connected to the onshore electricity grid. Instead, all generated electricity is used for hydrogen production, and the produced hydrogen is transported to shore via a pipeline. The PEM electrolyser is placed on an offshore platform near the OWF. This setup reflects emerging offshore hydrogen concepts and pilot projects, such as PosHYdon and NortH2, and allows for a focused analysis of system behaviour under realistic offshore conditions. Both the OWF and electrolyser capacity are assumed equal at 400kW. The electrolyser consists of 4, 100kW stacks. This modular configuration enables the exploration of stack-level operational strategies. The scope includes the electrochemical behaviour of the PEM electrolyser stack but assumes a simplified balance-of-plant[3] (BoP), to maintain computational feasibility and focus on the core research objectives. To quantify the degradation behaviour, the study uses a combination of literature-based degradation data, manufacturer specifications, and insights from industry experts.

This thesis does not cover the detailed design of offshore infrastructure (e.g., platforms, pipelines, or compressors), nor does it include the full lifecycle assessment or environmental impact analysis of offshore hydrogen systems.

To answer the research question, within the scope of this thesis, following sub-questions are considered:

- *What is electrolysis?*
- *Why is PEM the most suitable electrolyser technology for offshore renewable applications?*
- *What causes PEM electrolyser degradation and how does power intermittency influence this degradation?*
- *Which technical and operational factors affect the LCOH of offshore PEM systems?*
- *What are the PEM electrolyser operating characteristics under various load conditions and how can they be modelled?*
- *How can PEM electrolyser degradation be quantified under intermittent power?*
- *Which operational strategies are applied and why are these strategies selected?*

The key objectives of this thesis are:

- Understanding electrolysis and electrolyser technologies and substantiate why PEM electrolysers are the most suitable for offshore renewable applications
- Understanding degradation mechanisms and quantifying a degradation relation based on intermittent power operation.
- Modelling a PEM electrolyser and simulating its characteristics such as hydrogen production, efficiency and a polarization curve[4] under different load conditions.
- Evaluating operational strategies and reflect how they influence the hydrogen production, degradation and ultimately which strategy results the lowest LCOH.

[3] The balance of plants includes all components of the PEM systems other than the stacks, such as heat exchangers, dehumidifiers, pumps and pipelines.

[4] A polarization curve shows how the voltage of a PEM electrolyser changes with increasing current density, revealing its efficiency and internal losses. It is a key characteristic of an electrolyser cell.

## 1.4 Research Methodology

This thesis adopts a simulation-based, techno-economic research approach. The methodology consists of two interrelated phases:

- A literature-based research phase
- A simulation-modelling phase, consisting of:
    - The PEM electrolyser model
    - The operational strategy model

This methodological structure is chosen as simulations allow for exploration of long-term effects and strategic trade-offs between efficiency, hydrogen production, degradation, and ultimately the LCOH. The literature research ensures the models and inputs are grounded in theory and evidence. Experimental research was deemed infeasible for this thesis.

### 1.4.1 Literature Research Phase

The research phase establishes the academic foundation for the simulations. It systematically addresses the sub-questions and supplies validated input for the simulation models. It comprises five key components:

1. Fundamentals of Electrolysis; A review of the electrochemical principles of water electrolysis, focusing on core reactions and governing equations.

2. Comparison of Electrolyser Technologies; A comparative analysis of PEM electrolysers to other types (Alkaline, Anion Exchange Membrane, and Solid Oxide) in terms of working principles, performance, and materials to substantiate why PEM electrolysers are most suitable for offshore renewable applications.

3. Degradation Mechanisms and Data of PEM Electrolysers; An in-depth study of PEM degradation mechanisms and how they are affected by variable power loads. This includes an extensive analysis of degradation data to derive a quantitative relation between operating conditions and the degradation rate.

4. Modelling Approaches for PEM Electrolysers; A review of state-of-the-art PEM modelling methods and model structures. This establishes the foundation for the PEM electrolyser model.

5. Techno Economic Parameters: A review of representative CAPEX and OPEX values for offshore PEM systems.

Findings from the literature research are used to justify the PEM model assumptions and parameters. Findings from the degradation data analysis are integrated into the operational strategy model.

### 1.4.2 Simulation Modelling Phase

The modelling phase consists of two interconnected models that simulate both technical and economic aspects of the offshore PEM system.

1. PEM Electrolyser Model (Simulink)

The PEM electrolyser model is developed in Simulink and represents a single PEM stack (assumed 100 kW nominal capacity) consisting of 50 electrolytic cells connected in series. The model incorporates fundamental electrochemical equations and performance characteristics derived from literature. The result of this model is a validated PEM electrolyser simulation that defines the polarization curve, hydrogen production, and efficiency for any given power input across its nominal capacity.

2. Operational Strategy Model (Python)

Building on the stack performance characterisation from the Simulink model, the second part of the modelling phase is the development of an operational strategy simulation implemented in Python. This model represents the full 400 kW offshore PEM system (composed of 4, 100 kW stacks) operated over a period of 15 years, subject to a time-varying power input from an OWF. The model integrates technical performance, degradation effects, and economic calculations to evaluate different operational strategies.

The output of the operational strategy model is a dataset describing how each strategy performs in terms of efficiency, total hydrogen produced, the degradation behaviour of each stack, and the resulting LCOH. These outputs directly feed into answering the research question by quantifying the impact of the operational strategy on the LCOH. A schematic overview of the modelling methodology can be found in Figure 1-1.

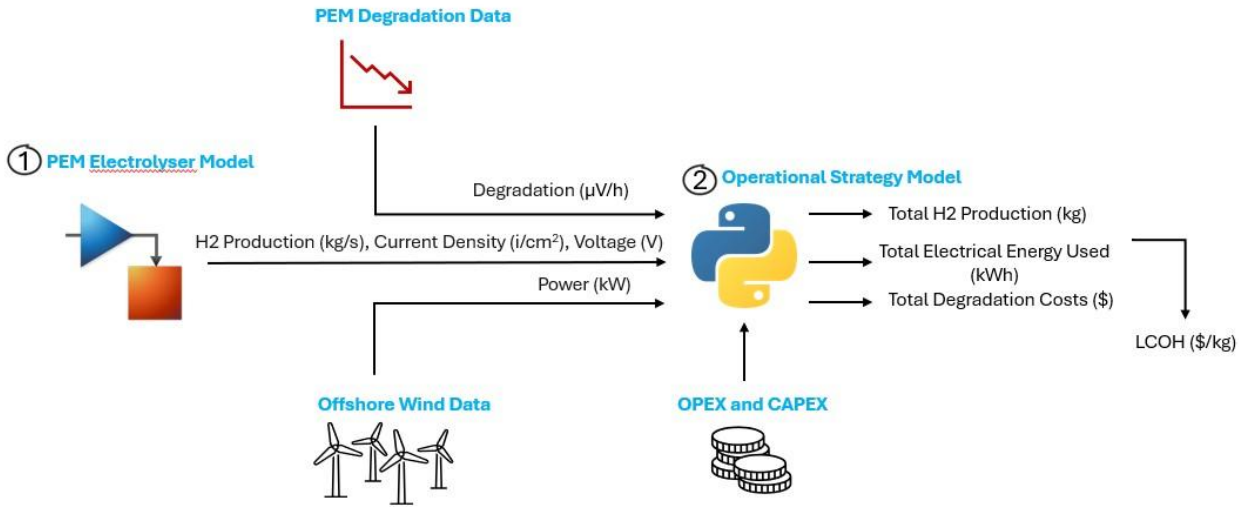


*Figure 1-1: Schematic overview of thesis' models*

## 1.5 Thesis structure

This thesis guides the reader through the technical, economic, and operational aspects of offshore hydrogen production using PEM electrolysers, according to the following structure:

- Section 2 presents the state-of-the-art in electrolysis and PEM technology. It covers the fundamentals of electrolysis, compares electrolyser technologies, and focuses on PEM-specific degradation mechanisms, modelling approaches, and techno-economic parameters.
- Section 3 introduces the PEM electrolyser Simulink model, detailing its structure, equations, parameters, and outputs, which serve as inputs for the operational strategy model.
- Section 4 covers the collection and analysis of degradation data, addressing challenges under intermittent operation and quantifying relation between operating conditions and the degradation rate.
- Section 5 presents the operational strategy model and simulation results, comparing three operational power distribution strategies and analysing their impact on efficiency, hydrogen production, degradation, and the LCOH.
- Section 6 concludes the thesis by answering the research question and summarising key findings.
- Section 7 discusses the results, reflects on limitations, and offers recommendations for future research.

Each section begins with a description of the relevance of the section and a conclusion for that section. Where needed, subsections end with a short summary to guide the reader through the thesis. Additional background information on certain sections can be found in the appendix.

# 2 State-Of-The-Art of Electrolysers for Hydrogen Production

This section covers the state-of-the-art of electrolysers for hydrogen production to understand what electrolysis is, give insights into the different types of electrolysers and substantiate why PEM is the most suitable technology for offshore renewable applications. Furthermore, it covers the key degradation mechanisms of PEM electrolysers, explores relevant modelling approaches, and assess the techno-economic parameters.

## 2.1 What is Electrolysis?

**Relevance**
A basic understanding of the process of (water) electrolysis is required to understand the different types of electrolysers, electrolyser degradation and models that are covered in this section.

**Conclusion**
Electrolysis is an electrochemical process where electrical energy drives an otherwise non-spontaneous redox reaction to decompose chemical compounds. Water electrolysis is the electrochemical reaction where liquid water is decomposed into hydrogen- and oxygen gas under specific potentials.

Hydrogen can be produced via the electrolysis of water. Section 2.1.1 and 2.1.2 aim to provide a basic understanding of the fundamentals of (water) electrolysis.

### 2.1.1 Basic Principles of Electrolysis

Electrolysis is an electrochemical process that uses electricity to drive a non-spontaneous redox reaction, breaking down compounds. “Lysis” means breaking down or loosening in ancient Greek; electrolysis means “breakdown via electricity” (Wang et al., 2005).

Redox reactions are a transfer of electrons between two reactants. Oxidation (ox) is defined as an increase in oxidation state, which is typically accompanied by the loss of electrons. Conversely, reduction (red) is a decrease in oxidation state, usually associated with the gain of electrons (Tsutsumi, n.d.). In a redox reaction the oxidation and reduction processes occur simultaneously within an electrolytic cell. The cell comprises of two plates called electrodes. The positive electrode is called the Anode and the negative electrode the Cathode. The electrodes are connected through an electrolyte. The electrolyte is a substance containing free ions, such as an electrolytic solution or molten ionic compound. The electrolyte gives the possibility for ions to transfer between the electrodes (Mustafa Ergin Şahin, 2024).

When a direct current (DC) is applied to the electrodes, a potential difference occurs and cations (positively charged ions) migrate towards the Cathode to undergo reduction, while anions (negatively charged ions) move towards the Anode for oxidation. The external voltage facilitates these reactions which are thermodynamically unfavourable under standard conditions (Smolinka, 2009).

Michael Faraday first formulated the principle of electrolysis in 1820 with the two fundamental laws (Sundén, 2019):

1. The first law states: “The mass of a substance deposited at any electrode is directly proportional to the amount of charge passed”. This law is defined by (2.1) where *m* is the mass in (kg), *Q* is the charge in Coulomb (C) and *Z* is the electrochemical equivalent which defines the mass of an element transported by a specific quantity of charge (kg/C).

$$\frac{m}{Q} = Z \tag{2.1}$$

2. The second law states: “If the same amount of electricity is passed through different electrodes in series, the masses of ions deposited at the electrodes are directly proportional to their chemical equivalents”. The second law is defined by (2.2). Here, *E* is the chemical equivalent in (kg/mol) as defined by (2.3) where *M* is the molar mass in (kg/mol) and *v* is the valency (-).

$$m \propto E \tag{2.2}$$

$$E = \frac{M}{v} \tag{2.3}$$

From the first and second law and together with the Avogadro constant ($N_A$), which defines the number of units in one mole of any substance ($mol^{-1}$), the Faraday constant (*F*) can be derived. The Faraday constant defines the quantity of electric charge carried by one mole of electrons, it is expressed in units of coulombs per mole (C/mol).

The mechanism of electrolysis and its basic principles as defined by Faraday’s Laws are fundamental in various processes including metal extraction, electroplating and the production of chemicals such as hydrogen. Hydrogen can be produced by the electrolysis of water which will be covered in the next section.

**In short:** Electrolysis is an electrochemical process that uses electrical energy to drive non-spontaneous redox reactions, causing the decomposition of chemical compounds. Governed by Faraday’s laws, it involves ion migration in an electrolyte between two electrodes, oxidation at the Anode and reduction at the Cathode. Electrolysis of water is the basis for hydrogen production.

### 2.1.2 Water electrolysis

Water electrolysis involves the decomposition of water into hydrogen and oxygen gases using electrical energy according to (2.4).

$$2H_2O\ (l) \xrightarrow{energy} 2H_2\ (g) + O_2(g) \tag{2.4}$$

The two half-cell reactions, also known as the reduction- and oxidation reaction, take place at the two half-cells, the Cathode and Anode respectively. These are connected by the electrolyte to form a

balanced system. To balance the half-cell reactions, the electrolyte needs to be either acidic or basic. The half-cell reactions are often catalysed by a transition metal catalyst to lower the required activation energy of the reaction.

In the presence of an acidic electrolyte the half-cell reactions are according to (2.5) and (2.6) (Gonçalves et al., 2021).

$$2H_2O(l) \rightarrow O_2(g) + 4H^+(aq) + 4e^- \tag{2.5}$$

$$4H^+(aq) + 4e^- \rightarrow 2H_2(g) \tag{2.6}$$

In the presence of a basic electrolyte the half-cell reactions are according to (2.7) and (2.8).

$$4H_2O(l) + 4e^- \rightarrow 2H_2(g) + 4OH^-(aq) \tag{2.7}$$

$$4OH^-(aq) \rightarrow O_2(g) + 2H_2O(l) + 4e^- \tag{2.8}$$

The difference between these two half-cell reactions can be explained by the Pourbaix diagram for water. The Pourbaix diagram for water at 25 $^0$C in Figure 2-1 shows the thermodynamic stability regions of water as a function of the electrode potential (*E*) and pH. Below the red line, also known as the hydrogen evolution reaction (HER) line, water is thermodynamically unstable and tends to reduce to hydrogen gas. Above the purple line, also known as the oxygen evolution reaction (OER) line, water tends to oxidize to oxygen gas. Between the two lines water is considered thermodynamically stable. The pH of the electrolyte determines which HER and OER take place.

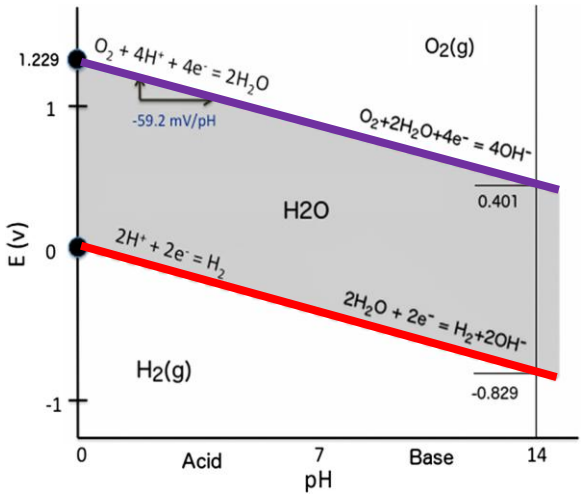


*Figure 2-1: Pourbaix diagram of water (Gonçalves et al., 2021)*

As can be seen from the Pourbaix diagram electrolysis occurs outside the thermodynamic stable region of water, meaning that the potential difference needs to be at least as large as the difference between the OER and HER line. This potential is called the standard cell potential, $E^0_{cell}$ (V). The standard cell potential is used to overcome the Gibbs-free energy, $\Delta G$ (kJ/mol). It represents the minimum electrical energy per unit of charge needed to split water without considering thermal energy.

The standard cell potential ($E^0_{cell}$) is defined by the difference between the Cathode and Anode standard half-cell potential according to (2.9).

$$E^0_{cell} = E^0_{cathode} - E^0_{anode} \tag{2.9}$$

The (half-) cell standard potential is the potential at standard state, meaning that a species in the condensed phase is at unit activity and any species in the gas phase is at a partial pressure of 1 atm. In aqueous systems, the hydrogen standard potential, as seen by the Cathode reaction in equation (2.6), is taken as the universal reference electrode, and its potential is set to 0V (Sundén, 2019). The standard potential of the Anode half-cell reaction in (2.5) is 1.299V (4.3: Electrochemical Potentials, 2019).

The (half-)cell potential under different conditions other than the standard conditions can be calculated using the Nernst-equation as in (2.10).

$$E = E^0 - \frac{RT}{n_e \cdot F} \ln (Q) \tag{2.10}$$

Where $R$ (J/mol) is the gas constant, $T$ (K) the temperature, $F$ (C/mol) the constant of Farraday, $n_e$ (-) the number of electrons involved and $Q$ is the reaction quotient that is related to the pressure and activities of the speciess involved in the reaction.

The standard potential as defined by (2.9) can also be written in terms of the Gibbs free energy as seen in (2.11). Under standard conditions the Gibbs free energy of water is 237.2 (kJ/mol). The standard potential ($E^0$) represents the minimum electrical energy per unit of charge needed without considering thermal energy.

$$E^0_{cell} = -\frac{\Delta G}{n_e \cdot F} \tag{2.11}$$

The thermoneutral voltage ($E_{tn}$) corresponds to the enthalpy change, $\Delta H$ (kJ/mol) which includes both the electrical and thermal energy to drive the reaction without a net temperature change. The thermal neutral voltage is defined by (2.12).

$$E_{tn} = -\frac{\Delta \mathrm{H}}{n_e \cdot F} \tag{2.12}$$

The Gibbs-free energy, enthalpy and corresponding (thermo)neutral voltages determine the Pourbaix diagram of water and are crucial to understand water electrolysis and the potential behaviour of an electrolysis cell. Their values under standard conditions can be found in Table 2-1.

*Table 2-1: Electrolysis energy values ((Tsutsumi, n.d.).*

| Metric | Value |
|---|---|
| $\Delta G$ | 237.2 [kJ/mol] |
| $\Delta H$ | 285.8 [kJ/mol] |
| $E^0_{rev}$ | -1.229 [V] |
| $E^0_{tn}$ | -1.481 [V] |

**In short:** Water electrolysis uses electrical energy to split water into hydrogen and oxygen through redox reactions at the Cathode and Anode, which are facilitated by either an acidic or basic electrolyte and often catalysed to reduce activation energy. The Pourbaix diagram helps to explain the required cell voltage by showing that electrolysis must occur outside water's thermodynamically stable region, requiring a minimum voltage defined by the standard cell potential and influenced by pH, Gibbs free energy, and enthalpy.

## 2.2 Electrolyser Technologies: An Overview

**Relevance**
Water electrolysis can be done in different type of electrolytic cells. The scope of this thesis focusses on PEM electrolysis. This section aims to understand and compare the different electrolyser technologies and substantiate why PEM electrolysers are most suitable for offshore renewable applications.

**Conclusion**
PEM electrolysers are the most suitable for offshore renewable applications due to their unique combination of high operational flexibility, compact design, and ability for pressurized operation. Unlike Alkaline, AEM, and SOEC systems, PEM electrolysers can rapidly respond to fluctuating power input, making them ideal for integration with offshore wind power. They are the only electrolyser technology currently deployed at scale in offshore environments.

There are several types of electrolyser technologies. Section 2.2.1 covers the different types of electrolysers and highlights the four most important technologies. Section 2.2.2 and 2.2.3 will dive deeper into these technologies. Section 2.2.4 compares the four major electrolyser technologies and substantiates why PEM electrolysers are most suitable for offshore renewable applications.

### 2.2.1 Introduction to The Different Types of Electrolysers

Electrolysers are made of multiple electrolytic cells stacked together. There are different types of electrolysers that each have slightly different electrolytic cells and working principles. An overview of the different types of electrolysers can be found in Figure 2-2. The most common electrolysers are Alkaline, Proton Exchange Membrane (PEM) and more recently Anion Exchange Membrane (AEM) and Solid Oxide (SOEC) electrolysers. Other technologies such as Acid-Alkaline Amphoteric, Microbial and Photoelectrochemical are still at research level, and not commercially available yet. They are therefore excluded from the state-of-the-art.

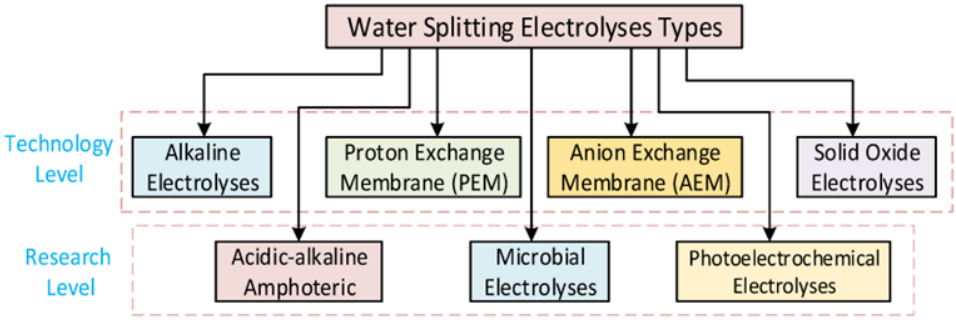


*Figure 2-2: Electrolysis technologies for hydrogen production (Mustafa Ergin Şahin, 2024)*

The next section will give a short overview of Alkaline-, AEM- and SOEC electrolyser technologies. This is followed by an extensive overview of PEM electrolysers.

**In short:** Electrolysers consist of electrolytic cells stacked together. The four main, commercially available, electrolyser technologies are Alkaline, Proton Exchange Membrane (PEM), Anion Exchange Membrane (AEM), and Solid Oxide (SOEC) Electrolysers.

### 2.2.2 Alkaline-, AEM- and SOEC- Electrolysers

Alkaline, AEM and SOEC are key electrolyser technologies. It is useful to understand their working principles, operating conditions and challenges to evaluate their potential for offshore renewable applications. This section gives a short summary of those characteristics. Extensive research on Alkaline-, AEM- and SOEC electrolysers can be found in Appendix A, B and C respectively.

**Alkaline Electrolysers**

The technology of Alkaline electrolysers is the most mature, with over 840 MW installed capacity worldwide (IEA, 2023). Alkaline electrolysers employ a liquid KOH or NaOH electrolyte and nickel-coated stainless-steel electrodes, separated by a porous asbestos or $ZrO_2$ diaphragm (Sampangi et al., 2017)(IEA, 2023)(Knop, 2022). A schematic overview of an Alkaline cell can be seen in Figure 2-3.

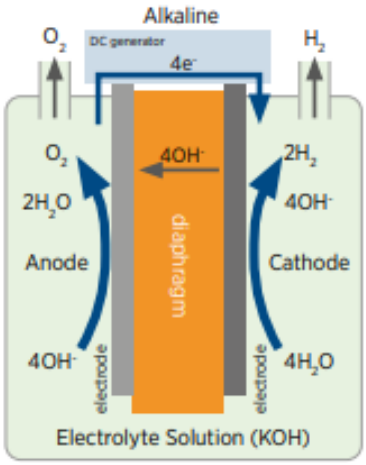


*Figure 2-3: Alkaline electrolyser cell (IRENA, 2020)*

The Cathodic hydrogen evolution reaction (HER) and Anodic oxygen evolution reaction (OER) are given by equation (2.13) and (2.14) respectively.

$$4H_2O\ (l) + 4e^-(aq) \rightarrow 2H_2(g) + 4OH^-(aq) \tag{2.13}$$

$$4OH^-(aq) \rightarrow 2H_2O(g) + O^2(g) + 4e^- \tag{2.14}$$

The overall reactions is given by equation (2.15).

$$H_2O\ (l) \rightarrow H_2(g) + \frac{1}{2}O_2(g) \tag{2.15}$$

Due to limited $OH^-$ conductivity, gas bubble formation, and thick diaphragms, Alkaline systems exhibit low current densities between 0.2 and 0.8 A/cm², cell voltages ranging from 1.4 to 3 V, and moderate efficiency of 43 to 66 percent (IRENA, 2020)(IEA, 2023)(Millet and Grigoriev, 2013). Alkaline electrolysers operate at 70 to 90 °C and 1 to 30 bar, limited by the boiling point of water and material stability (Seddiq Sebbahi et al., 2024). Diaphragm permeability and electrolyte drag limit hydrogen purity to between 99.9 and 99.9998 percent (Carmo et al., 2013). Cold start requires 10 to 50 minutes, and ramp rates vary from 30 seconds to several minutes due to thermal inertia and slow electrode kinetics (Li et al., 2022)(Carmo et al., 2013). Lifetime reaches approximately 60,000 hours and is affected by Anode corrosion, $Ni(OH)_2$ formation, diaphragm degradation, and electrolyte contamination (Zeng and Zhang, 2010)(Carmo et al., 2013). Capital expenditure for systems of 10 MW or larger is estimated at 500 to 1000 USD per kW, with 45 percent allocated to the stack and 55 percent to the BoP. The majority of stack costs stems from the electrodes and diaphragm, and half of the BoP costs is attributed to power electronics (IRENA, 2020). Due to the low current density, heavy electrolyte, and complex auxiliary systems, Alkaline systems are heavy and have a large footprint (Nel Hydrogen, 2024). Major limitations include low efficiency, gas crossover, and limited dynamic operability (Zeng and Zhang, 2010)(Li et al., 2022)(Seddiq Sebbahi et al., 2024). Current research targets cost and performance improvements through the development of non-precious catalysts such as TiN and MoN and advanced diaphragms with higher conductivity and lower permeability (Emam et al., 2024).

**AEM Electrolyser**

AEM electrolysers are an emerging electrolysis technology that combines the low-cost materials and mild conditions of Alkaline electrolysers with the compactness and pressurization ability of PEM electrolysers (IRENA, 2020). First reported in literature in 2011 (Shiva Kumar and Lim, 2022), AEM systems are still in early development, with low global installed capacity and ongoing challenges in membrane stability and durability (Du et al., 2022). The German company Enapter commercializes a modular 1 MW AEM system, indicating initial market entry (Enapter, 2025). AEM electrolysers use a solid Anion Exchange Membrane, typically quaternary ammonium-based (e.g. Sustanion®), that conducts $OH^-$ and functions as both separator and electrolyte. This membrane is often supported by a KOH solution to enhance conductivity (Shiva Kumar and Lim, 2022)(Xu et al., 2022). Non-noble metal catalysts such as Ni and NiFeCo alloys are used at the electrodes, benefiting from the alkaline pH environment (Xu et al., 2022). A schematic overview of an AEM cell can be seen in Figure 2-4.

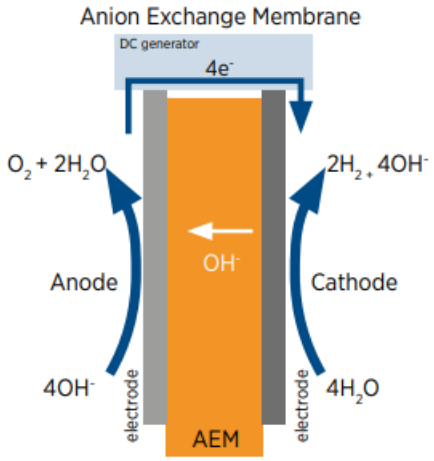


*Figure 2-4: AEM electrolyser cell (IRENA, 2020)*

The Cathodic hydrogen evolution reaction (HER) and Anodic oxygen evolution reaction (OER) are given by equation (2.16) and (2.17) respectively. The overall reaction is given by equation (2.15).

$$4H_2O\ (l) + 4e^- \rightarrow 2H_2(g) + 4OH^- \tag{2.16}$$

$$4OH^- \rightarrow 2H_2O(l) + O_2(g) + 4e^- \tag{2.17}$$

AEM electrolysers typically operate between 40 to 60 °C, because higher temperatures would degrade ammonium groups in the membrane and cause mechanical instability due to swelling of the membrane (Du et al., 2022). While solid membranes suggest pressurized operation is possible, most systems operate at low pressure due to immature and expensive membrane development (Shiva Kumar and Lim, 2022)(IRENA, 2020). Current densities range from 0.2 to 2 A/cm², limited by the low conductivity of $OH^-$ compared to $H^+$ and the immature membrane-electrolyte design (Xu et al., 2022). Voltage ranges from 1.4 to 2.0 V, with overpotentials driven by kinetic and ohmic losses (Shiva Kumar and Lim, 2022). Reported hydrogen purity is 99.95 percent and up to 99.999 percent after drying (Enapter, 2025)(IRENA, 2020). Lifetime varies widely, some reports suggest 5000 to 10,000 hours (Du et al., 2022)(IRENA, 2020), where others mention values up to 30,000 (Shiva Kumar and Lim, 2022). Cold start times are about 20 minutes and ramp rates range from seconds to minutes depending on thermal mass and system design (IRENA, 2020)(Enapter, 2025). System efficiency is reported to be between 48 and 57 percent (IRENA, 2020). BoP requirements are similar to PEM systems, with purification, pressure and temperature control, and power rectifiers. However, AEM systems may eliminate gas separation depending on water feed strategy (Koch et al., 2022). Due to less use of precious metals, AEM systems are expected to be cheaper than PEM in the long term (Xu et al., 2022). Major challenges include membrane degradation, gas crossover, catalyst layer delamination, and instability under dynamic operation (IRENA, 2020). Current research focuses on improving membrane conductivity and lifetime, and on developing robust, non-precious catalysts with high activity and stability.

**SOEC Electrolysers**

SOEC Electrolysers are high-temperature electrolyser systems that operate between 700 and 850 °C and use steam instead of water. They offer high electrical efficiency by using thermal energy to reduce electrical demand (Flis and Wakim, 2023). Development began in the 1970s (Shiva Kumar and Lim, 2022), and recent installations include a 2.6 MW unit in the Netherlands and a 4 MW unit at the NASA research centre (Collins, 2023). However, the total installed capacity is still less than 1 percent of the global electrolyser capacity (IEA, 2023). SOEC electrolysers use a dense ceramic oxide-ion conducting membrane, typically yttria-stabilized zirconia (YSZ), placed between a nickel-YSZ Cathode and a perovskite-based Anode such as LSCF or LSM (Shiva Kumar and Lim, 2022)(Dwi et al., 2023). Nickel provides catalytic activity and electronic conductivity, while the ceramic materials ensure thermal and chemical stability (Dharini et al., 2023). A schematic overview of an SOEC cell can be seen in Figure 2-5.

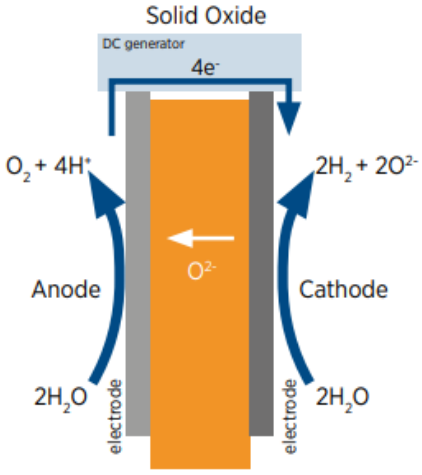


*Figure 2-5: SOEC electrolyser cell (IRENA, 2020)*

The cathodic hydrogen evolution reaction (HER) and anodic oxygen evolution reaction (OER) are given by equation (2.18) and (2.19) respectively. The overall reaction is given by equation (2.15).

$$H_2O\ (g) + 2e^- \rightarrow H_2(g) + O^{2-} \tag{2.18}$$

$$2O^{2-} \rightarrow O_2(g) + 4e^- \tag{2.19}$$

SOEC electrolysers generally operate at 1 bar, with only a few systems pressurized up to 30 bar for integration with downstream processes (IRENA, 2020)(Wolf et al., 2023). Current densities range from 0.3 to 1 A/cm², limited by ceramic membrane's thickness and gas diffusion resistance (Shiva Kumar and Lim, 2022). Operating voltages are typically low, between 1.0 and 1.5 V, as high temperature reduces the Gibbs free energy. Efficiency is reported between 66 and 82 percent, with values near 100 percent possible when coupled to waste heat sources (Wolf et al., 2023). However, high temperatures introduce mechanical stresses due to thermal expansion mismatch and material degradation, especially in the Cathode and sealants (IRENA, 2020). Hydrogen purity is approximately 99.9 percent but is affected by steam residue and sealant failure. Lifetimes reach up to 20,000 hours under stable conditions, but thermal cycling reduces durability (IRENA, 2020). SOECs have extremely slow cold starts exceeding 600 minutes and ramp-up times of about 10 minutes due to low thermal conductivity and risk of hotspot formation (Flis and Wakim, 2023). The BoP requires an evaporator, pre-heaters, thermal insulation, and conventional components such as power rectifiers and gas

separators (IRENA, 2020). Stack compactness is comparable to PEM systems, although weight is higher due to the heavy ceramics. CAPEX data is not publicly available. Ongoing research targets stability improvements, enhanced membrane conductivity, and new material integration to mitigate thermal degradation and expand system viability (Koch et al., 2022).

**In short:** Alkaline-, AEM-, and SOEC electrolysers offer advantages in terms cost and efficiency, but face challenges such as limited dynamic operability, instability, weight and compactness.

### 2.2.3 PEM Electrolysers

To overcome the drawbacks of Alkaline water electrolysis such as low current density and pressurized operation, General Electric developed the 1st PEM electrolyser in 1966 (Shiva Kumar & Lim, 2022). In 2023, the total installed PEM electrolyser capacity was 300MW worldwide (IEA, 2023). PEM electrolysers are known for their high current density, $H_2$ purity and flexibility.

A PEM electrolyser cell comprises of two electrodes, the Anode and Cathode, separated by a perfluoro sulfonic acid (PFSA) membrane such as a Nafion® membrane (IRENA, 2020). The solid membrane conducts protons ($H^+$) and functions as both the separator and the electrolyte. A schematic view of a PEM electrolyser cell can be seen in Figure 2-6.

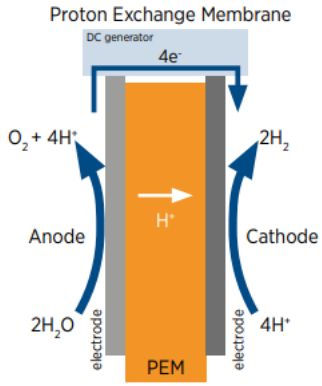


*Figure 2-6: PEM electrolyser cell (IRENA, 2020)*

**PEM Electrolysers - Electrochemical Reactions**

The electrochemical reactions of a PEM electrolyser cell consist of two individual half-cell reactions. The process is initiated at the positive Anode with the Oxygen Evolution Reaction (OER). Here water ($H_2O$) is split into protons ($H^+$), electrons ($e^-$) and oxygen ($O_2$), according to equation (2.20) (Shiva Kumar & Lim, 2022). The oxygen is removed from the Anodic surface and the protons travel through the proton-conducting membrane towards the negative Cathode. The electrons travel through an external circuit towards the Cathode (Sezer et al., 2025). At the Cathode the protons and electrons react to form hydrogen ($H_2$), according to the Hydrogen Evolution Reaction (HER) in equation (2.21). One can recognise these reactions from the acidic region in the Pourbaix diagram in Figure 2-1. The overall reaction is the same as the Alkaline technology given by equation (2.15).

$$2H_2O\ (l) \rightarrow O_2(g) + 4H^+ + 4e^- \tag{2.20}$$

$$4H^+ + 4e^- \rightarrow 2H_2(g) \tag{2.21}$$

The PEM electrolyser reactions can be found in Table 2-2.

*Table 2-2: PEM electrolyser half-cell reactions*

| Reaction | Equation |
|---|---|
| OER | $2H_2O\ (l) \rightarrow O_2(g) + 4H^+ + 4e^-$ |
| HER | $4H^+ + 4e^- \rightarrow 2H_2(g)$ |
| Total | $H_2O\ (l) \rightarrow H_2(g) + \frac{1}{2}O_2(g)$ |

**PEM Electrolysers - Materials**

The main component of the PEM electrolyser cell is the Membrane Electrode Assembly (MEA) which consist of the membrane, Anode and Cathode materials. Other components are the gas diffusion layer, bipolar plates and gaskets, further described in Section 2.3.

The membrane of a PEM electrolyser is made of perfluoro sulfonic acid (PFSA), the one most widely used is Nafion® (Sezer et al., 2025). PFSA is a linear fluorocarbon polymer, and the terminal portions of its side chains are equipped with the sulfonic acid group to facilitate proton transport within the membrane when it is sufficiently hydrated. These membranes, especially Nafion® offer several advantages such as high proton conductivity, high current density, high mechanical strength, and chemical stability (Shiva Kumar & Lim, 2022).

The Anode and Cathode materials are based on noble metals to resist corrosion. The Anode is commonly made of a porous titanium base with an iridium oxide ($IrO_2$) layer (Carmo et al., 2013). The coated iridium layer is measured in mg/cm$^2$. The OER at the Anode creates a strongly acidic environment in combination with high voltages and exposure to oxygen. Iridium oxide ($IrO_2$) is one of the few catalysts that is stable enough in this high potential, oxidizing, low pH environment. The titanium used is also relatively corrosion resistant in acidic and oxidizing environments and stable at high potentials. Furthermore, titanium provides mechanical strength and good electronic conductivity. The porous structure increases the active area and helps to effectively deliver water to the catalyst and remove oxygen from the Anode. However, Iridium is a scarce and expensive material which is a challenge for the PEM electrolyser technology.

The Cathode catalyst is usually platinum (Pt) as platinum has a high catalytic activity for the HER, a low overpotential and good corrosion resistance in low pH environments (Shiva Kumar & Lim, 2022). As pure platinum would be too dense, the platinum is usually deposited onto carbon black (C). The high porosity of carbon black increases the active surface area and facilitates efficient hydrogen transport. Teflon (PTFE) is often added to the carbon black because of its hydrophobicity. This helps to remove hydrogen gas from the pores and prevents possible blockage of gas transport channels with water. An overview of the materials can be found in Table 2-3.

*Table 2-3: PEM electrolyser materials*

| Component | Material |
|---|---|
| Membrane (electrolyte and separator) | perfluorosulfonic acid |
| Anode | Iridium oxide ($IrO_2$) on a titanium (Ti) base |
| Cathode | Platinum (Pt) on carbon black (C) |

**PEM Electrolysers - Operating Conditions**

PEM electrolyser cells operate at temperatures between 50-80 $^0$C for an optimal balance of performance and durability (IRENA, 2020). Both the HER and OER are thermally activated and at higher temperatures the Nafion® membrane is more conductive to protons. Thus, an increase in temperature enhances reaction kinetics, proton conductivity and reduces activation overpotentials (Bornemann et al., 2024). The Nafion© needs to stay hydrated to maintain conductivity, however at higher temperatures the risk of water evaporation increases which can dry out the membrane. Higher temperatures can also lead to chemical degradation and shrinkage of the membrane. Furthermore, the carbon black and sealing components in the stack increase degradation risk under higher temperatures. Thus, for commercial membranes 50-80 $^0$C is the optimal balance between performance and durability.

PEM electrolysers are well-suited to operate at elevated pressures which is a major advantage compared to Alkaline systems. Hydrogen is commonly transported or stored under high pressure (Salehmin et al., 2022). Pressurized production would thus reduce the need for external compression, reducing the total systems energy consumption. Currently PEM electrolysers operate at pressures between 1-70 bar (Shiva Kumar & Lim, 2022). The pressure in the PEM electrolyser is built up as the hydrogen outflow at the Cathode is restricted. The dense solid membrane can withstand higher pressure differentials and still prevents significant gas crossover while remaining conductive to protons. Apart from energy consumption, the pressure also increases reaction kinetics. However, higher pressure does increase the risk of mechanical membrane and seal degradation and eventually gas crossover. There are developments of cells operating even above 70 bars, although these high-pressure PEM electrolyser cells are not common (yet) (Salehmin et al., 2022).

PEM electrolysers typically operate at a current density between 1-2 A/cm$^2$. The perfluorsulfonic acid membranes are quite thin (50-200µm) and have high proton conductivity and low ohmic resistance compared to the thick (mm-range) Alkaline membrane, enabling efficient transport at higher current densities before the ohmic resistance becomes a limiting factor (Carmo et al., 2013). Also, the porosity of the catalyst allows for better mass transportation and gas removal compared to the liquid environment of Alkaline systems. A higher current density means higher hydrogen production and reduction of the systems size. However, extensive thermal management is needed, and the cell degradation increases with a higher current density (Feng et al., 2017).

The voltage range of PEM electrolyser cells is typically between 1.4-2.5V (IRENA, 2020). Compared to Alkaline cells the PEM electrolyser cells can sustain higher currents with moderate voltage increases. The ohmic losses in the membrane tend to increase with the current density but less than with the thick diaphragm of the Alkaline cell (Carmo et al., 2013). Also, the activation potential is more favorable in a PEM electrolyser cell. Operating at higher voltage, however, does accelerate catalyst dissolution, membrane degradation and thermal stress if not managed properly (Feng et al., 2017).

The hydrogen purity of PEM electrolysers is highest of all and ranges between 99.9%-99.9999% (Shiva Kumar & Lim, 2022). The dense solid Nafion® membrane effectively separates the $H_2$ and $O_2$ gasses quite efficiently. Under the right conditions there is little to no crossover and no further purification is needed (Carmo et al., 2013). If operated under higher pressures and temperatures, crossover becomes a more significant risk. Furthermore, PEM systems use pure water feed and a solid electrolyte, which eliminates the risk of electrolyte droplets in the gas stream.

PEM electrolysers have a reported a stack lifetime of about 50.000–80.000 hours (IRENA, 2020), although literature is inconclusive about the actual degradation and lifetime (Schofield et al., 2024). The main degradation mechanisms are membrane thinning and catalyst layer degradation. Especially the dissolution of Iridium at the Anode leads to the loss of active surface area. The degradation and lifetime of PEM electrolysers also depend strongly on the operating conditions. PEM electrolyser stacks tend to degrade faster under higher current density and variable load (IRENA, 2020). Section 2.3 will dive deeper into PEM electrolyser degradation.

PEM electrolysers tend to have high operational flexibility. The thermal mass of a PEM electrolyser cell is relatively low as there is no liquid electrolyte that needs to be heated and stabilized. Also, the Nafion© membrane is sufficiently conductive even at room temperature. A cold start of a PEM electrolyser takes less than 5 minutes (IRENA, 2020) and PEM cells can ramp up/down in a matter of milliseconds (Carmo et al., 2013). However, ramping up cannot outpace the water transport as this causes the membrane to dehydrate, therefore humidification control within the cell is needed.

The system efficiency of PEM electrolysers is typically between 40-66% (IRENA, 2020). The losses are caused by ohmic losses and activation potentials like in Alkaline systems. The BoP also requires a notable portion of the electrical input. An overview of the PEM electrolyser operating conditions can be found in Table 2-4.

*Table 2-4: PEM electrolyser operating conditions*

| Operating condition | Range |
|---|---|
| Temperature | 50-80 [$^0$C] |
| Pressure | 1-70 [bar] |
| Current Density | 1-2 [A/cm$^2$] |
| Voltage | 1.4-2.5 [V] |
| Purity | 99.9%-99.9999% |
| Lifetime | 50.000-80.000 [hours] |
| Cold start | < 5 [minutes] |
| Ramp-up/down | milliseconds – seconds |
| Efficiency | 40-66% |

**PEM Electrolysers - Balance of Plants**

Just like Alkaline, PEM systems require a water purification system, temperature and pressure management, gas separation units, a transformer and rectifier (IRENA, 2020). However, PEM systems don't require a complex liquid electrolyte management system and therefore have a simpler BoP than Alkaline systems. An overview of a PEM system's BoP can be seen in Figure 2-7.

**PEM Electrolyser - Weight and Dimensions**

PEM electrolyser systems tend to be compact. An entire 1.25MW system by NEL fits in a container with dimensions of 12x2.5x3m (90m3) and a weight of 17,300kg (PEM Electrolyser - MC Series, 2019).

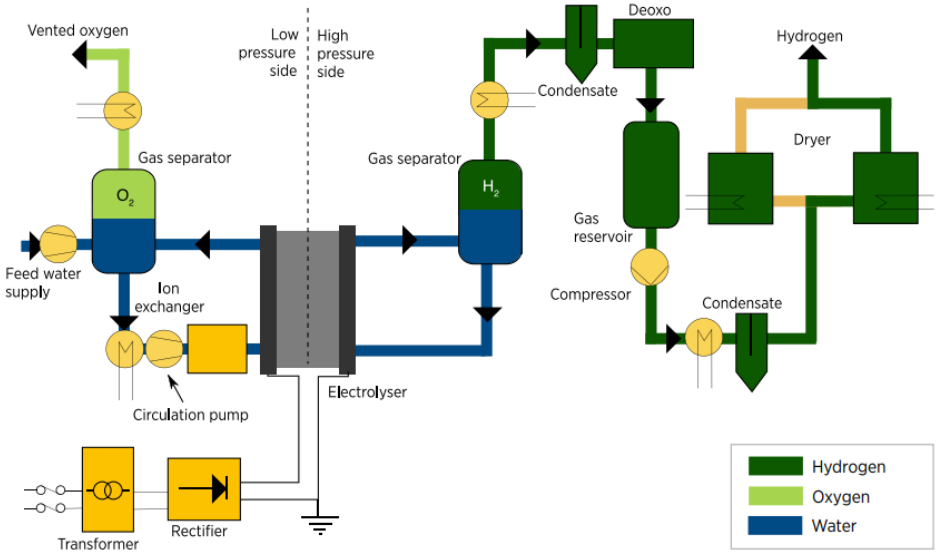


*Figure 2-7 PEM electrolyser BoP (IRENA, 2020)*

**PEM Electrolysers - CAPEX**

According to the International Renewable Energy Agency (IRENA, 2020), PEM electrolyser systems are 50-60% more expensive than Alkaline systems. A PEM electrolyser system of minimum 10MW costs around 700-1400 USD/kW of which 55% is due to the BoP and 45% due to the stack. Just as with AEM Electrolysers, the BoP costs consist for 50% of the power supply system. The use of noble materials such as iridium and platinum used in the bipolar plates take up a large portion of the total stack costs. Furthermore, membranes are complex and expensive to manufacture. Developments for cost reduction focus on reducing expensive coatings, redesigning electrodes and the catalyst coated membranes (IRENA, 2020). Especially the use of the very rare iridium and expensive platinum are areas of focus.

**PEM Electrolysers - Challenges and Technological Developments**

The main challenges for PEM electrolysers are:

1. High stack cost due to expensive membranes and metals such as iridium and platinum. Specially iridium is extremely scarce with less than 10 tons of production per year (Shiva Kumar & Lim, 2022).
2. Membrane durability: Due to thermal and mechanical stress and chemical attacks by radicals the membrane thins over time leading to higher ohmic losses and a lower efficiency (Carmo et al., 2013).
3. Water purity requirements: The membrane is sensitive to ionic contamination such as $Ca^{2+}$ or $Mg^{2+}$ commonly found in water. Ultrapure water needs to be used to prevent membrane fouling and catalyst poisoning (IRENA, 2020).

Current developments in PEM electrolysis are the production of thinner membranes to reduce electricity consumption and increase efficiency, reducing the quantity of expensive metals and progress in stack and system engineering for flexible operation (IRENA, 2020).

**In short:** Proton Exchange Membrane (PEM) electrolysers are a promising technology. The use of a solid membrane allows for compact design, high current densities and operational flexibility. Their ability to produce hydrogen at higher pressures reduces to need for external compression. These characteristics make PEM electrolysers suitable for applications that require pressurized operation, rapid response and compact system design such as offshore renewable hydrogen production. However, PEM electrolysers make use of expensive rare earth materials and complex membranes, and its components are prone to degradation. Furthermore, several resources report rapid degradation due to intermittent operation. Ongoing research aims to reduce the cost and improve durability.

### 2.2.4 Technology Comparison and PEM Justification for Offshore Renewable Applications

In the previous sections four major electrolysis technologies have been discussed. An overview of the technologies and their characteristics can be seen in Table 2-5, which is a result from the extensive literature research in Appendix A, B and C and Section 2.2.3.

By comparison of the technologies one can conclude that PEM electrolysers are currently the most suitable technology for offshore renewable applications. Their technical performance, compact design, and maturity distinguish them from Alkaline, AEM, and SOEC electrolysers.

PEM electrolysers offer superior operational flexibility. They can perform cold starts in under five minutes and ramp up or down in a matter of milliseconds. This is a direct result of their high proton conductivity and low thermal inertia. Alkaline electrolysers, by contrast, rely on a liquid electrolyte with high thermal mass, making them slow to respond and less suitable for dynamic operation. SOEC electrolysers require operating temperatures above 700 °C, making cold starts and fast ramping infeasible. AEM systems show potential in flexibility but are not mature enough yet. In offshore applications, where wind power is intermittent, an electrolyser must respond quickly to fluctuating power inputs. PEM systems are built to do exactly that.

Also. the systems footprint and weight are critical constraints for offshore platforms. Alkaline systems are bulky and heavy due to their liquid electrolyte systems and low current densities, which demand large stack sizes. SOEC electrolysers also have a high structural mass due to their ceramic components. SOEC electrolysers are usually integrated with waste heat which is uncommon offshore (Lamagna et al., 2023). PEM systems, in contrast, are compact and relatively lightweight. This is beneficial for transport, installation, and integration in offshore environments. AEM systems share this advantage in theory, but in practice, the lack of large-scale field validation currently makes them an unreliable choice for offshore deployment.

Another key advantage of PEM electrolysers is their ability to operate at high pressure (up to 70 bar). Offshore hydrogen production often requires compression for transport to shore via pipeline. With PEM systems, pressurized hydrogen can be produced directly at the stack, reducing or eliminating the need for external compression equipment. This not only simplifies the system design but also lowers energy losses and maintenance requirements.

Crucially, PEM electrolysers are the only technology currently used in real-world offshore hydrogen projects. The PosHYdon project in the Dutch North Sea integrates a 1.25 MW PEM electrolyser on a

repurposed offshore gas platform, powered directly by a nearby offshore wind farm (Poshydon, 2024). At the Hollandse Kust Noord wind farm, a 2.5 MW PEM electrolyser is being deployed (Brinck, 2025). In France, the Sealhyfe project recently demonstrated offshore hydrogen production using a 1 MW PEM unit (SeaLhyfe, 2024). These projects set the benchmark for offshore hydrogen systems.

In conclusion, PEM electrolysers offer the best combination of technical readiness, operational flexibility, compactness, and pressure capability for offshore hydrogen production. No other electrolyser technology currently meets the demanding requirements of offshore conditions or has been demonstrated successfully in practice. PEM is not just the most suitable option, it is the industry standard for offshore electrolysis today.

**In short:** PEM electrolysers outperform Alkaline, AEM, and SOEC systems in offshore renewable applications due to their operational flexibility, compact design and high-pressure operation. They are the only technology currently used in real-world offshore hydrogen projects, making PEM the industry standard.

*Table 2-5 Overview of electrolyser technologies characteristics*

| | Alkaline | AEM | PEM | SOEC |
|---|---|---|---|---|
| Anode reaction | $2OH^- \rightarrow H_2O + ½\ O_2 + 2e^-$ | $2OH^- \rightarrow H_2O + ½\ O_2 + 2e^-$ | $H_2O \rightarrow 2H^+ + ½\ O_2 + 2e^-$ | $O^{2-} \rightarrow ½\ O_2 + 2e^-$ |
| Cathode reaction | $2\ H_2O + 2e^- \rightarrow H_2 + 2OH^-$ | $2\ H_2O + 2e^- \rightarrow H_2 + 2OH^-$ | $2H^+ + 2e^- \rightarrow H_2$ | $H_2O + 2e^- \rightarrow H_2 + O^{2-}$ |
| Overall cell | $H_2O \rightarrow H_2 + ½\ O_2$ | $H_2O \rightarrow H_2 + ½\ O_2$ | $H_2O \rightarrow H_2 + ½\ O_2$ | $H_2O \rightarrow H_2 + ½\ O_2$ |
| Current density | 0.2-0.8 A/cm$^2$ | 0.2-2 A/cm$^2$ | 1-2 A/cm$^2$ | 0.3-1 A/cm$^2$ |
| Voltage | 1.4-3 V | | 1.4-2.5 V | 1.0-1.5 V |
| Cell pressure | 1-30 bar | < 35 bar | 1-70 bar | 1 bar |
| Operating temperature | 70-90 °C | 40-60 °C | 50-80 °C | 700-850 °C |
| System efficiency | 40-65% | 50-60% | 40-65% | 65-85% |
| Purity | 99.9-99.9998% | 99.95-99.9999% | 99.99-99.9999% | 99.9% |
| Lifetime | 60.000 hours | - hours | 50.000-80.000 hours | 20.000 hours |
| Cold start | 10-50 minutes | 20 minutes | < 5 minutes | > 600 minutes |
| Ramp-up/down | 30 seconds – a few minutes | - | milliseconds - seconds | 10 minutes |
| Capital cost (minimum 1MW stack) | 270$/kW | N/A | 400$/kW | 2000$/kW |
| Relative Footprint | Large | Small | Small | Small |
| Relative Weight | High | Low | Low | High |
| Development status | Widely commercially available, large-scale projects operational | Some commercial distributors, extensive research on laboratory scale | Commercially available, medium scale projects operational | Some commercial distributors, many small scale experiments |

## 2.3 Degradation Mechanisms in PEM Electrolysers

**Relevance**
Understanding the degradation mechanisms in PEM electrolysers is essential to understand how PEM electrolyser performance deteriorates over time, particularly under the influence of intermittent power. Since stack degradation directly affects system efficiency, hydrogen production, and replacement costs, it is a key driver of the LCOH. By understanding the degradation mechanisms and the influence of operating conditions, this section lays the foundation for degradation data analysis.

**Conclusion**
PEM electrolyser degradation (µV/h) is a complex and mostly irreversible process that occurs across all cell components. It is strongly influenced by intermittent operation, particularly through high current densities, temperature fluctuations, and frequent start-up and shut-down cycles. These conditions accelerate key degradation pathways such as ionomer breakdown, catalyst detachment, and (electro)chemical corrosion ultimately influencing the LCOH.

PEM electrolyser degradation is complex and poorly understood and is therefore still an active area of research (Suermann et al., 2019)(Sayed-Ahmed et al., 2024). The Austrian HyCentA, a research and testing centre for hydrogen technologies, researched and published one of the most extensive papers on degradation mechanisms in current literature. This research will be used as a guideline to understand PEM electrolyser degradation mechanisms (Wallnöfer-Ogris et al., 2024).

### 2.3.1 PEM Electrolyser Degradation in General

Electrolyser degradation is a gradual process that impacts long-term performance, efficiency, and economics. As the system operates, it requires progressively higher cell voltages to maintain the same production rate of hydrogen. This phenomenon occurs because the total energy losses in the system, referred to as overpotentials, increase during operation. Overpotentials include various types of losses, such as resistive (ohmic) losses, kinetic limitations and activation potentials. Degradation is commonly quantified by measuring the rate at which the cell voltage rises over time, expressed in microvolts per hour (µV/h).

Different degradation mechanisms occur in each component of the PEM electrolyser cell; therefore Section 2.3.2 covers the PEM components in more depth and Section 2.3.3 covers the different types of degradation mechanisms.

Degradation is characterized by (a combination of) the following aspects:

- **Chemical degradation** – The loss of material functionality caused by unwanted chemical reactions.
- **Electrochemical degradation** – The performance declines due to changes in electrochemical properties or reactions at the electrodes.
- **Mechanical degradation** – Physical degradation resulting from mechanical stresses such as pressure, temperature and load cycling.

In addition, degradation mechanisms can be classified as either reversible or irreversible:

- **Reversible degradation** – Temporary degradation that can be restored by for example adjusting operating conditions.
- **Irreversible degradation** – Permanent performance loss.

These characterisations will be further covered in Section 2.3.4.

**In short:** PEM electrolyser degradation is a gradual process that increases system overpotentials causing the cell voltage to rise over time. Degradation is typically measured in microvolts per hour (μV/h) and affects long-term performance.

### 2.3.2 Detailed Components of a PEM Cell

Degradation occurs in all components of a PEM cell. Therefore, it is important to consider a PEM cell in more detail. As mentioned in Section 2.2.3 a PEM-cell consists of a Membrane Electrode Assembly (MEA) containing the membrane, Anode and Cathode catalyst. Other PEM electrolyser components are the bipolar plates, porous transportation layer (also known as the current collector) and gaskets. The materials used in each component are of great importance as they directly affect performance and degradation. A more detailed representation of a PEM-cell can be seen in Figure 2-8.

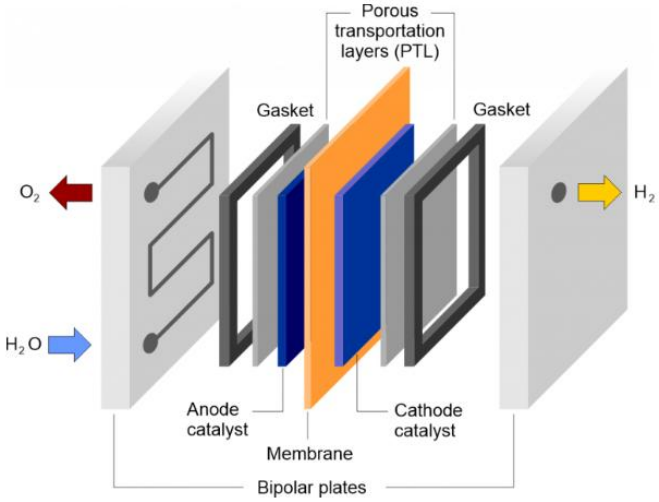


*Figure 2-8: PEM-cell components (Sezer et al., 2025)*

An overview of the components, their functions and materials can be found in Table 2-6. A more elaborate analysis of the PEM electrolyser components can be found in Appendix D.

**In short:** Since degradation affects all components of a PEM electrolyser, understanding the cell's structure, functions, and material is essential to understand PEM electrolyser degradation mechanisms.

*Table 2-6: PEM Components Functions and Materials*

| Component | Function | Material |
|---|---|---|
| Membrane (electrolyte and separator) | Conducts protons from Anode to Cathode; separates hydrogen and oxygen gases | Perfluorosulfonic acid |
| Anode catalyst | Facilitates the OER by accelerating water oxidation | Iridium oxide ($IrO_2$) |
| Anode PTL | Conducts electrons to the catalyst layer and distributes water; allows oxygen removal | Porous titanium |
| Anode Bipolar plate | Provides structural support, conducts current between cells, distributes water, and removes oxygen; includes cooling channels | Titanium/stainless-steel |
| Cathode catalyst | Facilitates the HER by accelerating proton reduction | Platinum (Pt) |
| Cathode PTL | Transfers electrons to the catalyst layer and allows hydrogen removal; supports water diffusion | Porous carbon black |
| Cathode Bipolar plate | Conducts current, removes hydrogen gas, distributes water, and provides thermal management | Titanium/stainless-steel |
| Gaskets | Seal the cell to prevent gas and water leakage; ensure electrical insulation and mechanical compression | Anticorrosive, high strength elastomer |

### 2.3.3 Overview of PEM Degradation Mechanisms

All components of a PEM electrolyser cell are subjected to degradation through various chemical, mechanical, and electrochemical pathways. Understanding how these degradation mechanisms work and what their consequences are is essential to gaining an understanding of degradation in PEM electrolysers.

Appendix E gives a detailed analysis of the degradation mechanisms that occur within a PEM electrolyser (Wallnöfer-Ogris et al., 2024). A short overview of these mechanisms and their consequences can be seen in Table 2-7.

**In short:** All components of a PEM electrolyser are vulnerable to degradation through interconnected chemical, mechanical, and electrochemical mechanisms, influencing proton conductivity, gas crossover, contact resistance, activation overvoltage, mass transport, system efficiency, safety, and ultimately the systems lifetime and LCOH.

*Table 2-7: PEM electrolyser degradation mechanisms descriptions and consequences*

| Degradation mechanism | Description | Consequence |
|---|---|---|
| Chemical ionomer degradation | Radicals like OH• and OOH• formed from $H_2O_2$ attack vulnerable C–H bonds in the PFSA membrane. This leads to chain scission, polymer fragmentation, thinning, and pinhole formation. The radicals arise from gas crossover and side reactions, especially during shutdown and transient operation. | Loss of membrane integrity, increased gas crossover, lower proton conductivity, and safety risks. Efficiency and durability decline. |
| Ionomer inhibition by impurities | Cations such as $Na^+$, $Cu^{2+}$, $Fe^{2+}$ from feedwater or system components displace protons in the sulfonic acid groups of the membrane. This inhibits ion exchange, disrupts hydration behaviour, and leads to uneven proton distribution and local heating. | Reduced ionic conductivity and increased ohmic losses. Proton starvation leads to local heating and accelerated degradation. |
| Mechanical membrane damage | Thermal expansion mismatch, pressure differentials, water swelling, and mechanical clamping induce stress in the membrane. This leads to plastic deformation, micro-cracks, and pinholes, which compromise gas separation and structural integrity. | Formation of pinholes and cracks increases gas crossover and reduces efficiency and lifetime. Synergizes with chemical degradation. |
| Mechanical electrode degradation | Electrode structure suffers from clamping pressure and mechanical mismatch with the membrane. Delamination and morphological changes in the catalyst layers result from thermal and mechanical cycling, affecting charge and mass transport. | Morphological instability in catalyst layers reduces contact with the membrane, increasing resistance and reducing performance. |
| Chemical carbon degradation | Carbon PTLs are chemically attacked by peroxide radicals, leading to fiber oxidation and structural degradation. Weak van der Waals bonding and pressure spikes contribute to mechanical weakening and catalyst layer detachment. | Loss of catalyst support and structural integrity of PTL. Leads to increased ohmic and mass transport resistances. |
| Pt dissolution and redeposition | Ir and Pt catalysts dissolve under electrochemical conditions, especially at high potentials. Dissolved species may redeposit, potentially altering the electrode structure. The process is enhanced by impurities and transient conditions. | Reduction in catalyst layer stability and efficiency. Irreplaceable noble metals lost, increasing cost and environmental impact. |
| Pt detachment / coalescence | Nanoparticles merge through coalescence or agglomerate due to mechanical stress or dissolution/redeposition cycles. This reduces the surface area and changes catalyst morphology, decreasing effectiveness. | Larger particle size reduces ECSA, leading to higher activation overvoltages and lower hydrogen production efficiency. |
| Pt poisoning / blocking | Impurities like $Fe^{2+}$ or $Zn^{2+}$ adsorb onto the catalyst surface, physically blocking active sites. Titanium ions from upstream components can also contribute. This contamination inhibits catalytic activity and increases interfacial resistance. | Loss of active catalytic area, higher activation losses, and increased energy consumption. Reversible under specific treatments. |
| Ir/Ir oxide dissolution / redeposition | Ir and $IrO_2$ dissolve during the OER under high potentials. Chloride ions accelerate dissolution. Dissolved species reduce ECSA and increase | Irretrievable loss of Ir/$IrO_2$, reduction in catalytic activity and durability. |

| | | |
|---|---|---|
| | activation losses. Dissolution can be partial or complete depending on potential and pH. | Reduced efficiency and higher costs. |
| Ir/Ir oxide detachment / coalescence | Detachment occurs due to mechanical vibration, bubble stress, and poor adhesion between catalyst and support. Coalescence reduces the number of independent active sites, degrading performance. | Reduced ECSA and catalyst contact area, leading to reduced current density, increased voltage losses, and lifetime decay. |
| Ir/Ir oxide poisoning / blocking | Surface poisoning by metal ions or contaminants blocks active Ir/$IrO_2$ sites, increasing activation overpotentials and reducing reaction rates. Chlorine and titanium contaminants are especially problematic. | Blocked active sites cause localized overpotentials and hinder catalyst performance. Performance can degrade quickly. |
| Chemical metal BPP/PTL degradation | Fluoride ions and radicals attack the $TiO_2$ passivation layer on titanium PTLs and BPPs, causing corrosion and forming non-conductive Ti-F complexes. This reduces durability and conductivity. | Increased contact resistance and loss of mass transport function. Structural damage reduces current density and reliability. |
| Electrochemical metal BPP/PTL corrosion | $TiO_2$ passivation layer increases resistance due to poor electrical conductivity. To prevent this, some BPPs are coated with precious metals. However, oxide growth still limits efficiency and is hard to control. | Reduced efficiency due to higher resistance. Necessitates expensive coatings. Impairs water/gas management functions. |
| Mechanical metal BPP/PTL damaging | Mechanical compression and thermal cycling deform pore structures in PTLs and BPPs. Hydrogen embrittlement forms brittle hydrides, especially under high pressure and temperature, promoting crack formation. | Cracking and mechanical failure reduce structural stability and conductivity. Accelerates aging and increases failure risk. |
| Polymer sealing gaskets degradation | Peroxide radicals and oxygen exposure chemically attack PTFE-based gaskets. Mechanical clamping stress and stack assembly flaws lead to physical deformation. Leaks and contamination of adjacent components may occur. | Leaks, reduced sealing, and contamination of the catalyst or PTL. Efficiency drops and safety hazards increase. |

### 2.3.4 PEM Electrolyser Degradation Classification, Probabilities and Effects on Overpotentials.

Table 2-8 created by the HyCentA (Wallnöfer-Ogris et al., 2024) provides a comprehensive overview of the characteristics of the key degradation mechanisms. It shows the type of degradation, the affected material, the probability of influences on the stack components and the effect on various overpotentials.

The table also shows the complexity of PEM electrolyser degradation. Degradation mechanisms may affect multiple components and multiple overvoltages/resistances. One can notice that apart from ionomer inhibition, all degradation mechanisms are irreversible and thus impact the PEM electrolysers lifetime. It can also be seen that almost all degradation mechanisms have a high probability/effect on at least one type of overvoltage/resistance, thereby increasing the cells potential and reducing the performance. The largest contributors to an increase of overvoltage are the Anodic/Cathodic activation overpotentials and membrane resistance.

*Table 2-8: Classification, probabilities and effects of PEM electrolyser degradation mechanisms (Wallnöfer-Ogris et al., 2024)*

x match

probability / effect:
++ high
+ significant
o possible

* under constant operating conditions at
- medium current density,
- low hydrogen pressure (< 10 bar),
- low temperature (< 60° C),
- no external introduction of impurities

| | Type | | | | | Material | | | | | | | | Probability of influence on the component * | | | | | | | Effect on increase of overvoltage / resistance | | | | |
|---|---|---|---|---|---|---|---|---|---|---|---|---|---|---|---|---|---|---|---|---|---|---|---|---|---|
| **Class of degradation mechanisms** | chemical | electrochemical | mechanical | reversible | irreversible | PFSA ionomer | carbon black / fiber | platinum | iridium / iridium oxide | titanium | stainless steel | metal coatings, passive layers | PTFE / ETFE / PSU | membrane | anode active layer | cathode active layer | anode transport layer | cathode transport layer | bipolar plate | sealing gasket | anodic activation overvoltage | cathodic activation overvoltage | electrical & contact resistance | membrane resistance | mass transport resistance |
| chemical ionomer degradation | x | | | | x | x | | | | | | | | + | o | ++ | | | | | o | + | | ++ | o |
| ionomer inhibition by impurities | x | | | x | | x | | | | | | | | o | o | o | | | | | o | + | | ++ | |
| mechanical membrane damaging | | | x | | x | x | | | | | | | | o | | | | | | | | | + | o | |
| mechanical electrode degradation | | | x | | x | x | x | x | x | | | | | | + | + | | | | | + | + | + | | ++ |
| chemical carbon degradation | x | | | | x | | x | | | | | | | | | + | | o | | | | ++ | + | | + |
| Pt dissolution and redeposition | x | x | | | x | | | x | | | | | | | | o | | | | | | ++ | | | |
| Pt detachment / coalescence | x | x | x | | x | | | x | | | | | | | | + | | | | | | ++ | | | |
| Pt poisoning / blocking | x | | | x | x | | | x | | | | | | | | o | | | | | | ++ | | | |
| Ir/Ir oxide dissolution / redeposition | x | x | | | x | | | | x | | | | | | ++ | | | | | | ++ | | | | + |
| Ir/Ir oxide detachment / coalescence | x | x | x | | x | | | | x | | | | | | + | | | | | | ++ | | | | + |
| Ir/Ir oxide poisoning / blocking | x | | | | x | | | | x | | | | | | o | | | | | | ++ | | | | |
| chem. metal BPP/PTL degradation | x | | | | x | | | | | x | x | x | | | | | o | | o | | | | ++ | | + |
| electrochem. metal BPP/PTL corrosion | | x | | | x | | | | | x | x | x | | | | | o | | o | | | | + | | + |
| mechanical metal BPP/PTL damaging | | | x | | x | | | | | x | x | x | | | | | o | | | | | | + | | + |
| polymer sealing gaskets degradation | x | | x | | x | | | | | | | | x | | | | | | | o | | | | | |

**In short:** PEM electrolyser degradation is a complex and mostly irreversible process. It affects multiple components and overpotentials/resistances, particularly anodic and cathodic activation overpotentials and membrane resistance, all of which play a key role in performance loss.

### 2.3.5 Overview of The Influence of Operating Conditions on Degradation Mechanisms

Table 2-9 created by the HyCentA (Wallnöfer-Ogris et al., 2024) provides a comprehensive overview of the influence of operating conditions on initiating or accelerating degradation mechanisms, and the propagation of degradation through primary degradation pathways.

The table shows that several operating conditions exhibit a high influence on degradation. Among these are high current density and cell voltage, high temperatures (> 80°C) and temperature peaks, transient operation and start-up/shut-down, and the presence of impurities in feedwater. For example, high current density/voltage has a significant to high influence on several degradation mechanisms including Pt and Ir detachment/coalescence, Ir dissolution/redeposition and (electro)chemical BBP/PTL degradation. Transient operation and start-up/shut-down both have a high influence on these degradation mechanisms as well. These operating characteristics are typical for operation

under intermittent power input. This shows the impact that intermittent operation has on PEM electrolyser degradation.

The influence of primary degradation shows the compounding nature of degradation in PEM electrolysers. For example, chemical ionomer degradation is significantly influenced by transient operation whereas transient operation has a high influence on (electro)chemical BBP/PTL degradation. Demonstrating that operating conditions not only have direct, but also indirect influence on degradation mechanisms, ultimately resulting in cumulative performance losses.

Table 2-9 reveals that degradation in PEM electrolysis is not confined to a single failure mode but arises from a complex interplay of operating conditions, (electro)chemical, and mechanical stressors, many of which are reinforcing. Understanding this complex degradation is essential for developing degradation relations for PEM electrolysers intended for intermittent renewable applications. This remains an active area of investigation in the current literature (Feng et al., 2017).

**In short:** PEM electrolyser degradation is strongly influenced by intermittent operation, where transient operation, start-up/shut-down and high voltage/current density accelerate multiple degradation mechanisms. These effects often reinforce each other, making degradation cumulative and harder to predict.

*Table 2-9: Influence of operating conditions of PEM electrolyser degradation (Wallnöfer-Ogris et al., 2024)*

influence:
++ high
+ significant
o possible

| Class of degradation mechanisms | Influence of operating conditions | | | | | | | | | | Influence of primary degradation | | | | | | | | | | | | | | |
|---|---|---|---|---|---|---|---|---|---|---|---|---|---|---|---|---|---|---|---|---|---|---|---|---|---|
| | low current density < 0.5 A/cm² | high current densities / high voltage | transient operation | start-up / shut-down | insufficiencies in feed water supply | temperatures 60 - 80 °C | temperatures > 80 °C / temp. peaks | high hydrogen pressure | mechanical load / pressure peaks | intake of impurities (water / BoP) | chemical ionomer degradation | ionomer inhibition by impurities | mechanical membrane damaging | mechanical electrode degradation | chemical carbon degradation | Pt dissolution and redeposition | Pt detachment / coalescence | Pt poisoning / blocking | Ir/Ir oxide dissolution / redeposition | Ir/Ir oxide detachment / coalescence | Ir/Ir oxide poisoning / blocking | chem. metal BPP/PTL degradation | electrochem. metal BPP/PTL corr. | mech. metal BPP/PTL damaging | polymer sealing gaskets degradation |
| chemical ionomer degradation | + | + | + | | o | + | ++ | | | ++ | ++ | | + | | | o | | | | | | ++ | ++ | | |
| ionomer inhibition by impurities | | | | | o | | | | | ++ | | | | | | o | | | o | | | + | + | | + |
| mechanical membrane damaging | | | + | + | | o | ++ | ++ | + | | ++ | | ++ | + | | | | | | | | | | | |
| mechanical electrode degradation | | | | o | o | o | + | o | + | | | | + | ++ | | | | | | | | + | + | ++ | |
| chemical carbon degradation | + | + | + | | o | + | ++ | | | ++ | | | | | ++ | | | | | | | ++ | ++ | | |
| Pt dissolution and redeposition | | | | | | | | | | o | | | | | | ++ | | | | | | | | | |
| Pt detachment / coalescence | | + | ++ | ++ | | o | ++ | | | | | | | | | ++ | ++ | | | | | | | | |
| Pt poisoning / blocking | | | | | | | | | | ++ | ++ | | | | | | | | o | | | + | + | | + |
| Ir/Ir oxide dissolution / redeposition | + | + | ++ | ++ | | o | ++ | | | ++ | | | | | | | | | ++ | | | | | | |
| Ir/Ir oxide detachment / coalescence | | + | ++ | + | | + | ++ | | | | | | | | | | | | + | + | | | | | |
| Ir/Ir oxide poisoning / blocking | | | | | | | | | | o | | | | | | | | | | | | + | ++ | | o |
| chem. metal BPP/PTL degradation | | ++ | ++ | + | | + | ++ | + | | + | ++ | | | | | | | | | | | ++ | o | + | |
| electrochem. metal BPP/PTL corr. | | ++ | ++ | + | | o | ++ | | | | | | | | | | | | | | | ++ | ++ | + | |
| mech.metal BPP/PTL damaging | | | | | | | | o | + | | | | | | | | | | | | | ++ | + | ++ | |
| polymer sealing gaskets degradation | o | o | o | | | o | o | o | | | | | | | | | | | | | | o | o | + | ++ |

### 2.3.6 Conclusion of PEM Electrolyser Degradation Mechanisms

The degradation behaviour of PEM electrolysers is complex and governed by a multitude of interrelated chemical, electrochemical, mechanical, and operational factors. Over time, these degradation mechanisms lead to increased overvoltage, reduced efficiency, and ultimately a decline in electrolyser performance and lifetime, influencing the LCOH.

Degradation occurs across the entire cell and is driven by both material vulnerabilities and operational conditions. It accumulates over time, is mostly irreversible, and frequently involves interactions between different mechanisms. Renewable energy input introduces transient operation, start-up/shut-down and possibly high current density and temperature operation. These operating patterns accelerate key degradation pathways such as ionomer breakdown, catalyst detachment, and (electro)chemical BBP/PTL degradation.

One can conclude that intermittent power supply significantly impacts PEM electrolyser degradation. Understanding this effect is critical for quantifying degradation behaviour and developing operational strategies.

## 2.4 PEM Electrolyser Models

**Relevance**
Understanding the different characteristics of PEM electrolyser models is essential because no single modelling approach is universally applicable. The characteristics of the model are important to select a model that is sufficiently accurate without being unnecessarily complex.

**Conclusion**
PEM electrolyser models differ widely in complexity, accuracy, and applicability. For system-level studies with fluctuating loads, a semi-empirical, zero-dimensional, non-isothermal, multiphase model offers a practical balance between realism and efficiency.

### 2.4.1 PEM Electrolyser Modelling in General

PEM electrolyser modelling enables the creation of a digital representation of the physical system, enabling prediction and analysis of its performance under varying conditions. Such a model, often referred to as a “digital twin”, is essential for evaluating system behaviour, identifying performance characteristics and ultimately to develop control strategies.

The polarization curve is the most important characteristic of a PEM electrolyser and defines the relation between the current density (A/cm$^2$) in the cell and the potential (V). An example of a polarization curve can be seen in Figure 2-9. The cell voltage reflects the sum of various overpotentials all of which are closely linked to the electrochemical behaviour and degradation. The polarization curve determines the possible operating points of the PEM electrolysers and defines the current density/potential combination, given a certain power input. Current density is closely linked to hydrogen- and heat production, while cell potential influences reaction rates and is strongly associated with various degradation mechanisms. Both are key control parameters and therefore important to model.

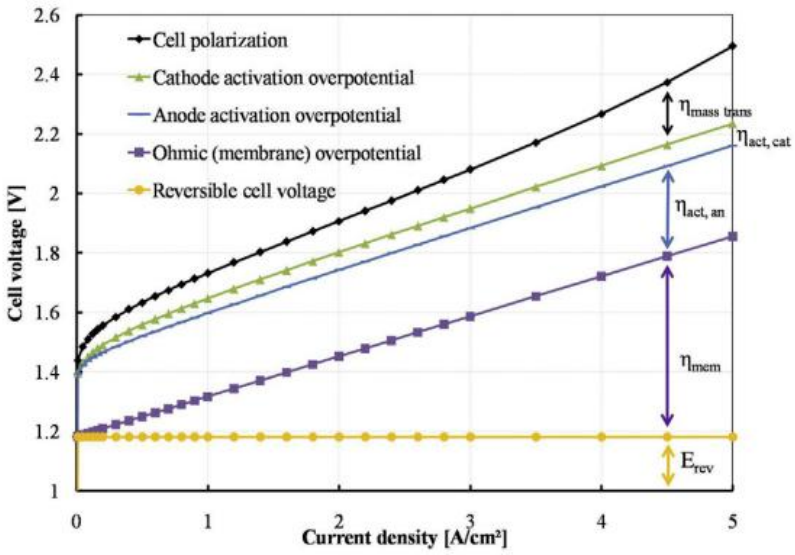


*Figure 2-9: Example of a PEM electrolyser polarization curve and its components (Ojong et al., 2017)*

Other than the polarization curve, PEM models provide insights into key aspects of system operation such as the mass flow of water ($H_2O$), oxygen ($O_2$) and hydrogen ($H_2$), temperature, pressure and

membrane hydration. Depending on the level of detail, models can range from simplified system-level approximations to high-resolution simulations of local proton flux and thermal hotspots.

**In short:** PEM electrolyser modelling enables the creation of a digital representation of the physical system to capture important characteristics such as the polarization curve and hydrogen production.

### 2.4.2 Different Types of PEM Electrolyser Models

PEM electrolyser models can be categorized based on various characteristics. This section presents the different types of models, highlighting their respective strengths and weaknesses. Section 2.4.3 discusses the current state of research in PEM electrolyser modelling, providing a clear overview of the literature and supporting the selection of the most appropriate model in Section 3.

PEM models can be divided into three groups: Analytical, Semi-empirical and Mechanistic. The state of the models can be further divided into steady-state and dynamic, its dimensions, phase and whether the model is isothermal or not. An overview of the PEM electrolyser models classification can be seen in Figure 2-10. A deeper understanding of each of these features can be found in Appendix F.

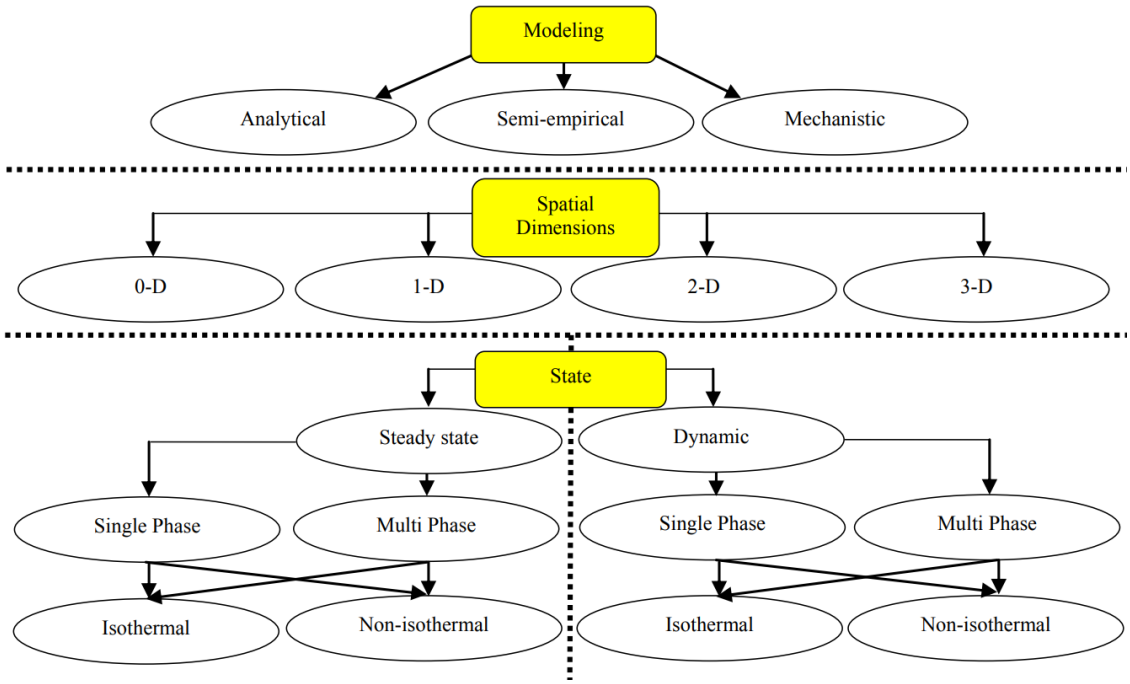


*Figure 2-10: PEM electrolyser model classification (Hernández-Gómez et al., 2020)*

The selection of a model depends heavily on the intended application, required level of accuracy, computational resources, and the specific physical or operational phenomena being studied. For system-level studies, simplified models are often sufficient. These models typically rely on analytical or semi-empirical formulations. They are often implemented in a zero-dimensional (0D) framework, which treats the cell as a lumped system and is well-suited for control development, real-time simulations, or early-stage feasibility studies.

When the goal is to understand detailed electrochemical or material behaviour on component level, mechanistic models are more appropriate. Mechanistic models are typically spatially resolved, non-

isothermal and multiphase to capture heat generation, water transport, and gas evolution more accurately. This level of detail is essential for component design, though it comes at the cost of higher computational complexity and longer simulation times.

For applications where the PEM electrolyser operates under intermittent loads, such as coupling with wind or solar power, dynamic models are required. These models capture time-dependent changes in current, temperature, pressure, and other internal states. Depending on the desired level of detail, both semi-empirical and mechanistic formulations can be used dynamically. Analytical models, by contrast, are rarely suitable for dynamic applications due to their limited flexibility and oversimplification.

Thermal treatment is another key consideration. Isothermal models assume uniform temperature whereas non-isothermal models include energy balance equations and can simulate thermal gradients that influence performance, membrane hydration, and degradation, particularly relevant under intermittent conditions.

Finally, multiphase modelling becomes important when water management and phase change play a role. While single-phase models may suffice under steady operation, multiphase models are necessary to simulate the behaviour of both gaseous and liquid species at higher current densities or during intermittent operation.

**In short:** The choice of model depends on the intended application, the required accuracy, available computational resources, and the specific physical or operational phenomena. For system-level studies involving intermittent operation, it is important to find a balance between accuracy and computational efficiency. A semi-empirical, zero-dimensional, non-isothermal, multiphase model is well-suited for this purpose, as it enables sufficiently accurate prediction of system behaviour under fluctuating loads while keeping the complexity manageable for long-term, large-scale simulations.

### 2.4.3 Status of PEM Electrolyser Modelling

PEM electrolyser modelling is a relatively underdeveloped field. Although the fundamental electrochemical principles of water electrolysis are well established, accurate and validated models for PEM systems are still limited in number and scope (Falcão & Pinto, 2020). Compared to PEM fuel cell modelling, which has reached a high level of maturity, PEM electrolyser modelling falls behind in both depth and standardisation. Since the first publication on PEM electrolyser modelling in 2002 (Onda et al., 2002), research activity seems to increase but remains relatively scarce. Figure 2-11 illustrates the number of publications over the years (Hernández-Gómez et al., 2020).

Most available models focus on static, steady-state behaviour, often neglecting dynamic effects that are critical under intermittent operation, such as thermal transients, water and gas transport, and time-dependent degradation (Abdin et al., 2015). In addition, mass transport phenomena within the cell are frequently oversimplified or ignored, despite their significant influence on performance and durability (Hernández-Gómez et al., 2020).

A further challenge lies in the lack of experimental validation. Many models rely on assumed or fitted values for key parameters such as exchange current density, ionic conductivity, or Faraday efficiency. This limits their reliability and predictive power.

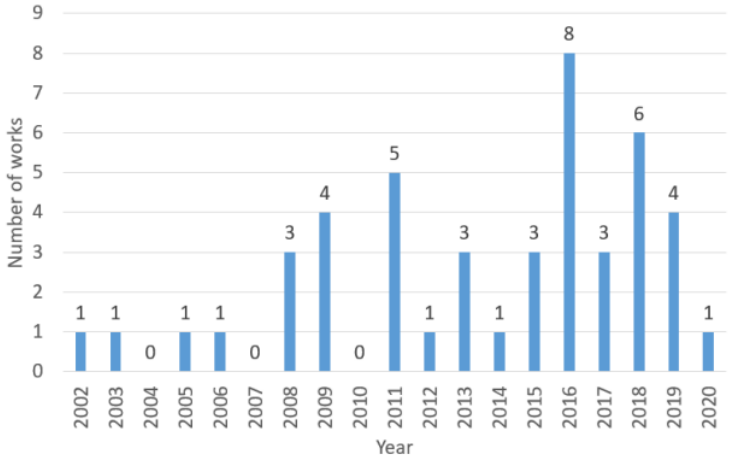


*Figure 2-11: Number of published PEM electrolyser model works (Hernández-Gómez et al., 2020)*

Altogether, the limited number of validated, comprehensive PEM electrolyser models, particularly those that address transient and transport phenomena, highlights the need for further research in this area. Developing such models is essential for accurate system design, control, and integration in renewable-powered applications.

**In short:** PEM electrolyser modelling remains underdeveloped, with limited works often neglecting transients, mass transport, or degradation. Many models lack experimental validation, limiting reliability, underscoring the need for further research. Therefore, one should critically assess model assumptions and limitations.

## 2.5 CAPEX and OPEX of PEM Electrolyser Systems

**Relevance**
To evaluate the LCOH, it is important to understand the capital (CAPEX) and operational (OPEX) expenditures of PEM electrolyser systems, as they are the key cost drivers and directly influence the economic feasibility.

**Conclusion**
The CAPEX of PEM electrolyser systems ranges from 700 to 1,400 USD/kW for a 10 MW installation, with costs roughly split between the stack and BoP. The CAPEX of the offshore infrastructure depends strongly on the site. For standard PEM systems, the OPEX is assumed to be 5% of the CAPEX although it is likely this percentage is higher for offshore systems.

### 2.5.1 Introduction to PEM Electrolysers CAPEX and OPEX

Despite progress in PEM technology and system integration, economic viability, due to high costs, remains a key barrier to large-scale deployment (IRENA, 2020). This section breaks down the capital (CAPEX) and operational (OPEX) costs of PEM systems, which are essential for evaluating the LCOH.

Accurate cost data is difficult to obtain due to its confidential nature; suppliers are often unwilling to share detailed figures. Additionally, costs are rapidly evolving. Saba et al. (2018) reported a sharp decline in PEM system costs over the past 30 years, but current estimates show extreme variations, from a low 306 $/kW to a high 4,748 $/kW. This makes it extremely challenging to identify representative values.

Further costs insights are gained from IRENA's comprehensive report on renewable hydrogen (IRENA, 2020) and the public cost analysis by the North Sea Wind Power Hub (NSWPH), a major European initiative aiming to deploy large-scale offshore PEM electrolysers (Offshore Energy Hubs, 2021). This is further detailed in the following sections.

**In short:** High costs and limited transparency continue to challenge the economic viability of PEM electrolysers, though recent studies and projections suggest promising cost reductions that could support broader deployment.

### 2.5.2 CAPEX of PEM Electrolysers Systems

The CAPEX of an offshore PEM electrolyser installation can be divided into three main components:

1. The PEM electrolyser stack
2. The PEM electrolyser BoP
3. The offshore platform, cables and pipelines

As mentioned in Section 2.2.3, the CAPEX of a minimum 10MW system (stack and BoP) ranges between 700-1400 USD/kW. IRENA (2020) concluded that the system costs are divided among the stack and BoP according to Figure 2-12.

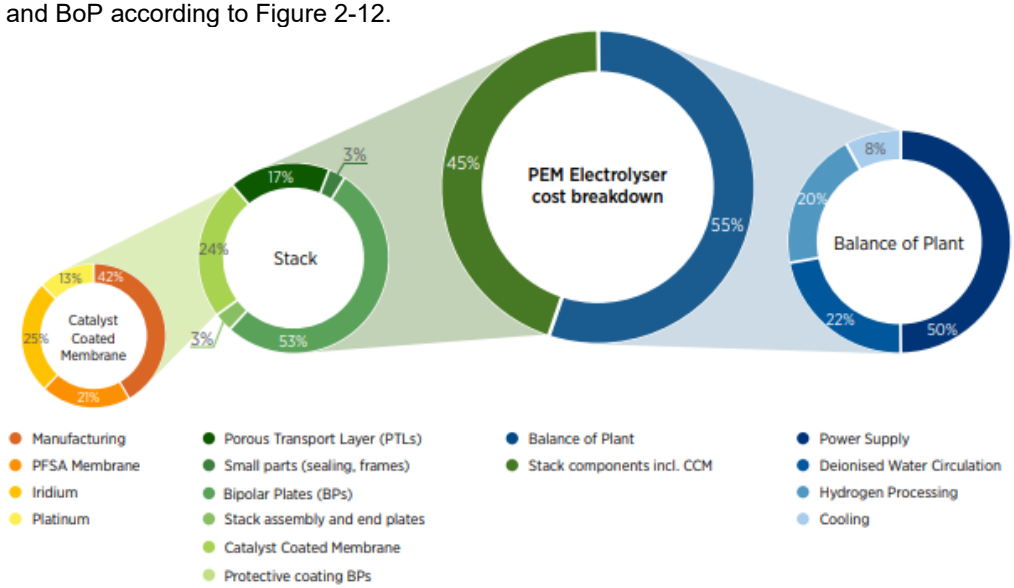


*Figure 2-12 PEM electrolyser system cost breakdown (IRENA, 2020)*

The stack and BoP make up 45% and 55% of the total cost, respectively. In the BoP the power supply equipment is the dominant cost component. In the stack, the bipolar plates make up for just over 50% of the costs. The build up of stack assembly and endplates is further specified in Figure

2-12. An overview of the breakdown of the dominant components according to its percentages and the reference of a 10MW system by IRENA (2020) can be seen in Table 2-10.

*Table 2-10: PEM Electrolyser CAPEX breakdown*

| Component | CAPEX (USD/kW) |
|---|---|
| **Stack** | 315-630 |
| PTL's | 54-107 |
| Bipolar Plates | 167-333 |
| MEA | 75-151 |
| **BoP** | 385-770 |
| Power supply components | 193-385 |
| Water system | 85-170 |
| Hydrogen processing | 77-154 |

The CAPEX of an offshore platform depends strongly on the size of the platform, the water depth, soil, location and ocean conditions. For the NSWPH for example, the platforms make up for 30% of the total costs. However, it is good to notice that this is a 4GW electrolyser project consisting of 8 platforms of 500MW each (Offshore Energy Hubs, 2021). Therefore the project can benefit economies of scale. The PosHydon project on the other hand is making use of an already existing platform that is stationed at an empty gas field (Poshydon , 2024).

Cables and pipelines also strongly depend on the water depth, soil conditions and the distance to shore. The cost of electricity cables and gas pipelines can be into the millions of USD/km (Poshydon, 2024)( Statista, 2021). Another possibility would be to make use of the already existing gas pipeline infrastructure from empty gas field. Other factors to consider are the regulatory and permitting process offshore, extensive research of the offshore sights and possible environmental impact of placing an electrolyser offshore.

**In short:** Offshore PEM electrolyser CAPEX consists of the stack, BoP, and offshore infrastructure. The stack and BoP each account for about half the system cost, with power supply and bipolar plates being major cost drivers. Offshore platform and pipeline costs vary widely based on site conditions and can be reduced through economies of scale or by reusing existing infrastructure.

### 2.5.3 OPEX of PEM Electrolyser Systems

The OPEX of an offshore PEM electrolyser system can roughly be divided into:

1. Routine operations and regular maintenance
2. Operational power consumption
3. Logistics and downtime

Routine operation and regular maintenance costs for PEM electrolysers include tasks such as stack inspections, system maintenance, safety checks, remote monitoring, insurance, and fixed labour. For standard PEM systems, these costs are estimated to be around 5% of the total CAPEX (Offshore Energy Hubs, 2021), although this percentage can vary significantly depending on the system size. In

offshore applications, this share is expected to be higher due to additional factors such as transportation to the platform and the inspection and maintenance of offshore infrastructure.

The operational energy consumption of a PEM electrolyser system includes the energy used by the platform, electrolyser, and the BoP. When calculating the LCOH, these energy costs must be considered as opportunity costs. This can be approached by assuming an average electricity price, or ideally, by using the market price at the specific time the energy is consumed (Schofield et al., 2024).

Logistics and maintenance are a key factor that distinguishes offshore PEM systems from onshore installations. Regular tasks become significantly more costly due to the need for specialized personnel and transportation to remote platforms. Stack replacements for example, are more expensive under these conditions. Additionally, due to these challenging logistics, offshore systems are more susceptible to downtime, which can result from unforeseen maintenance, or external factors such as heavy weather conditions that delay access to the platform. This downtime translates into lost production and can be accounted for in the OPEX as the cost of missed revenue.

**In short:** Offshore PEM electrolyser OPEX includes maintenance, energy consumption, and logistics. Routine maintenance typically costs around 5% of CAPEX but is higher offshore due to access and infrastructure challenges. Logistics and weather-related downtime further increase costs and reduce revenue.

## 2.6 Conclusion and Discussion of Electrolyser State-of-the-Art

In summary, this literature review has substantiated that PEM electrolysers emerge as the most suitable technology for offshore renewable hydrogen production among the various electrolyser types reviewed. PEM electrolysers offer high current densities, rapid responsiveness, and compact designs, making them well-adapted to the fluctuating power outputs of wind and solar sources (Shiva Kumar & Lim, 2022). Their ability to operate under high pressure and deliver high-purity hydrogen further justifies the focus on PEM electrolysers for offshore applications (Carmo et al., 2013). At the same time, PEM electrolysers face challenges common to all electrolyser technologies, such as high capital costs due to expensive materials and degradation mechanisms that can shorten their effective lifetime (Wallnöfer-Ogris et al., 2024). Thus, while the state of the art indicates PEM electrolysers are promising for offshore renewable applications, it also underscores that the following critical issues need to be addressed to realize their full potential:

**Degradation and Lifetime**
Literature shows that PEM electrolyser performance declines over time due to chemical, mechanical, and thermal stress affecting nearly all components. Dynamic operation, such as load fluctuations and frequent shutdowns, accelerates degradation, causing issues like catalyst dissolution, membrane damage, and mechanical stress. These effects increase overpotentials and reduce efficiency. However, the long-term impact of intermittent operation on lifetime remains unclear, as most lifetime data is based on steady-state conditions. Without consistent definitions and testing protocols, quantifying durability under dynamic loads remains a key research gap.

**PEM Modelling**
Most existing PEM electrolyser models are steady-state and oversimplified, making them unsuitable for offshore systems exposed to fluctuating renewable power. Few dynamic models exist, and even fewer include degradation or mass transport effects. Lack of experimental validation and reliance on fitted lab data further limit their reliability. Compared to fuel cell modelling, PEM electrolyser modelling is still immature. A validated, dynamic, and degradation-integrated model is needed to evaluate control strategies for offshore deployment, but no such standard model currently exists.

**Economics**
PEM electrolysers remain expensive, with CAPEX around $700–1,400/kW, roughly 50–60% higher than Alkaline systems. Costs are split evenly between stack and BoP, with bipolar plates and catalyst-coated membranes being major contributors. Potential stack replacements due to accelerated degradation and the nature of offshore OPEX can drive the costs up further. Improving durability is therefore critical to lower the LCOH through fewer stack replacements. Reliable data on offshore lifetime is scarce, increasing uncertainty in cost estimates.

Considering the reviewed literature, several recommendations and opportunities for further research stand out, both for this thesis and for the PEM electrolyser research community at large:

I. Long-Term Dynamic Testing: Conduct dedicated long-duration experiments of PEM electrolysers under realistic fluctuating power profiles. Standardized test protocols (e.g. cell configurations, load cycle definitions and measurement conditions) should be developed to enable comparison across studies. This would help capture true degradation rates and failure modes that short-term tests miss, providing data to validate models and refine lifetime predictions.

II. Integrated Modelling Frameworks: Develop and validate comprehensive PEM models that incorporate electrochemical performance, heat/mass transfer, transient operation, and component degradation simultaneously. Such models should be calibrated with (standardized) experimental data and capable of simulating months or years of operation. This would allow researchers to test different operational strategies and optimize them against criteria like hydrogen output, efficiency, and degradation cost.

III. Materials and Design Innovation: Invest in research on durability-enhancing materials and designs. For example, improved catalyst materials or alternatives to iridium could reduce catalyst degradation, and advanced membrane materials might better withstand chemical attack at high voltage. Likewise, smart cell and stack design such as better stress distribution or improved water management can mitigate some of the damage from dynamic operation. Any such improvements directly feed into longer life and lower costs.

IV. Hybrid Energy Systems: Explore the integration of energy storage or other buffering techniques. These techniques could help to manage and dampen the intermittent power profile to reduce degradation. Research should quantify how much these methods can extend electrolyser life or improve efficiency and at what cost. A rigorous techno-economic analysis is needed to determine if adding storage yields net positive returns by lowering the LCOH in an offshore wind-to-hydrogen system.

V. Operational Optimization and Control: Develop advanced control algorithms for multi-stack electrolyser systems under variable input. This could involve predictive control that anticipates fluctuations (using forecasts) and adjusts load distribution among stacks to minimize wear-and-tear. Machine learning or adaptive control strategies might also be employed to balance efficiency versus degradation in real-time. By optimizing at the system level (multiple stacks + possibly storage), operators could significantly reduce unnecessary stress on components while still meeting hydrogen production targets.

VI. Economic and Lifecycle Analysis: Finally, undertake comprehensive life-cycle cost analysis that accounts for degradation. Traditional LCOH calculations often assume fixed lifetimes or stack replacements after arbitrary periods; instead, coupling a degradation model with cost analysis will give more accurate predictions of hydrogen cost over a plant's life. Such analysis can reveal the most cost-sensitive factors and thereby guide both operational decisions and research priorities.

Through this critical evaluation of current literature, it becomes evident that while PEM electrolyser technology holds great promise for enabling offshore renewable hydrogen production, significant work remains to ensure its viability under real-world, dynamic conditions. The new insights and gaps identified here provide a direct justification for the research done in this thesis. By focusing on the interplay between intermittent operation, electrolyser degradation, and economic outcomes, this thesis will address a currently unresolved aspect of the field. The expected outcome is not only an optimized operational strategy, but also an insight into degradation mechanisms and data.

# 3 PEM Electrolyser Simulink Model

**Relevance**
The Simulink model captures the characteristics of a PEM electrolyser under varying power inputs, which is essential for the development of the operational strategy model presented later in this thesis. By providing insight into the relationships between power input, hydrogen production, efficiency and the polarization curve, the model forms a foundational element for optimizing system operation over time.

**Conclusion**
The Simulink model reliably captures the dynamic behaviour of a PEM electrolyser under variable power inputs. Its outputs, validated against theoretical and experimental data, demonstrate internal consistency and credible system-level trends. Despite simplifying assumptions, the model offers a robust basis for evaluating operational strategies and power-input scenarios in subsequent analysis.

This section presents the development of a Simulink model to simulate the behaviour of a PEM electrolyser stack. The model builds upon an existing framework (MATLAB, 2018) and was selected for its suitability and the time constraints associated with developing a model from first principles. The objective of this section is to describe the model's structure, including its key parameters, governing equations, and operational boundaries. This section also presents the output results, including verification and validation. It concludes with a critical discussion of the model's underlying assumptions and limitations.

## 3.1 Model Characteristics

A zero-dimensional Simulink model is introduced that serves as a "digital twin" of a PEM electrolyser stack. By neglecting spatial gradients, the model captures system-level behaviour while significantly reducing computational demand. This simplification is appropriate given the thesis's focus on system operational optimization rather than component-scale design.

The model is non-isothermal, enabling the simulation of temperature-dependent effects such as membrane hydration, ionic conductivity, and heat generation from electrochemical and resistive losses. The thermal management of the system is modelled by a standardized Simulink heat exchanger.

A multiphase formulation is included to simulate liquid water supply, gas evolution, and vapor transport across the membrane. This allows the model to capture key processes such as diffusion, electro-osmotic drag, and condensation, all of which impact performance. It supports the development of control strategies to prevent membrane drying and flooding.

The model runs as a transient simulation, tracking the time-dependent evolution of current, voltage, pressure, and temperature. It requires initial conditions at $t$=0 and enables the analysis of dynamic system behaviour under variable input conditions.

The chosen model's architecture is well suited for the aim of this thesis. It provides the necessary resolution to evaluate operational trade-offs and system constraints, while maintaining the computational speed required to characterize the stack under various power inputs.

**In short:** A zero-dimensional, non-isothermal Simulink model is used. It captures system-level behaviour, including thermal and multiphase effects, while enabling transient simulations. The model suits the thesis' focus on operational system optimization under variable input conditions.

## 3.2 Model Boundaries

Figure 3-1 shows the full PEM system model, which includes components such as power converters, gas compressors, and thermal management systems. This thesis focuses on the Membrane Electrode Assembly (MEA), narrowing the model boundaries to the core processes relevant to hydrogen production and the polarization curve. BoP elements, such as piping, water supply, recirculation, heat exchanger, dehumidifier, and fluid channels, are not explicitly modelled. Their behaviour is represented using standard Simulink blocks with predefined equations.

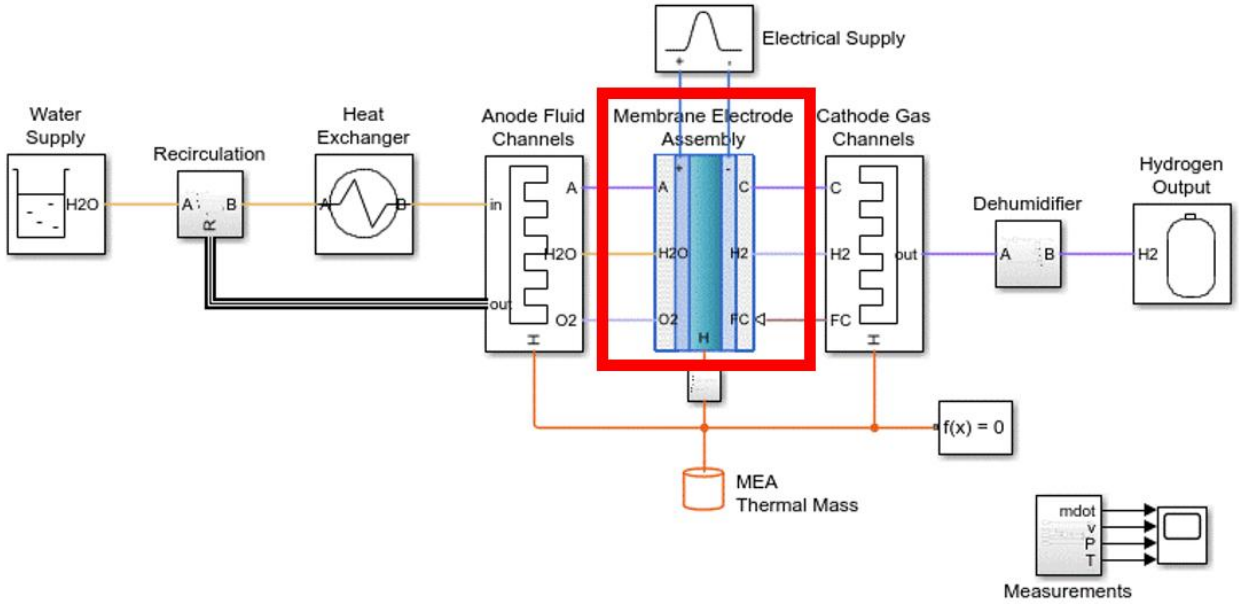


*Figure 3-1: PEM electrolyser Simulink Model (MATLAB, 2018)*

## 3.3 Governing Equations

The following sections present the governing equations used in the PEM electrolyser simulation model, organized by key physical domains: power input, voltage, mass flow, pressure and temperature, and efficiency. The complete model and its equations are provided in Appendix G.

### 3.3.1 Power input

The electrical power input of the model is defined by equation (3.1), where *P* is the power input (kW), *U* is the voltage (V) and *I* is the current (A).

$$P = U * I \tag{3.1}$$

The electrolyser operates in current mode, where input current is controlled to regulate hydrogen production. This mode is commonly used, as hydrogen output is directly proportional to the current (Abdin et al., 2015). The current is divided by the cell area and defined as the current density (A/cm$^2$) according to equation (3.2).

$$i_{cell} = \frac{I}{A_{cell}} \tag{3.2}$$

Cells within a stack are connected in series meaning that the current is equal in each cell according to equation (3.3) and the total stack voltage can be calculated according to equation (3.4). Stacks are usually connected in parallel so that the voltage of each stack equals that of the system.

$$i_{stack} = i_{cell,1} = i_{cell,2} = i_{cell,3} \dots = i_{cell,n} \tag{3.3}$$

$$V_{stack} = N_{cells} * V_{cell} \tag{3.4}$$

### 3.3.2 Voltage

When a specific current is applied to a cell, it results in a corresponding voltage across the cell, governed by the electrochemical behaviour of the cell as defined by its polarization curve. The electrolyser voltage consists of the open circuit cell potential ($V_{nernst}$) and three overpotentials: activation ($V_{act}$), ohmic ($V_{ohm}$) and concentration ($V_{con}$). The total cell voltage is defined by equation (3.5). The concentration overpotential is negligible compared to the other voltage contributions and is therefore excluded to simplify the model (Abdin et al., 2015). The potentials are covered below.

$$V_{cell} = V_{nernst} + V_{act} + V_{ohm} \tag{3.5}$$

<u>$V_{nernst}$</u>

The open circuit potential, also known as the Nernst potential, is the difference in voltage between the Anode and the Cathode when no current is flowing. It represents the minimum potential needed for water electrolysis as covered in Section 2.1.2. The Nernst potential can be determined with the Nernst equation (3.6) where $E^0$ is the standard potential as defined by equation (2.11) and $a_{H2}$, $a_{O2}$ and $a_{H2O}$ are the species activities.

$$V_{nernst} = E^0 - \frac{RT_{stack}}{n_e \cdot F} \ln\left(\frac{a_{H2O}}{a_{H2} * \sqrt{a_{O2}}}\right) \tag{3.6}$$

The theoretical equation (2.11) for $E^0$ does not account for the influence of temperature, therefore in this model the semi-empirical relation as defined by equation (3.7) is used to determine $E^0$ , where $T_{stack}$ is the stacks temperature in Kelvin (Abdin et al., 2015).

$$E^0 = 1.299 - 0.9 * 10^{-3} (T_{stack} - 298) \tag{3.7}$$

<u>$V_{act}$</u>

The activation overpotential represents the additional voltage required beyond the open-circuit potential to drive the electrochemical reactions at the Anode and Cathode. The total activation

overpotential is the sum of the voltages of both electrodes and is calculated using the Butler–Volmer equation, as in equation (3.8). The fitting parameters ($\alpha_{Anode}$, $\alpha_{Cathode}$, $i_{0,Anode}$ and $i_{0,Cathode}$) are determined according to experiments by (Liso et al., 2018) and can be found in Table 3-1.

$$V_{act} = \frac{RT_{stack}}{\alpha_{anode}F}\operatorname{arcsinh}\left(\frac{i_{cell}}{2 * i_{o_{anode}}}\right) + \frac{RT_{stack}}{\alpha_{cathode}F}\operatorname{arcsinh}\left(\frac{i_{cell}}{2 * i_{o_{cathode}}}\right) \tag{3.8}$$

$V_{ohm}$

The ohmic overpotential arises from the total internal resistance ($R_{ohm}$) which is primarily due to ionic resistance in the membrane. Other resistive contributions, such as those from electrodes and bipolar plates, are minor and therefore omitted in this model (Liso et al., 2018)(Abdin et al., 2015).

The ohmic voltage depends on two key membrane properties: its thickness ($t_{membrane}$) and ionic conductivity ($\sigma_{mem}$). Membrane conductivity is modelled as a function of the water content ($\lambda$), which is defined as the number of water molecules per sulfonic acid group ($SO_3^-$) in the Nafion® membrane (Liso et al., 2018) (Abdin et al., 2015) (Lu et al., 2023). The ohmic voltage can be calculated using equation (3.9), where $R_{ohm}$ is the membrane resistance. The membrane resistance can be calculated using equation (3.10) (Lu et al., 2023).

$$V_{ohm} = R_{ohm} * i_{cell} \tag{3.9}$$

$$R_{ohm} = \frac{t_{membrane}}{\sigma_{mem}} = \frac{t_{membrane}}{(0{,}005139\lambda - 0{,}00326)e^{(1268(\frac{1}{303} - \frac{1}{T_{stack}}))}} \tag{3.10}$$

The power input, together with the overpotentials determine the polarization curve, which is a crucial characteristic of a PEM electrolyser.

### 3.3.3 Mass Flows

As mentioned in Section 2.1.1, Faraday's law of electrolysis relates the electric charge to the amount of substance that reacts. Faraday's law can be used to calculate the mass flows of $H_2O$, $O_2$ and $H_2$ according to equation (3.11), (3.12), and (3.13), respectively. Here $M$ is the molar mass (kg/mol). Since Faraday's law assumes all charge goes into the reaction, the hydrogen mass flow is corrected with the Faraday's efficiency ($\eta_{faraday}$) that accounts for side reactions and cross-over.

$$H_2O\ \left[\frac{kg}{s}\right] = N_{cells} * M_{H2O} * A_{cell} * (\frac{i_{cell}}{2F}) \tag{3.11}$$

$$O_2\ \left[\frac{kg}{s}\right] = N_{cells} * M_{O2} * A_{cell} * (\frac{i_{cell}}{4F}) \tag{3.12}$$

$$H_2\ \left[\frac{kg}{s}\right] = N_{cells} * M_{H2} * A_{cell} * \left(\frac{i_{cell}}{2F}\right) * \eta_{faraday} \tag{3.13}$$

### 3.3.4 Pressure and Temperature

Temperature has a major influence on the PEM electrolyser operation not only within the governing equations but also on the degradation as discussed earlier. The cell temperature results from heat generated during operation. This heat ($Q$) is defined as the power dissipated, which is the difference

between the electric power and the net power used for the electrochemical reaction, as shown in equation (3.14).

$$-Q = P_{dissipated} = P_{elec} - P_{net} \tag{3.14}$$

The electric power has already been defined in equation (3.1). The net power consists of the energy consumed by the hydrogen-producing reaction ($R_{rxn}$), as well as corrections for bringing reactants and products to standard conditions ($R_{std}$) and water transport effects ($R_{trans}$), as given in equation (3.15).

$$P_{net} = R_{rxn} - R_{std} - R_{trans} \tag{3.15}$$

$R_{rxn}$ is defined according to equation (3.16) and $R_{std}$ and $R_{trans}$ can be found in Appendix G.

$$R_{rxn} = -HHV_{H_2} * \frac{H_{2,produced}}{M_{H2}} \tag{3.16}$$

The cell temperature is treated as an input to the computation in the membrane electrode assembly. It increases due to the generated heat (-Q) and is modelled using a thermal mass block, shown in Figure 3-1, which simulates internal energy storage. The rate of temperature change is simulated by equation (3.17), where $\rho$ is the density of the liquid (kg/m$^3$), $c_p$ is the specific heat capacity (J/(kg·K) and $V$ is the volume (m$^3$). The model's heat exchanger allows for a maximum temperature of 80 °C.

$$\frac{dT}{dt} = \frac{Q}{\rho * c_p * V} \tag{3.17}$$

The Anode and Cathode fluid channels, as also seen in Figure 3-1, simulate pipe flow dynamics including viscous losses and convective heat exchange to the pipe wall. These dynamics lie outside the model boundaries defined in Section 3.2, and their governing equations are covered in Appendix G. The increase in pressure is caused by a restricted outflow at the Cathode. The increase in pressure is simulated by applying compressible mass conservation to the gas volume. The resulting rate of pressure change is simulated by equation (3.18), where $p$ is the internal pressure, $T$ is the gas temperature, and $V$ is the volume of the control region. The terms $R_a$, $R_w$, and $R_g$ represent the specific gas constants of dry air, water vapor, and trace gas, respectively. The variables $\dot{m}_{total}$, $\dot{m}_w$ and $\dot{m}_g$ represent the total-, water vapor-, and trace gas mass inflow rates. The first term on the right-hand side captures the effect of temperature rise on pressure, while the second term accounts for pressure changes due to mass accumulation, corrected for differences in gas properties. The total pressure at the Cathode is restricted at 3MPa.

$$\frac{dp}{dt} = \frac{p}{T} * \frac{dT}{dt} + \frac{T}{V}(R_a * \dot{m}_{total} - (R_a - R_w) * \dot{m}_w - (R_a - R_g) * \dot{m}_g \tag{3.18}$$

### 3.3.5 Efficiency

The total efficiency of a PEM electrolyser is a combination of the voltage efficiency ($\eta_{voltage}$), faraday efficiency ($f_{faraday}$) and the efficiency of the BoP ($\eta_{BoP}$) according to equation (3.19). The average efficiency of the BoP is about 80-90% (Electric Hydrogen, 2024). In this model, $\eta_{BoP}$ is assumed to be 85%.

$$\eta_{PEM} = \eta_{voltage} * \eta_{faraday} * \eta_{BoP} \quad (3.19)$$

The voltage efficiency is based on the HHV and can be calculated using equation (3.20) (Lu et al., 2023).

$$\eta_{voltage} = \frac{V_{nernst}}{V_{cell}} \quad (3.20)$$

The Faraday efficiency reflects the losses caused by gas crossover. It depends on the operating pressure ($p_{cell}$) and is defined by equation (3.21) (Lu et al., 2023).

$$\eta_{faraday} = \frac{-0{,}0034 * p_{cell} - 0{,}001711}{i_{cell}} + 1 \quad (3.21)$$

**In short:** This section presents the governing equations used in the Simulink model to describe key processes within the MEA. The model operates in current mode, neglects concentration overpotential, and accounts for temperature- and pressure-dependent effects such as ionic conductivity and Faraday efficiency.

## 3.4 Model Parameters

Table 3-1 lists the parameters used in the Simulink model, categorized into fixed and fitted values. The fixed parameters are adopted from the PEM cell configuration presented by Liso et al. (2018), who provided a characterisation of a 1 kW commercial PEM electrolyser. These values include intrinsic design features such as active cell area and catalyst loadings, which are treated as constants in the simulation. The exchange current density and charge transfer coefficient are fitted parameters and they are calibrated by experiments done by Liso et al. (2018). Their validity is supported by consistency with values reported by Espinoza et al. (2018), Biaku et al. (2008), and Choi et al. (2004).

*Table 3-1: Fixed and fitted model parameters*

| Parameter | Value |
|---|---|
| Rated power | 100 kW |
| Number of cells | 50 |
| Cell area | 280 $cm^2$ |
| Cathode catalyst loading | 0.5 $mg/cm^2$ (Pt/C) |
| Anode catalyst loading | 0.3 $mg/cm^2$ $IrO_2$ and 2.7 $mg/cm^2$ Ir, with porous Ti. |
| Membrane thickness | 125 µm |
| Anode diffusion layer thickness | 25 µm |
| Cathode diffusion layer thickness | 250 µm |
| Density of dry membrane | 2000 $kg/m^3$ |
| Overall density of MEA | 1800 $kg/m^3$ |
| Overall specific heat of MEA | 870 J/(kg K) |
| | |
| Universal gas constant | 8.31446 J/K/mol |
| Faraday constant | 96485.332 C/mol |
| Gibbs free energy of water | -237.14 kJ/mol |
| Higher heating value of water | 285.8 kJ/mol |
| | |
| Standard temperature | 20 °C |
| Standard pressure | 1 atm |
| | |
| *Fitting parameters according to Liso et al., (2018)* | |
| Exchange current density Anode ($I_{0,an}$) | $5*10^{-12}$ $A/cm^2$ |
| Exchange current density Cathode ($I_{0,cat}$) | $1*10^{-3}$ $A/cm^2$ |
| Charge transfer coefficient Anode ($\alpha_{an}$) | 1.2 |
| Charge transfer coefficient Cathode ( $\alpha_{cat}$) | 0.5 |

## 3.5 Model Output, Verification and Validation

The output of the model gives the characteristics of the PEM electrolyser under various power inputs and serves as an input for the operational strategy model. This section presents the model output, as well as its verification and validation. Verification confirms that the model has been implemented correctly according to its theoretical specifications, ensuring that the underlying equations and logic behave as intended. Validation assesses how well the model reflects real-world system behaviour by comparing its output against independent experimental data under similar operating conditions.

The section presents the Simulink outputs that are crucial for the operational strategy model. Other outputs such as $H_2O$ and $O_2$ mass flows, temperature and pressure curves and individual overpotentials can be found in Appendix H.

### 3.5.1 Simulated Polarization Curve

The simulated polarization curve can be seen in Figure 3-2. As known from equation (3.5), the polarization curve is the sum of $V_{nernst}$, $V_{act}$, and $V_{ohm}$. The individual curves of each of these potentials can be found in Appendix H.

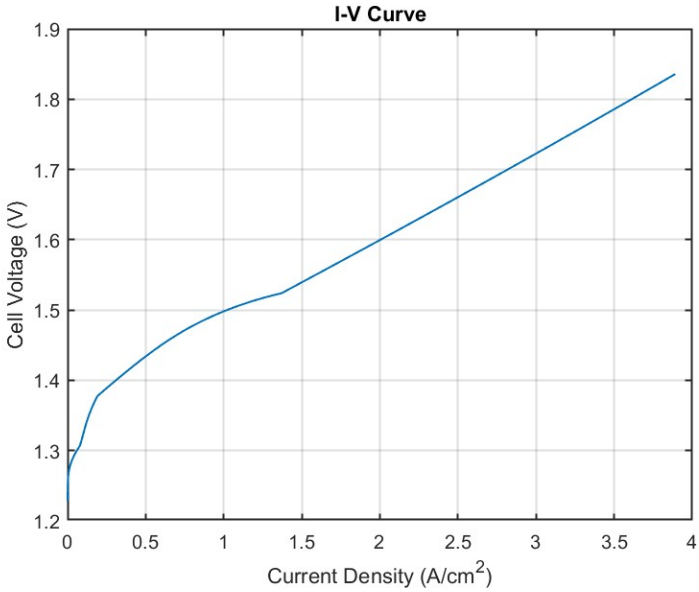


*Figure 3-2: Simulated polarization curve*

**Verification**

The polarization curve of the PEM electrolyser can be verified by confirming the simulated results with established theoretical behaviour as defined in Section 3.3.2. As the current density increases, the cell voltage rises due to increasing activation and ohmic losses, which is consistent with the Butler–Volmer formulation and Ohm's law for ionic conduction.

It can also be verified that the model accurately captures the effect of operating temperature: as temperature increases with the current density, the gradient of the activation overpotential decreases. The simulated temperature curve can be found in Appendix H. At a current density of around 1.4 ($A/cm^2$) the model reaches a constant temperature, in Figure 3-2 one can see that the polarization curve reaches a constant gradient when the cell reaches a constant temperature.

Furthermore, the power input as defined by equation (3.1), should match the stacks total potential (V) and current (I). At its highest point the polarization curve shows a current density of 3.89 ($A/cm^2$) and a potential of 1.84 (V). In a 50-cell stack with a cell area of 280 $cm^2$ according to Table 3-1, this results in a power of P = 1.83 (V) * 50 * 3.89 ($A/cm^2$) * 280 ($cm^2$) ≈ 100kW. Which makes sense as this is the rated power of the stack.

The consistency between the simulated curve and electrochemical theory confirms that the model provides a physically meaningful and realistic representation.

**Validation**

To validate the model, its simulated polarization curve is compared against simulation results from literature. Figure 3-3 shows the polarization curve as found by (Liso et al., 2018). This curve follows

the same trend. However, it shows a slight difference at the first part of the curve. The main reason for this is that (Liso et al., 2018) assumes a constant temperature of 80 °C whereas the Simulink model starts at ambient temperature (20 °C) and allows for a temperature increase up to 80 °C.

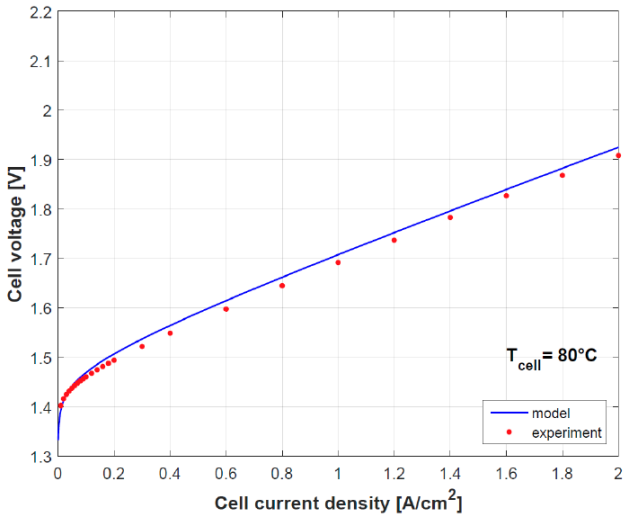


*Figure 3-3: Polarization curve as found by (Liso et al., 2018)*

Figure 3-4 shows another research which found polarization curves for different catalyst compositions. The trend of these curves is similar to that of the polarization curve found by the simulation. However, it also indicates that polarization curves are difficult to compare as they are highly dependent on the materials and operating conditions. Figure 3-4 underscores this by showing the influence of catalyst composition on the polarization curve.

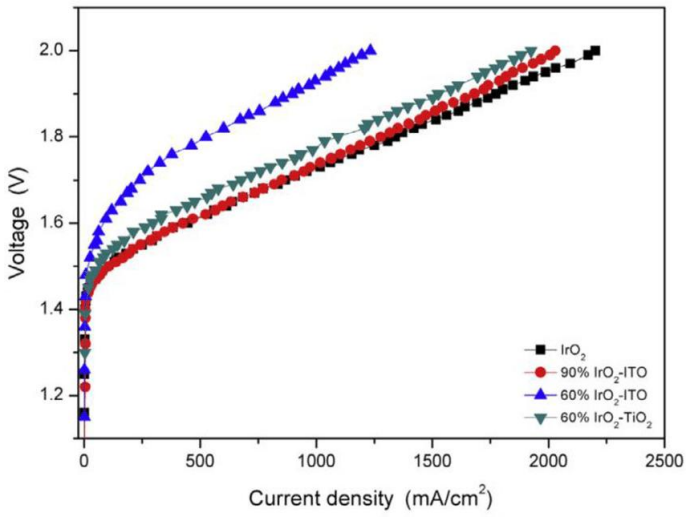


*Figure 3-4: Polarization curve as found by (Sapountzi et al., 2017)*

The comparison of the simulated polarization curve with literature relations confirms that the model captures the correct overall trend. Deviations are explained by differences in operating conditions, such as temperature and PEM cell compositions such as that of the catalyst materials.

### 3.5.2 Simulated Hydrogen Production

Figure 3-5 shows the simulated hydrogen production rate (g/s) as a function of current density (A/cm²). The mass flow rates of $H_2O$ and $O_2$ can be found in Appendix H.

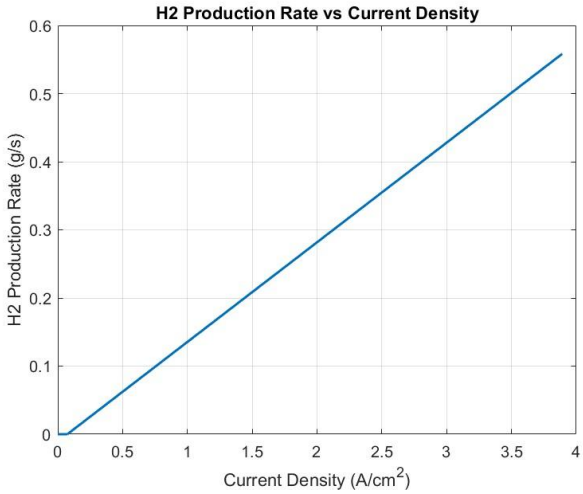


*Figure 3-5: Simulated $H_2$ production rate vs. current density*

**Verification**

The hydrogen production curve of the PEM electrolyser can be verified by comparing the simulated results with expected production behaviour. The rate of hydrogen production seems to increase linear with the current density. This is logical when considering the hydrogen production relation as defined by equation (3.13), which states that $H_2$ production is linearly related to the current density. However, for hydrogen production one does have to consider that an increase in power doesn't necessary lead to an equal increase in current as can be seen from the polarization curve. Also, one must consider the Faradaic efficiency. The curve for hydrogen production vs. power can be seen in Figure 3-6. It shows that the $H_2$ production rate has a slight decrease in the gradient as the power input increases. This is in line with the decrease in the current density gradient as the power input increases as dictated by the polarization curve.

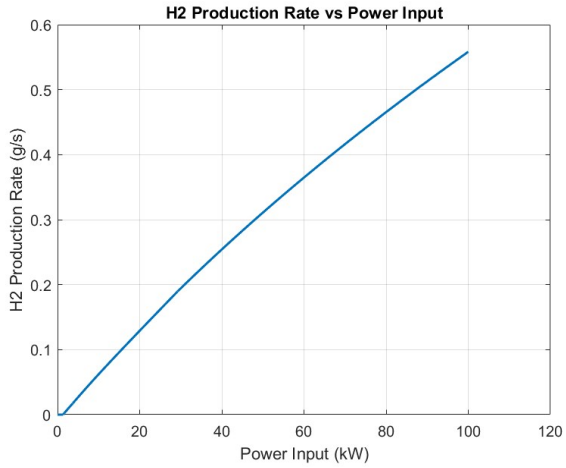


*Figure 3-6: Simulated $H_2$ production rate vs. power input*

This verification confirms that hydrogen production generally increases linearly with current density, as expected, but also highlights that the relationship between power input and hydrogen output is influenced by nonlinearities in the polarization curve and Faradaic efficiency.

**Validation**

The simulated production rate can be validated by comparison to stacks of a similar size. A 100kW stack as listed by (PEM Water Electrolysis System, 2024) reports a maximum hydrogen production rate of 20.000 L/h which translates to 1.79 kg/h at a hydrogen gas density of 0.08988 g/L (Yang et al., 2024). At peak power (100kW) the simulation shows a production rate of 0.558 g/s which equals to around 2kg/h. This production rate is in the same range as the production rate listed by the supplier; this validates the simulation.

### 3.5.3 Simulated Efficiency

Figure 3-7 shows the total efficiency of the stack vs. the current density. The efficiency steeply increases up to about 0.5 A/cm$^2$. It remains almost constant until about 1.5 A/cm$^2$ after which it declines.

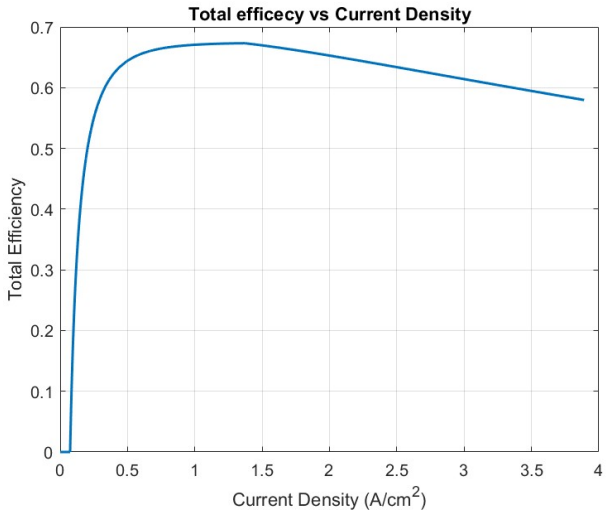


*Figure 3-7: Simulated efficiency vs. current density*

**Verification**

The efficiency curve of the PEM electrolyser can be verified by confirming the simulated results with expected efficiency behaviour. The efficiency as defined by equation (3.19) is the product of the voltage, Faradaic and BoP efficiency. The BoP efficiency is assumed as a constant. The Faradaic- and voltage efficiency can be seen in Figure 3-8 and Figure 3-9 respectively.

The steep incline at the beginning of the total efficiency curve is mainly caused by the steep incline in Faradaic efficiency. In line with equation (3.21), the Faradaic efficiency is influenced by both the operating pressure and the current density. The pressure curve in Appendix H shows that the system reaches a steady pressure of 30 bar at a relatively low current density of approximately 0.2 A/cm². While elevated pressure tends to reduce Faradaic efficiency, primarily due to increased crossover, the continued increase in current density has a counteracting effect. This makes sense, as with the increase in current density the temperature increases which in turn enhances reaction kinetics and mass transport and thus the Faradaic efficiency.

The voltage efficiency, as defined by equation (3.20), is the ratio of the Nernst voltage to the actual cell voltage. It can be derived directly from the polarization curve in Figure 3-2 and the Nernst voltage plot in Appendix H. As current density increases, the cell voltage rises due to growing overpotentials, initially dominated by activation losses, followed by a linear contribution from ohmic resistance.

Simultaneously, the stack temperature increases with current density due to internal heat generation, eventually stabilizing. Beyond this point, the rate of voltage increase flattens, and the polarization curve transitions to a steady gradient. The voltage efficiency declines accordingly but follows a predictable path consistent with theory. This close match between simulated voltage behaviour confirms the correct implementation of the electrochemical model and verifies the internal consistency of the voltage efficiency calculation.

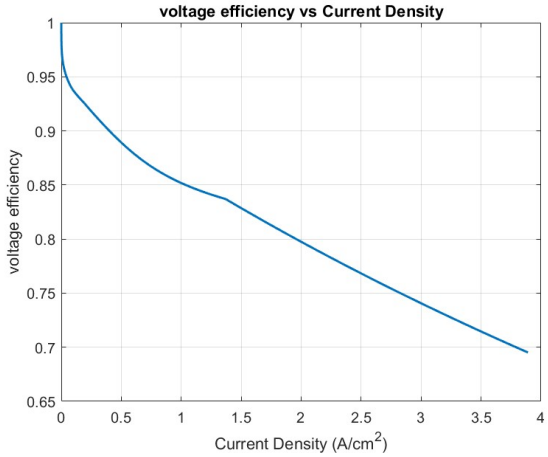


*Figure 3-8: Simulated voltage efficiency vs. current density*

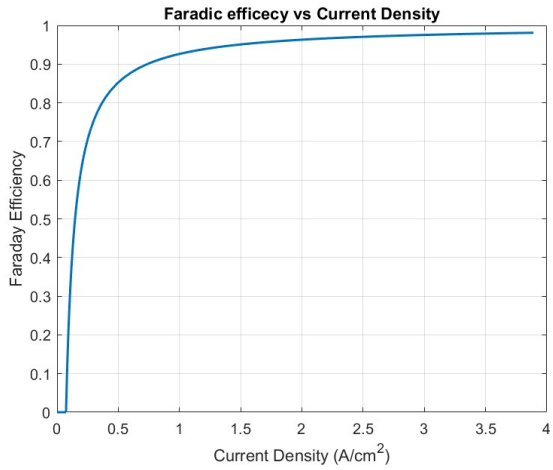


*Figure 3-9: Simulated Faradaic efficiency vs. current density*

Figure 3-10 shows the current total efficiency at a given power input. It can be seen that optimal efficiency is at a power input of approximately 30kW at 67%. At 30kW Figure 3-6 shows a hydrogen production rate of around 0.2g/s which equals about 0,72kg/h. A simple calculation with a specific energy of 33kWh/kg$_{H2}$ (Idealhy, n.d.) and a fixed BoP efficiency of 85% can verify this efficiency as in equation (3.22). This verification confirms that the simulated efficiency aligns with theoretical expectations.

$$efficiency = \frac{0.72\ \left(\frac{kg}{h}\right) * 33(\frac{kWh}{kg})}{30\ (kW) * 1\ (h)} * 0.85 * 100 \approx 67\% \tag{3.22}$$

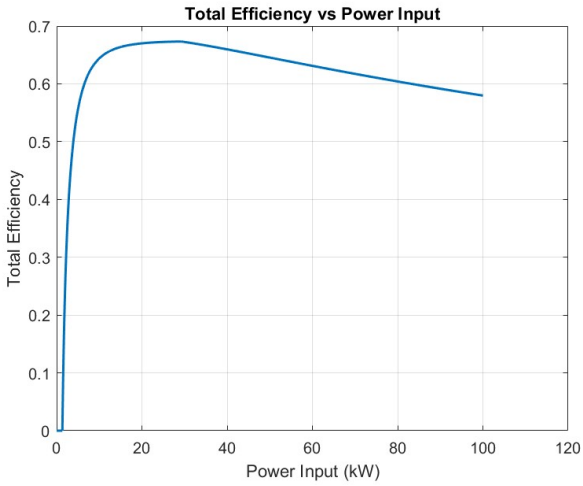


*Figure 3-10: Simulated total efficiency vs. power input*

**Validation**

To validate the simulation results, the model's predicted efficiency curve is compared against real-world experimental data from the PosHydon project and independent simulation results from the literature. The experimental data from the PosHydon project (Poshydon, 2024), as seen in Figure 3-11, show a similar trend as the simulated efficiency curve in Figure 3-10. Both show an optimal efficiency at 30% of the rated power. The PosHydon curve does start at a higher efficiency, presumably because it operates at a constant temperature whereas the simulation starts at ambient temperature. The efficiency curve in Figure 3-11 is given in kWh/kg $H_2$, which at a specific energy of 33kWh/kg translates to an optimal efficiency of (33/46,2)*100 = 71%. This is comparable to 67% optimal efficiency in the simulation.

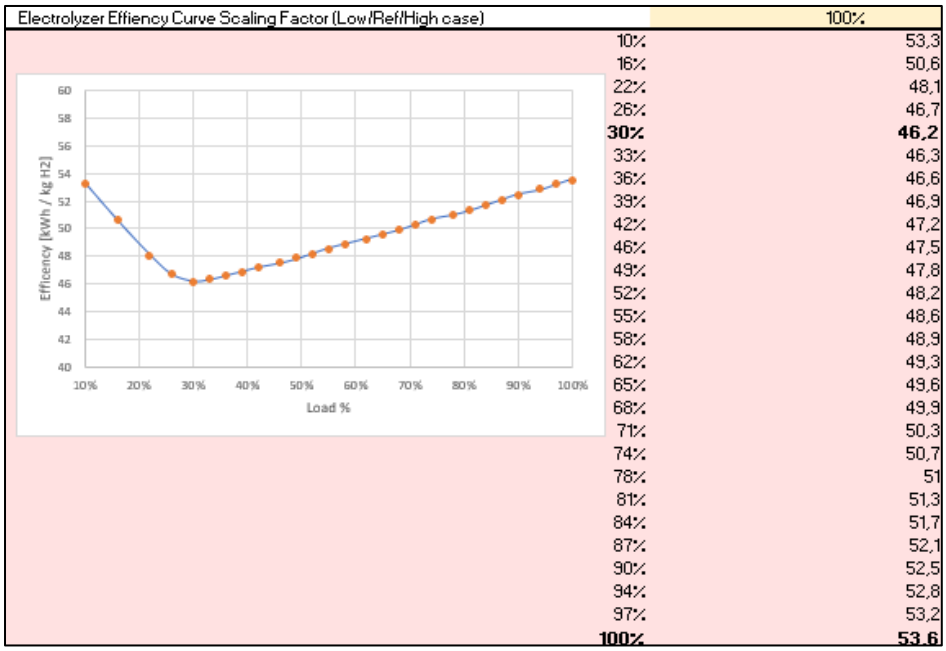


*Figure 3-11: Experimental efficiency curve of PosHydon project (Poshydon, 2024)*

A simulation model by Lu et al., (2023) assumes ambient temperature and allows for a temperature increase up to 80 ºC, like the Simulink simulation. The results in Figure 3-12 show a similar trend and a peak efficiency around 15/60 = 25% of the rated power. Moreover, Figure 3-12 also shows the influence of degradation on the efficiency curve. This is important to notice and will be further discussed in Section 4 by introducing the performance factor. Finally, the US department of energy reported a PEM electrolyser efficiency of 65%, similar to the 67% efficiency as found by the simulation (U.S. Department of Energy, n.d.).

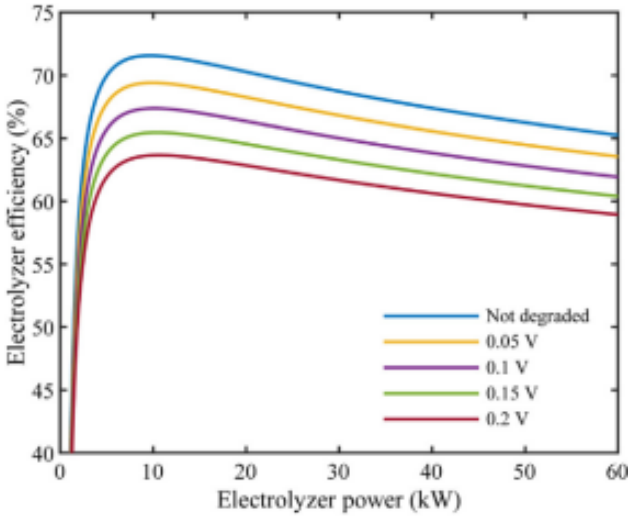


*Figure 3-12: Not degraded and degraded simulated efficiency curves as found by Lu et al., (2023)*

The validation shows that the simulated efficiency curve closely matches real world experimental data as that from the PosHydon project. Furthermore, the simulation matches with a similar model (Lu et al., 2023), both showing peak efficiency at around 25-30% of the rated power. Minor differences, such as a higher starting efficiency in the PosHydon data, are consistent with initial temperature conditions.

**In short:** This section confirms that the model accurately captures the expected behaviour of a PEM electrolyser under varying power inputs. The verification shows that the model behaves in line with theoretical relations, while the validation confirms agreement with literature and experimental data.

## 3.6 Model Assumptions and Limitations

This section presents a critical reflection on the assumptions and limitations of the Simulink PEM electrolyser model. Understanding these constraints is essential to properly interpret the simulation results, benchmarking the model's accuracy, and identifying directions for future research and development.

### 3.6.1 Electrochemical Dynamics

The model assumes a quasi-steady-state electrochemical response. Cell voltage is calculated instantaneously at each time step using algebraic expressions for the Nernst potential, activation overpotentials, and ohmic losses. It does not account for short-timescale dynamics such as interfacial charge accumulation or kinetic delays. This simplification is common in PEM electrolyser modelling due to the fast intrinsic kinetics of PEM cells. According to Liso et al. (2018), these transients occur

much faster than the load changes typical in renewable energy systems. As a result, the assumption is valid for simulations with varying inputs like solar or wind. While cell-level dynamics are simplified, the model still captures system-level transients such as temperature, mass flow, water transport, and gas production through time-dependent differential equations.

This assumption enables fast and stable simulations for renewable energy scenarios. However, it limits the model's ability to study fast electrochemical transients or sub-second control dynamics.

### 3.6.2 Dimensionality and Spatial Resolution

The model is built as a zero-dimensional representation, meaning it assumes spatial uniformity within and across all cells in the electrolyser stack. Current density, temperature, and species concentrations are treated as homogeneous within each cell and identical across the full stack. This simplifies the governing equations and reduces computational cost, but inherently neglects intra-cell and inter-cell heterogeneities. Effects such as membrane dehydration, thermal gradients, and non-uniform flow distribution along channels or between cells are not accurately captured. As a result, localized issues like dry-out, hot spots, or edge effects are beyond the model's scope.

This assumption is appropriate for system-level performance estimation but limits the model's applicability for investigating localized degradation, failure modes, or advanced cell design optimizations.

### 3.6.3 Parameter Scaling

The model uses a combination of fixed physical parameters (e.g., membrane thickness, catalyst loading) and fitted electrochemical parameters (e.g., exchange current density, charge transfer coefficients), primarily sourced from Liso et al. (2018). These are based on laboratory-scale experiments. The parameters were validated for a single cell with a relatively small active area.

In the simulation, these values are applied directly to simulate a 100 kW industrial-scale stack. This assumes geometric and operational similarity across scales, and that performance scales linearly with active area and cell count. However, large stacks can exhibit scale-dependent effects such as voltage drops, uneven water distribution, or inter-cell performance. Without recalibration using experimental data from a comparable full-scale system, the extrapolation introduces uncertainty into the model's accuracy. This limits the model's predictive accuracy for performance at full scale.

### 3.6.4 Governing Equations Simplifications

The governing equations for cell voltage include contributions from the Nernst potential, activation overpotential, and ohmic resistance, but explicitly neglect concentration overpotential. This simplification is valid under well-hydrated and moderate current density conditions, where gas transport limitations are relatively minor (Abdin et al., 2015). However, in high-performance or high-pressure designs, neglecting mass transport losses could underestimate overpotentials.

Additionally, the model assumes ideal thermodynamic behaviour for reactants and products, and that hydrogen and oxygen production follow Faraday's law exactly. These assumptions are reasonable for system-level modelling; however, they overlook second-order effects that may become relevant in detailed cell optimization studies.

These simplifications enable efficient simulation and are suitable for comparative and trend analyses, but they might limit the model's ability to predict performance losses in extreme operating conditions or to research component-level design improvements.

### 3.6.5 Species and Phase Behaviour

The model simplifies species transport by considering only the primary components ($H_2$, $O_2$, and $H_2O$). It assumes that gas-phase water vapor is always in equilibrium with liquid water at the local temperature. For example, the oxygen stream at the Anode is assumed to be saturated with water vapor. The entire system is also assumed to operate at a uniform temperature and limited at 80 °C. These assumptions eliminate the need to model two-phase flow explicitly and are common in first-order system models. However, this simplification neglects possible vapor-liquid phase transitions, condensation dynamics, and local humidity gradients. Under transient or high-load conditions, such assumptions may overlook effects such as flooding, membrane drying, or gas supersaturation, which could impact both efficiency and durability. While appropriate for average-condition modelling, this limits the model's ability to assess critical operational risks such as membrane dry-out.

### 3.6.6 Balance of Plant Efficiency

The model assumes a constant BoP efficiency of 85%, representing auxiliary components such as pumps, cooling systems, compressors, and control electronics. However, in practice, BoP loads fluctuate depending on operating conditions, system design, and control strategy. Ignoring these dynamics may lead to inaccurate system-wide efficiency estimates, particularly under variable operating profiles.

This assumption allows for simplified system efficiency estimation but may underestimate energy consumption variability, leading to too optimistic LCOH or efficiency projections in operational scenarios.

### 3.6.7 Simulink Component Constraints

The model uses standardized Simulink component blocks for flow channels, thermal resistances, and heat exchangers. While these accelerate development and improve modularity, they limit the flexibility to explore non-standard stack designs or customized components.

This makes the model well-suited for conceptual studies on system level, but less suitable for evaluating detailed design trade-offs or innovating on component-level architecture.

### 3.6.8 Degradation Modelling

The model represents a non-degraded, fresh stack, with no aging or performance degradation mechanisms included. Effects such as catalyst dissolution, membrane thinning, or increasing resistance over time are excluded. This limits the model's ability to predict long-term performance or stack replacement cycles. In this thesis, degradation was analysed by post-processing Simulink outputs in a Python model, due to the complexity of integration in the Simulink model. This approach decouples degradation from the system's transient response. Ideally, degradation mechanisms would be integrated directly into the Simulink framework to allow dynamic degradation analysis under varying load profiles. Furthermore, BoP degradation is not considered, even though Bop components do degrade.

The Simulink model cannot capture performance degradation over time, limiting its usefulness for lifetime analysis, maintenance scheduling, or reliability forecasting without external degradation modelling.

**In short:** The Simulink PEM electrolyser model relies on several simplifying assumptions, including quasi-steady-state electrochemical behaviour, spatial uniformity across and within cells, ideal gas-phase reactions, and fixed BoP efficiency. These assumptions support system-level modelling but inherently introduce limitations. Parameters are sourced from lab-scale experiments and applied to a 100 kW stack without recalibration, introducing uncertainty in full-scale predictions. Additionally, the model does not account for degradation over time, which means aging effects and long-term performance decline are not represented in the Simulink simulation.

# 4 PEM Electrolyser Degradation Data Analysis

**Relevance**
Quantifying PEM electrolyser degradation under intermittent operation is essential for optimising the trade-off between hydrogen production and PEM electrolyser degradation. This section collects and analyses degradation data in order to establish a degradation relation as input for the operational strategy model.

**Conclusion**
The degradation relation by Schofield et al. (2024) was selected as it showed the strongest statistical relevance ($R^2 = 0.63$) and allows for comparison with similar research. All other analysed relations failed to demonstrate a statistically significant correlation. Additionally, no useful or quantifiable data was found on the specific impact of power cycles or start/stop cycles. One can conclude that there is a lack of reliable insights into PEM electrolyser degradation under intermittent operation, which exposes a critical knowledge gap. This absence of consistent data could pose a serious problem for the industry, as it limits the ability to develop accurate operational strategies and may lead to poorly informed decisions that risk early stack failure and increased project costs.

This section presents the collection and analysis of degradation data for PEM electrolysers, with a focus on intermittent operation. The aim is to establish a quantitative relation between degradation rate, current density, and intermittent power patterns. This relation, together with the output from the Simulink model, is used as input for the operational strategy model.

## 4.1 Introduction to PEM Electrolyser Degradation Data

PEM electrolyser degradation refers to the gradual increase in the stacks overpotential measured in (µV/h). As seen in equation (3.1), an increase in voltage ($U$) leads to a decrease in current ($I$) given a certain power input ($P$). Equation (3.13) shows that the current is directly related to the hydrogen production thus an increase in voltage, decreases the hydrogen production, and thus decreasing the electrolyser's performance. This is also visualized in Figure 3-12.

Section 2.3 highlighted the complexity of PEM electrolyser degradation, which depends strongly on stack composition and operating conditions. Manufacturers typically base lifetime projections on steady-power operation, but renewable intermittent power supply makes degradation behaviour less predictable.

Quantifying degradation in PEM electrolysers as a result of intermittent power remains challenging. While several studies by for example Rakousky et al. (2017), Sun et al. (2014), Wallnöfer-Ogris et al. (2024) and Shaun et al. (2019) have investigated this, most rely on lab-scale cells, short-term tests, and inconsistent protocols, making comparisons and interpretation difficult. Large-scale PEM electrolysers are still emerging, and long-term degradation data under intermittent operation is

scarce. Manufacturers rarely share such data, possibly due to confidentiality or lack of availability. Overall, degradation data is limited, fragmented, and difficult to scale from lab to industry. Reported results often vary widely and sometimes contradict each other. The goal of this section is to collect and analyse the available PEM degradation data under intermittent operation and try to identify a relation between operating conditions and degradation rates.

**In short:** Degradation in PEM electrolysers reduces performance over time, especially under intermittent power input. While several lab-scale studies have explored the impact of intermittent operation on degradation, the data remains fragmented, inconsistent, and difficult to scale.

## 4.2 Approach to PEM Electrolyser Degradation Data Collection and Analysis

This section highlights a structured approach for the degradation data collection and analysis.

**The Objective**
The degradation data collection and analysis have the following objectives:

I. Quantify a relation between the degradation rate (µV/h) and the current density (i)
II. Quantify the influence of power cycles[1] and on/off cycles on the degradation rate (µV/h).

The first objective allows to determine the degradation rate at any given operating point of the stack. The second objective allows to capture the intermittent behaviour. Together, they define the dynamic degradation behaviour of a PEM electrolyser.

**Data Collection Methods**
To collect the required degradation data, a range of methods will be used:

- A thorough review of scientific literature and technical publications.
- Interviews with industry experts and researchers working in the field. and
- An outreach through LinkedIn
- Contacting PEM electrolyser suppliers and manufacturers
- Collecting in-house data available at Guidehouse or affiliated institutions and (research) projects.

The collected data is gathered in an overview that can be found in Appendix I. Some highlights of the correspondence can be found in Appendix J.

**The Data Analysis**
The collected data will be subjected to both a qualitative review and a quantitative analysis. The qualitative review in this context refers to the selection of datapoints by certain criteria such as materials, operating conditions and power inputs. The goal of this so called ‘sampling’ process is to try to filter and compare representative data points. The quantitative analysis refers to the statistical evaluation of the degradation relations found.

[1]A power cycle is defined as a 50% variation in stack power between two simulated time steps.

## 4.3 Results of PEM Electrolyser Degradation Data Collection and Analysis

The results of the degradation data collection are presented below, including an evaluation of data quality and consistency. Additionally, the analysis explores whether a meaningful relationship exists between degradation rate, current density, and patterns of intermittent operation

### 4.3.1 Overview of PEM degradation Data Collection

**Results of Industry Feedback**

The outreach on LinkedIn and meetings with several industry experts and professors made clear that degradation data is highly confidential and some manufacturers don't even have clear insights in the degradation of their own equipment under intermittent operation. Dedicated websites even speak of a "global risk' as hydrogen electrolysers could degrade faster than stated by manufacturers (Collins, 2024).

Associate Professor David A. Vermaas (TU Delft) confirmed both the scarcity of data and industry concerns about intermittent operation. Professor Atsushi Urakawa from Japan's HyPRO project indicated that this is a key research focus for them (HyPRO, 2024). Menno Landsmeer from the PosHydon project emphasized that degradation is a central study objective of their 1 MW pilot. He also noted that their supplier, NEL, lacks clear data on degradation under intermittent use. Most manufacturers either did not respond or stressed the confidentiality of their data. At Guidehouse, a simple degradation factor is used in project assessments, which does not account for intermittent operation, stack composition, or electrolyser type.

These communications underscore the relevance of this topic and the current lack of reliable degradation data for intermittent PEM operation. Unfortunately, no concrete data was obtained.

**Results of Literature and Technical Publications**

Extensive desktop research covered over 30 sources that provide degradation data. Each dataset is characterized by its data type (experimental, target, or review), catalyst material and loading (mg/cm²), and key testing conditions such as current density, temperature, and pressure. The initial results are visualized in Figure 4-1, plotting degradation rate (µV/h) against current density (A/cm$^2$).

A second-order polynomial was fitted to the data. Among all tested models, including linear, exponential, and higher-order polynomials, it achieved the highest coefficient of determination ($R^2$). This makes it the most suitable choice for capturing the observed non-linear trend without overfitting.

If the coefficient of determination ($R^2$) equals 1, the trendline is a perfect fit with the data. If $R^2$ is lower than 0.5 the model has a weak fit and is unreliable. The second-order polynomial for the data as shown in Figure 4-1 has a value of $R^2 = 0.12$, which means the trendline cannot be relied on. The spread within the data could be explained by the fact that the data includes experiments, reviews and targets, different loading conditions, timeframes and catalyst loadings. Section 4.3.2 tries to eliminate these uncertainties by sampling the data based on these characteristics to try and find a better fit.

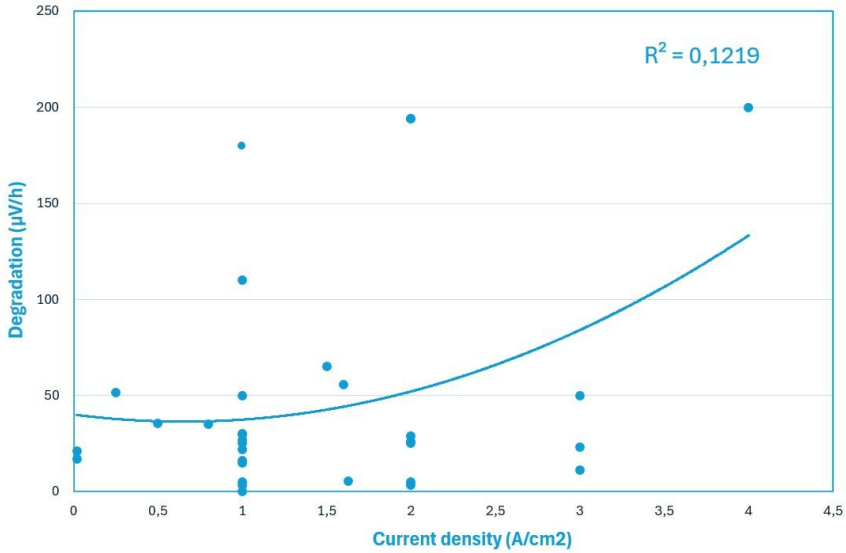


*Figure 4-1: Plot of initial collected degradation data*

In addition to the collected data, a separate relationship between current density and degradation was identified in the literature, as reported by Schofield et al. (2024). The relation, as seen in Figure 4-2, is based solely on square and hold wave power patterns, with degradation rates averaged over the lifetime of the cell. Negative degradation rates reported in some studies were excluded from this analysis. The trend shows that, for current densities greater than 1 A/cm², the degradation rate increases with the square of the current density as defined in equation (4.1). The combined parts of Schofield relation show a $R^2$ of 0.63 as seen in Appendix K.

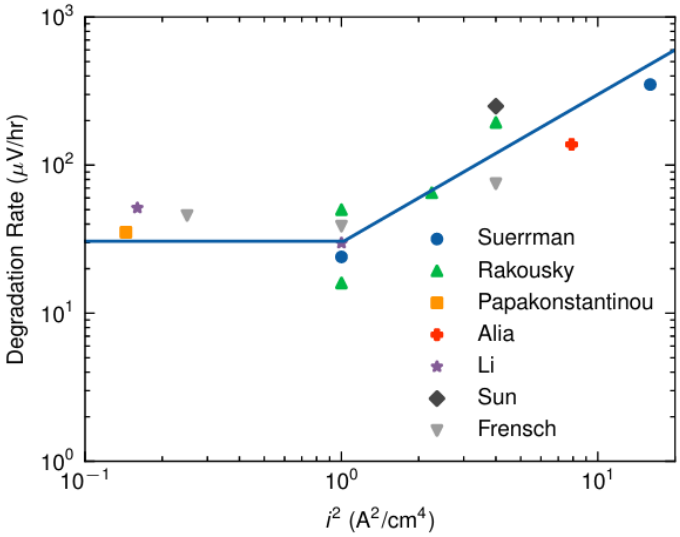


*Figure 4-2: Degradation relation according to (Schofield et al., 2024)*

$$degradation\ rate = \begin{matrix} 30 & i < 1 \\ 30 * i^2 & i > 1 \end{matrix} \quad (4.1)$$

Degradation due to power- or on/off cycles is hard to find in the literature. Some studies do include cyclic operation; however, they report degradation rates over the total observation period (Frensch et al., 2019)(Li et al., 2021)(Rakousky et al., 2017). Thus, not reporting degradation of single power- or

on/off cycle. Two publications were found that give some insights into cyclic degradation. One research by Weiß et al (2019) found that when a cell is operated alternately at high (3 A/cm$^2$) and low (0.1 A/cm$^2$) current densities, with idle periods during which no current was applied and the cell remained at open circuit voltage (Nernst potential) the degradation increased by a factor 1.6 after 718 cycles compared to a steady potential at 1.3V. This shows the impact of power cycles. However, on/off cycles reach an idle position of 0V and in other power cycles the idle position can be well above open circuit voltage, making it hard to draw conclusions from this data.

Another research by (Shaun et al., 2024) found that start-stop cycling (0-2V) increases the degradation to 5.5 µV/cycle compared to 3.2 µV/cycle for a power cycle (1.45-2V). This experiment concludes that on/off cycles have more impact than power cycles. However, the absolute values are not representative as low catalyst loadings are used as well as high frequency cycling to accelerate degradation and reduce experiment duration.

The combined findings from industry outreach and literature review confirm that high-quality degradation data for PEM electrolysers under intermittent operation is severely lacking. The next section focusses on the data analysis of the collected dataset and tries to establish a more significant relation by sampling datapoints based on certain characteristics.

**In short:** Despite growing concern over degradation in PEM electrolysers under intermittent operation, both industry experts and academic literature reveal a significant lack of reliable, detailed, and comparable data. The initial data show that degradation increases with current density but without a statistically significant trendline. The degradation relation found by Schofield et al. (2024) shows a better trendline but is based on limited datapoints.

### 4.3.2 PEM Electrolyser Degradation Data Analysis

To assess whether variability in PEM electrolyser degradation data can be reduced, the dataset was sampled by operational and material characteristics to evaluate their effect on the correlation between current density and degradation rate, as measured by the coefficient of determination ($R^2$).

The data is sampled based on (a combination of) the following characteristics:

1. Cyclic Loading – Includes only data points from experiments with intermittent power operation.
2. Constant Loading – Includes only data from steady-state (constant current) tests.
3. Experimental Data Only – Excludes target values and manufacturer specifications, only laboratory-based experimental data is considered.
4. Catalyst Loading Threshold – Includes only data with realistic Iridium catalyst loadings above 1.5 mg/cm².

The results are presented in Table 4-1, with the corresponding regression plots included in Appendix K. For each sample, multiple curve-fitting approaches were evaluated by their coefficient of determination, but none outperformed the second-order polynomial. Across all sampled datasets, the coefficient of determination remains below 0.5, indicating a weak correlation.

These results highlight the fragmented nature of the available degradation data. Even when controlling for critical variables, the lack of standardization in experimental procedures and reporting

continues to limit the ability to establish a reliable, generalizable degradation model. One can conclude that no significant correlation within the dataset is found. This could be explained by the limited data volume and inconsistent testing conditions, making it difficult to define a clear and reliable trend.

*Table 4-1: Data sample analysis results*

| Sample | # of data point | $R^2$ |
|---|---|---|
| All datapoints | 32 | 0.1219 |
| Experiments only | 28 | 0.1270 |
| Cyclic loading and experiments only | 10 | 0.2489 |
| Constant loading and experiments only | 20 | 0.1236 |
| Realistic catalyst loading and experiments only | 8 | 0.3863 |

**In short:** The collected PEM degradation data is highly fragmented and inconsistent. No significant correlation between current density and degradation rate was found, even after data sampling or testing various curve-fitting methods. No reliable data was identified on power- or on/off cycling. Only one degradation relation from literature, reported by Schofield et al. (2024), could be used.

## 4.4 Conclusion and Selection of PEM Electrolyser Degradation Dataset

This section aimed to collect and analyse degradation data for PEM electrolysers to quantify how performance degrades under intermittent operation including power cycling and on/off cycling. These insights are essential for modelling the operational strategies and optimizing the trade-off between hydrogen production and system lifetime. Unfortunately, no statistically significant correlation was found between current density and degradation rate. Even after sampling, $R^2$ remained below 0.5, and alternative curve-fitting methods failed to improve results. These results show the immaturity of this field of research and reveal the significant limitations in the availability and comparability of degradation data.

This has serious implications for the industry. The absence of robust degradation data under intermittent conditions exposes a critical knowledge gap. Many electrolyser operators rely on steady-state assumptions, while the reality of renewable-driven operation is far more variable. Without clear degradation data, stakeholders risk making poorly informed operational choices, which may result in premature stack failure, inflated costs, and underperformance of green hydrogen projects.

The only degradation relation that showed statistical relevance was reported by Schofield et al. (2024), with an $R^2$ of 0.63. Although it does not explicitly quantify degradation from single on/off- or power cycles, it inherently reflects intermittent operation effects due to the use of square and hold power profiles. This is the degradation relation selected for the remainder of this thesis. It is selected not only because it provides the strongest statistical correlation, but also because Schofield et al. (2024) applied a comparable modelling approach, although without implementing operational control strategies. Using this relation allows for comparison between the results of this thesis and those from

their LCOH assessment.

**In short:** The degradation relation by Schofield et al. (2024) is selected for this thesis due to its strong statistical correlation ($R^2 = 0.63$) and compatibility with a comparable LCOH study. Other data sources proved too fragmented, with no meaningful correlations found, even after sampling. This exposes a critical knowledge gap that could lead to poor operational decisions and higher costs in green hydrogen projects.

# 5 PEM Electrolyser Operational Strategy Model and Results

**Relevance**
Identifying how operational strategies affect hydrogen production, degradation, and cost is crucial for answering the research question. By comparing different strategies, this analysis enables more informed decisions about how to operate electrolysers in a way that balances performance with durability, an essential step toward scaling offshore hydrogen production.

**Conclusion**
Among the three strategies evaluated, equal distribution yields the lowest LCOH by avoiding high current densities and spreading degradation evenly across stacks. The efficiency-based strategy performs comparably in LCOH and achieves the highest system efficiency but leads to more frequent on/off cycling. The serial distribution strategy performs worst, resulting in accelerated degradation of one stack and the highest overall LCOH. These findings highlight that degradation behaviour, particularly under dynamic operation, is a decisive factor in the economic optimization of offshore PEM electrolysis systems.

The PEM electrolyser operational strategy model aims to answer the research question:

*How does the operational strategy for managing intermittent offshore wind power supply in an offshore PEM electrolyser system affect hydrogen production, stack degradation and the LCOH?*

In this model, several operational strategies are simulated and compared based on their LCOH, on/off- and power cycles. The operational strategy model uses input from the PEM electrolyser model, which relates the power input to stack-level behaviour such as the current density, efficiency and hydrogen production, together with the degradation relation as defined in Section 4. This allows for a time-resolved simulation of stack behaviour, degradation and hydrogen production over the system's lifetime. The power input of the model is from a North Sea offshore wind farm (OWF).

## 5.1 Operational Strategy Model Characteristics

This section aims to explain the characteristics of the operational strategy model such as inputs, working principles and assumptions.

### 5.1.1 The Operational Strategy Model - Inputs

The operational strategy model makes use of the following inputs:

- The Simulink PEM electrolyser model output: this model provides data about the operating points of the 100kW PEM electrolyser stack. The outputs of the PEM electrolyser model show the current density (A/cm$^2$), potential (V), efficiency (-), and hydrogen production (g/s) at any given power input ranging between 0-100 kW. The data can be found in Appendix H.

- Degradation relation: this relation provides the degradation rate in (µV/h) given the current density (A/cm$^2$) and is defined according to Figure 4-2 by Schofield et al. (2024). Degradation effects of power- and on/off cycling are not considered as no reliable data is found. Possible scenarios will be covered in the sensitivity analysis.

- North Sea OWF data: this data gives the capacity factors of a 2GW North Sea offshore wind farm, based on the year 2013. The power output is scaled to 400 kW capacity. The data can be found in Appendix L.

Together, these inputs enable a time-resolved simulation that links fluctuating renewable power availability to stack-level performance and lifetime, ensuring that both technical realism and degradation dynamics are incorporated into the model.

**In short:** The operational strategy model uses three essential data inputs: the Simulink PEM electrolyser model output, the degradation relation as defined by Schofield et al. (2024), and power output of an OWF.

### 5.1.2 The Operational Strategy Model - Working Principles

The Operational Strategy Model consist of 4x100kW PEM electrolyser stacks and an intermittent power input that ranges between 0-400kW over time. The goal of this model is to divide the power input over the 4 stacks based on different power dividing strategies or operational strategies. The power input that each stack gets determines its working point on the I-V curve. This working point defines hydrogen production and the degradation as they are related to the current density, I (A/cm$^2$). A schematic overview of the model can be seen in Figure 5-1, the code of the model can be found in Appendix N.

The model operates in a 1-hour timeframe over the course of 15 years. For each hour the power input for a stack (kW), the degradation (µV/h) and hydrogen production (kg/h) are determined. The degradation is accumulated and if a certain amount of degradation (V) is reached , stack is replaced, adding the replacement costs to the total costs and setting the degradation level back to 0. The hydrogen production and power usage (in kWh) are added up over the course of 15 years.

The LCOH is calculated based on the hydrogen output in 15 years (in kg) and the total cost of production. These costs include the BoP costs ($), the stack (replacement) costs ($) and opportunity costs of the power used ($). Dividing the costs by production volume results in a LCOH in $/kg.

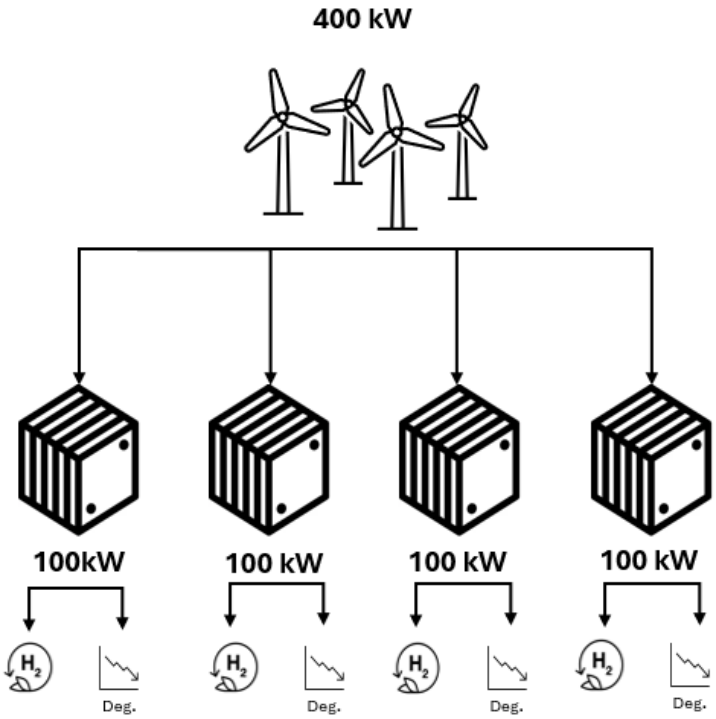


*Figure 5-1: Schematic overview of the operational strategy model*

Due to degradation the stack loses efficiency and the hydrogen production is reduced over the lifetime of the stack. This is accounted for by the performance factor according to equation (5.1), where 1.85 is the maximum voltage at standard conditions according to the I-V curve in Figure 3-2. ∑(stack degradation) is the sum of the stack degradation at any given moment. As the hydrogen production is linearly related to the current density according to equation (3.13), the hydrogen production is multiplied by the performance factor to account for decline in hydrogen production due to stack degradation.

$$Performance\ factor = 1 - \frac{\sum stack\ degradation\ (V)}{1.85\ (V)} \tag{5.1}$$

**In short:** The operational strategy model simulates how PEM stacks respond to varying wind power input by applying different power allocation strategies. It accounts for degradation accumulation, stack replacement, and hydrogen production over a 15-year horizon. The inclusion of a performance factor ensures that the decline in efficiency due to voltage degradation is directly reflected in hydrogen output, allowing for accurate LCOH calculations and long-term performance tracking under dynamic operating conditions.

### 5.1.3 The Operational Strategy Model - Assumptions

The operational strategy model makes use of the assumptions listed below, which are categorized based on their segments.

Power input assumptions:

- The OWF and electrolyser capacity are equal (both 400kW). It is assumed there are no power connections other than from the OWF.
- The power input is based on a 2GW OWF, operated in the year 2013.

- The power input is scaled to 400kW using the capacity factor.
- The power input is on an hourly basis.
- The yearly pattern is repeated 15 times to simulate a lifetime of 15 years based on the OWF lifetime.
- The OWF experiences a 15% wake loss.
- There are no losses assumed in terms of power transportation and conversion.

Simulation assumptions:

- The model runs on 1-hour intervals assuming an instant transition from one to the other state.
- The stacks' end-of-life is defined by accumulated degradation of 1V.
- No degradation recovery: degradation is assumed permanent and accumulative.
- Stack replacement happens immediately; no downtime is assumed.
- Stack operating points are only defined for discrete power inputs (e.g. 0,1, 2, …, 100kW). The simulation rounds to the nearest integer and does not use interpolation.
- PEM electrolyser stacks operate over its full power range (0-100kW), no minimum power is required.
- On/off cycles are considered to occur when a stack changes from 0 kW input to >0 kW or from >0 kW to 0 kW across two time intervals.
- Power cycles are considered to occur when a 50% variation in stack input power occurs across two time intervals.
- All generated hydrogen is assumed to be captured.
- The BoP performance is assumed constant, and no BoP degradation is considered.

Cost assumptions:

- The total BoP costs are 577,5 $/kW × 400 kW = $231.000 based on the average value of Table 2-10 and are assumed to have a lifetime of 15 years. No replacement or maintenance cost are considered within the BoP's lifetime.
- The stack replacement costs are 427,5 $/kW × 100 kW = $47.250 per stack replacement. based on the average value of Table 2-10, this assumption includes transportation and installation costs.
- The power costs are assumed to be constant over the course of 15 years at 0,04 $/kWh.

This section outlined the operational strategy model key assumptions regarding power input, simulation behaviour, and cost structure that form the foundation for the simulation.

## 5.2 Operational Strategy Simulations and Results

The simulation is run with 3 different operational strategies. The rationale behind these strategies is based on interviews with industry experts. This section defines and motivates the selected operational strategies, presents the corresponding results, and includes a brief verification to ensure that the simulation and strategies produce realistic and consistent outcomes. The conclusion from these results will be drawn in Section 6.

### 5.2.1 Strategy 1 – Equal distribution

The first operational strategy is an equal power distribution across the four stacks. This strategy is selected as the 'base case' as there is no active power dividing required, since stacks within an

electrolyser are typically placed in parallel. The motivation behind this strategy is to establish a simple, balanced reference scenario. The results of the equal distribution operation can be seen in Table 5-1 and Table 5-2, where the first presents the overall system results and the latter presents the results on stack level.

*Table 5-1: Equal distribution; system results*

| Metric | Value |
|---|---|
| LCOH without electricity cost | 9,78 $/kg |
| LCOH with electricity cost | 12,17 $/kg |
| Total hydrogen production | 352.211 kg |
| Total electricity used | 21.045.407 kWh |
| LHV efficiency | 55.2% |

*Table 5-2: Equal distribution; stack results*

| Metric | Stack 1 | Stack 2 | Stack 3 | Stack 4 | Total |
|---|---|---|---|---|---|
| Replacements | 17 | 17 | 17 | 17 | 68 |
| On/Off cycles | 946 | 946 | 946 | 946 | 3.784 |
| Power cycles | 15.329 | 15.329 | 15.329 | 15.329 | 61.316 |

**Verification**

The output of the equal distribution simulation is exported to an Excel, as seen in Appendix M. In the excel it can be verified that power distribution is indeed equal over all stacks and so is degradation and hydrogen production. This is in line with the results that show an equal number of stack replacements and power- and on/off cycles for each stack. The number of on/off cycles can be verified by analysing the power input data in Appendix L and checking for on/off cycles in the input power of the OWF.

The average capacity factor of the OWF is 0,47. A back of the envelope calculation shows that an average power input of 47kW per stack results in a current density of around 2 A/cm$^2$, which has an average degradation rate of 30*2$^2$ = 120 µV/h. Over the course of 15 years and with a stack replacement threshold at 1V this would result in 15 replacements. This supports that the replacement ratio is about right.

**In short:** The equal distribution strategy serves as baseline scenario and leads to uniform stack usage, degradation, and replacement rates.

### 5.2.2 Strategy 2 – Serial distribution

The second operation strategy is a serial distribution. In this operational strategy the power is first provided to stack 1, when stack 1 reaches is maximum capacity, stack 2 is activated, and so on. This strategy was inspired by an interview with the PosHydon project. The strategy has two main drivers. First, the maximization of hydrogen output as this strategy resulted in the most stacks operating at the highest current density. Second, by ‘sacrificing’ the first stack, other stacks could have a longer lifetime making it possible to optimize maintenance planning and avoid downtime. The results of the serial distribution can be seen in Table 5-3 and Table 5-4.

*Table 5-3: Serial distribution; system results*

| Metric | Value |
|---|---|
| LCOH without electricity cost | 13,33 $/kg |
| LCOH with electricity cost | 15,83 $/kg |
| Total hydrogen production | 336.332 kg |
| Total electricity used | 21.045.407 kWh |
| LHV efficiency | 52.7% |

*Table 5-4: Serial distribution; stack results*

| Metric | Stack 1 | Stack 2 | Stack 3 | Stack 4 | Total |
|---|---|---|---|---|---|
| Replacements | 39 | 27 | 19 | 5 | 90 |
| On/Off cycles | 946 | 2866 | 2970 | 2145 | 8.927 |
| Power cycles | 13.905 | 10.439 | 8.910 | 5.055 | 38.309 |

**Verification**

The output of the serial distribution simulation is exported to Excel as in Appendix M, where it can be verified that power is first allocated to Stack 1 until it reaches full capacity (100 kW), after which Stack 2 is activated, then Stack 3, and so on. This operational strategy results in significantly higher power input and thus degradation for Stack 1 compared to the others. This can be verified by the pattern of stack replacements in Table 5-4.

Also, on/off- and power cycles are unevenly distributed across the stacks. As expected for the serial distribution strategy, Stack 1 undergoes fewer on/off cycles due to its near-continuous operation. The subsequent stacks are operated with more intermittency and thus show more on/off cycles. Lastly, the on/off cycles of stack 1 (946) are equal to the on/off cycles of equal distribution strategy (946) which is in line with the analysis of the OWF power input.

The overall system hydrogen production was expected to be higher due to operation at higher current densities, but it turned out lower than with equal power distribution. This is explained by the performance factor: the gain in hydrogen production from higher current density does not compensate for the loss in performance due to increased degradation at higher current density, resulting in a lower total output.

**In short:** The serial distribution strategy concentrates usage on the first stack, significantly increasing its degradation and replacement frequency. Although this approach can simplify maintenance planning by localizing degradation, it results in reduced hydrogen production due to increased performance loss attributed to increased degradation.

### 5.2.3 Strategy 3 - Efficiency distribution

The third operational strategy is the efficiency-based distribution approach, which aims to operate all stacks at their optimal efficiency. As illustrated by the efficiency curve in Figure 3-7, the peak efficiency of a stack occurs around 30 kW, with a sharp decline in efficiency below this value. Therefore, under this strategy, a new stack is only activated if it can be supplied with at least 30 kW. Any remaining power is then evenly distributed among the active stacks. This strategy is also inspired by an interview with the PosHydon project and is designed to maximize energy efficiency. The results of the efficiency distribution can be seen in Table 5-5 and Table 5-6

*Table 5-5: Efficiency distribution; system results*

| Metric | Value |
|---|---|
| LCOH without electricity cost | 9,87 $/kg |
| LCOH with electricity cost | 12,25 $/kg |
| Total hydrogen production | 353.595 kg |
| Total electricity used | 21.045.407 kWh |
| LHV efficiency | 55,5% |

*Table 5-6: Efficiency distribution; stack results*

| Metric | Stack 1 | Stack 2 | Stack 3 | Stack 4 | Total |
|---|---|---|---|---|---|
| Replacements | 18 | 17 | 17 | 17 | 69 |
| On/Off cycles | 946 | 2.836 | 2.791 | 2.806 | 9.379 |
| Power cycles | 13.259 | 3.854 | 3.779 | 3.704 | 24.596 |

**Verification**

The output of the efficiency distribution simulation is exported to Excel as in Appendix M, where it can be verified that stacks are only activated when at least 30 kW of power is available per additional stack.

The simulation shows a slightly higher number of replacements for Stack 1 compared to the other stacks, which is consistent with Stack 1 being active most often, especially in low-wind periods when the total power input is insufficient to activate additional stacks. The on/off cycle data further support this: Stack 1 has the fewest on/off cycles, due to its frequent use. The 946 on/off cycles of stack 1 are in line with the analysis of the power input from the OWF as mentioned before.

**In short:** The efficiency-based strategy prioritizes operating at optimal efficiency points, activating additional stacks only when sufficient power is available to sustain high efficiency. This approach led to an increased number of power cycles in the first stacks and more frequent on/off cycles in the later ones.

## 5.3 Operational Strategy Model Validation

Model validation ensures the PEM electrolyser strategy model produces credible results by comparing outcomes to literature and benchmarks

The simulation results showed a LCOH ranging between $12.17 and 15.83 $/kg. At first, these values appear high, particularly when compared to conventional hydrogen production via Steam Methane Reforming (SMR), which typically yields LCOH values between $1 and $2 per kilogram (stargate hydrogen, 2024). The U.S. Department of Energy reported an LCOH target of $3/kg for PEM-based renewable hydrogen production as of 2022 (U.S. Department of Energy, n.d.).

However, what makes this thesis unique is the inclusion of degradation under intermittent renewable operation and the associated stack replacement costs. These factors are often overlooked in other research, yet shown here to have a significant impact on the LCOH. For example, the simulation results indicate that stacks require replacement approximately every 11 months under the equal

distribution strategy, whereas manufacturers such as NEL Hydrogen report stack lifetimes of 5–7 years under optimal steady conditions (PEM Electrolyser – MC Series, 2019). Studies that account for intermittent operation and corresponding degradation similarly report higher LCOH values. For instance, Schofield et al. (2024) demonstrated that incorporating usage-based degradation reduced the expected stack lifetime from seven to around two years, resulting in an LCOH of $6.60/kg. Table 5-7 presents the LCOH values from other studies that considered intermittent operation and the related degradation effects. The relatively high LCOH observed in this thesis reflects the impact of degradation under intermittent operation, precisely the challenge this research aims to highlight.

*Table 5-7: LCOH data from literature*

| Source | LCOH |
|---|---|
| (Schofield et al., 2024) | 6,60 $/kg |
| (DOE, 2025) | 6,20 $/kg |
| (Nasser et al., 2022) | 5-9,72 $/kg |
| (TNO, 2024) | 16,02 $/kg |

It is important to note that the LCOH is sensitive to several core assumptions such as the degradation rate, stack replacement costs and the electricity price. These aspects are explored in greater detail in the sensitivity analysis presented in the following Section 5.5.

**In short:** The model produces verified and validated LCOH results that align with literature when degradation under intermittent operation is considered, highlighting the critical impact of assumptions like stack lifetime and replacement costs.

## 5.4 Operational Strategy Simulations Conclusion

This section concludes the evaluation of the operational strategies. Among the three operational strategies evaluated, the equal distribution strategy is the most economically favourable under the current assumptions, achieving the lowest LCOH at $12.17/kg. This outcome is not coincidental, it is a direct result of avoiding high current density operation, which is known to accelerate degradation as found in Section 4. By distributing power evenly across all stacks, this strategy ensures a balanced load and minimizes stress on individual components, leading to lower maintenance requirements and improved system longevity. The notable downside of this strategy, however, is the higher number of power cycles, as each stack continuously adjusts its input to match the total available power.

The efficiency-based strategy demonstrates strong potential. It achieves the highest system efficiency (55.5%), has a limited number of power cycles and has a LCOH of $12.87/kg. However, this comes at the cost of increased on/off cycling, which could pose long-term reliability concerns depending on the degradation dynamics.

In contrast, the serial distribution strategy is clearly the least favourable, with an LCOH of $15.83/kg, over 30% higher than the equal distribution strategy. Its design inherently leads to disproportionate degradation, particularly in the first stack, which required 39 replacements. This imbalance not only drives up maintenance costs but also undermines system reliability. While the concept of sacrificing one stack to preserve others may have its applications, it is economically inefficient.

These findings underscore a critical insight: degradation behaviour is central to operational strategy design. Under current assumptions high current density significantly increases degradation. The strategy that best avoids this performs best in terms of LCOH. However, if future research reveals that power cycling is more detrimental than high current operation or on/off cycling, the efficiency-based strategy becomes more favourable. Conversely, if on/off cycling proves more damaging, the case for equal distribution becomes even stronger.

**In short:** Under the current degradation assumptions, the equal distribution strategy is the most cost-effective and operationally balanced approach with the lowest LCOH. If future insights shift the understanding of degradation impacts like power- and on/off cycling, different operational strategies may be favoured.

## 5.5 Sensitivity analysis

As mentioned, the results of the operational strategy model are sensitive to several assumptions and input variables. The goal of the sensitivity analysis is to understand how changes in these assumptions and input variables affect the output of the model. The sensitivity analysis helps to identify the most influential inputs and helps to determine how robust the model is to uncertainty or variation.

### 5.5.1 Degradation Sensitivity Analysis

One of the most uncertain input parameters in the operational strategy model is the degradation rate of the PEM electrolyser stacks. As extensively discussed in Section 4, degradation behaviour is highly variable across studies especially under dynamic operation.

To assess the sensitivity of the LCOH to assumed degradation, the simulation explored a ±50% deviation from the standard PEM electrolyser degradation curve to evaluate the impact of potential technological developments or inaccuracies in current degradation estimates. This approach is visualized in Figure 5-2.

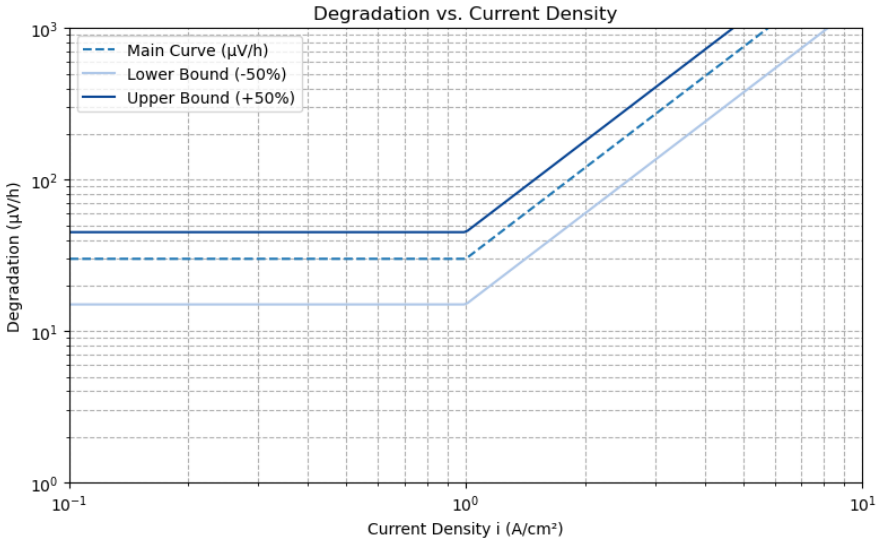


*Figure 5-2: Upper and lower bound of the degradation relation*

The results of the sensitivity analysis for equal distribution operation are shown in Figure 5-3. A reduction of the degradation rate by 50% leads to an LCOH decrease of nearly 40%, while a 50% increase raises the LCOH by the same amount. The discontinuity of the curve can be explained by the nature of stack replacements; degradation significantly influences the LCOH when it leads to one more/less stack replacement over the 15-year lifetime, which are discrete events. Additionally, the operational efficiency of the electrolyser as defined by the performance factor in equation (5.1), is influenced by degradation. This results in a lower hydrogen output per unit of electricity input, further raising LCOH.

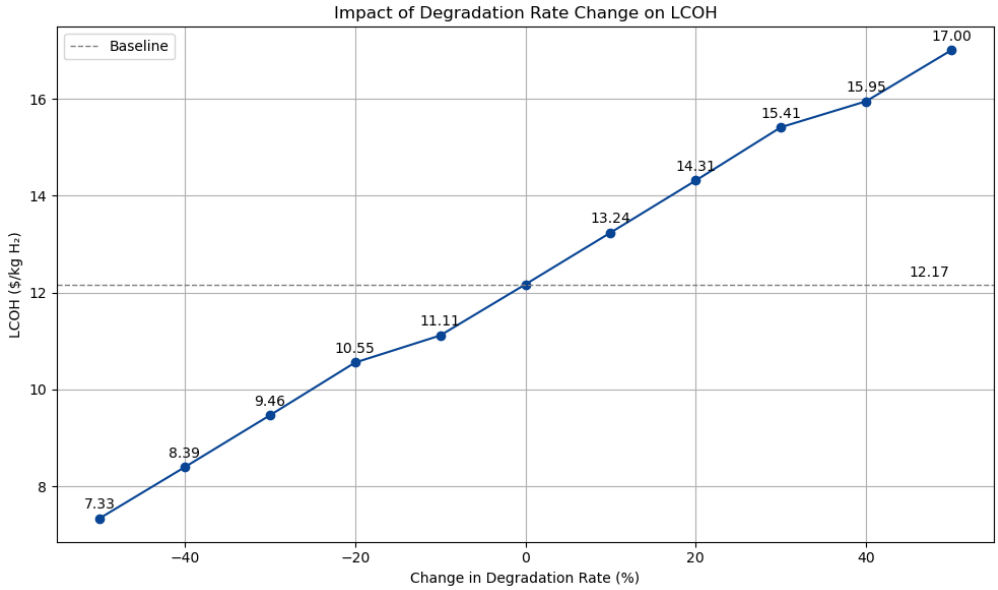


*Figure 5-3: Sensitivity analysis of degradation for equal distribution strategy*

The deviation of the degradation curve has a similar effect on the serial and optimal efficiency operational strategy can be seen in Table 5-8

*Table 5-8: Influence of degradation deviation on the LCOH with electricity cost*

| Operational strategy | LCOH with degradation upper bound | LCOH with degradation base case | LCOH with degradation lower bound |
|---|---|---|---|
| Equal distribution | 7,33 $/kg | 12,17 $/kg | 17,00 $/kg |
| Serial distribution | 9,22 $/kg | 15,83 $/kg | 22,17 $/kg |
| Efficiency distribution | 7,44 $/kg | 12,25 $/kg | 17,07 $/kg |

Furthermore, this study did not account for degradation effects from power- and on/off cycles due to the lack of available data. However, to get an impression of the potential impact, values from Shaun et al. (2024) were included in a sensitivity analysis. Although their experiments used low catalyst loading and high-frequency cycling, the data remains one of the few available sources. Their results indicate that a start-stop cycle causes an additional degradation of 5.5 µV/cycle, while a power cycle adds 3.2 µV/cycle.

The impact of this degradation on the LCOH is shown in Table 5-9. As shown, the effect is almost negligible, ranging from only $0.01/kg under equal distribution to $0.14/kg in the optimal efficiency scenario. This is expected, given that the assumed baseline degradation rate during operation is at least 30 µV/h. For example, 60,000 on/off cycles occur over 15 years under equal distribution, the additional degradation of 3.2 µV per cycle contributes relatively little to the total degradation over the system's lifetime. However, other studies referenced in Section 4 suggest a potentially larger effect but do not provide the degradation data. As a result, the true impact remains uncertain.

*Table 5-9: LCOH with power an on/off cycle degradation*

| Operational strategy | LCOH with power and on/off cycle degradation |
|---|---|
| Equal distribution | 12,18 $/kg |
| Serial distribution | 15,84 $/kg |
| Efficiency distribution | 12,39 $/kg |

In conclusion, degradation is both an uncertain and influential parameter of the LCOH. The analysis shows that deviations in the degradation relation can lead to substantial changes in the LCOH as seen in Table 5-8. Given its dual role in affecting both stack replacement frequency and production efficiency, degradation must be considered a key sensitivity in techno-economic assessments of PEM electrolysers. With the current knowledge the sensitivity of degradation due to power- and on/off cycles remains limited. Future research and modelling should place significant emphasis on refining degradation estimates, incorporating uncertainty bands, and linking degradation more closely to operational strategy and system design.

### 5.5.2 Cost Sensitivity Analysis

The total LCOH is primarily determined by three components: the cost of stacks and their replacements, the cost of the consumed electricity and the BoP cost. As section 2.5 outlined, the BoP cost is quite low compared to the reoccurring stack replacement costs and electricity cost.

Current research targets lower-cost stacks through non-precious metal catalysts and cost-effective membranes. The sensitivity of these stack costs is analysed for the equal distribution strategy in Figure 5-4, which presents the LCOH as a function of varying stack replacement costs between $5.000 and $75.000 per unit. A reduction in the stack replacement costs by 50%) resulted in a 37.4% reduction in LCOH (from 12,17 $/kg to 7,61 $/kg). On the other hand, increasing the stack cost by 10% (to $51.700) due to, for example, an increase in material prices, raised the LCOH by 7,4% to 13,08 $/kg. This highlights the significant impact of stack replacement costs on the LCOH, demonstrating that even moderate stack cost fluctuations can substantially influence the economic feasibility of PEM electrolysis.

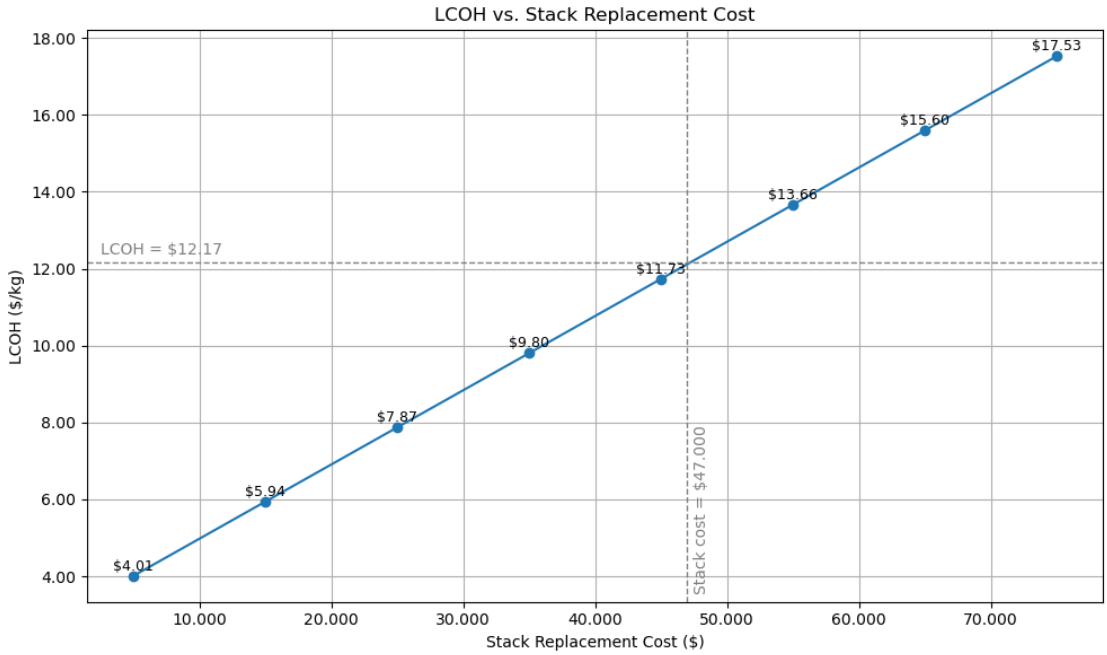


*Figure 5-4: Sensitivity analysis of stack replacement costs for equal distribution strategy*

The influence on the other operational strategies can be found in Table 5-10. The impact of the stack replacement costs is slightly higher on the serial distribution as this operational strategy results in more stack replacements over the system's lifetime.

*Table 5-10: Stack Replacement Cost Sensitivity*

| Operational strategy | 50% cost reduction | Cost base case | 10% cost increase |
|---|---|---|---|
| Equal distribution | 7,87 $/kg | 12,17 $/kg | 13,66 $/kg |
| Serial distribution | 9,88 $/kg | 15,83 $/kg | 17,91 $/kg |
| Efficiency distribution | 7,91 $/kg | 12,25 $/kg | 13,77 $/kg |

The LCOH is also influenced by the electricity cost. In this model, the electricity cost was assumed to be 0.04 $/kWh. A sensitivity analysis for the equal distribution strategy, as in Figure 5-5, reveals that reducing the electricity price by 50% leads to a 9.8% decrease in the LCOH and an increase in the electricity price by 50% leads to a 9,8% increase in the LCOH. The impact is not as significant as a 50% change in the stack replacement costs, which is to be expected as the electricity cost make up just under 20% of the LCOH for all 3 scenarios. However fluctuations in electricity prices are quite likely to occur due to the dynamic nature of electricity pricing and can be extreme. The absolute impact on the LCOH for the serial and efficiency distribution strategies can be assumed to be similar as all three strategies consume the exact same amount of electricity. Future model refinements could include a time-resolved electricity price profile, reflecting historical or projected market behaviour of electricity prices.

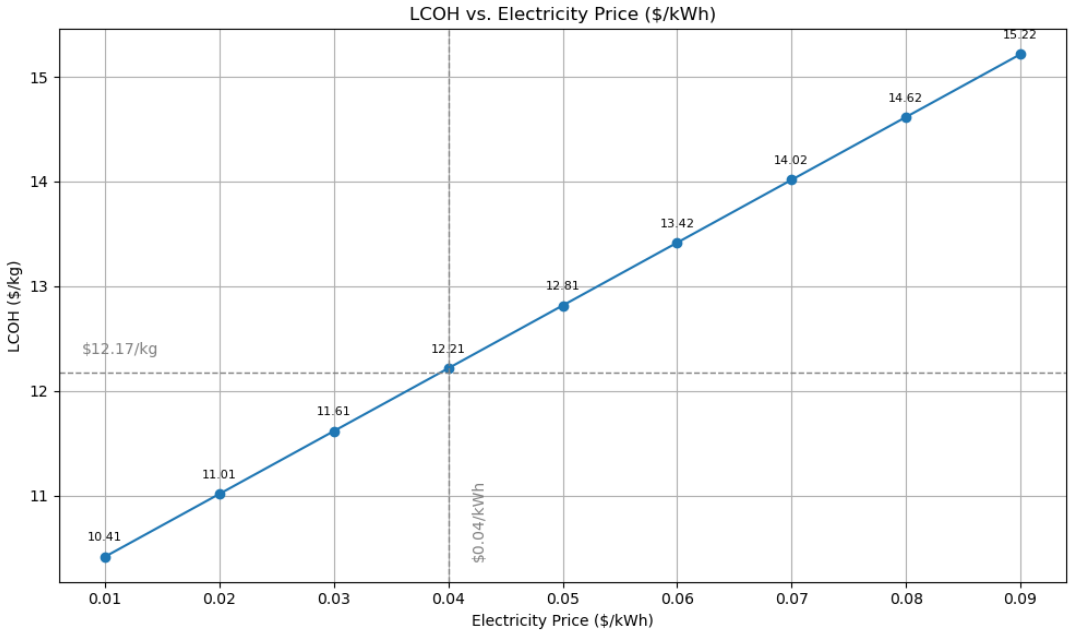


*Figure 5-5: Sensitivity analysis of electricity costs for equal distribution strategy*

The cost sensitivity analysis clearly demonstrates that among the key cost drivers of the LCOH, stack replacement costs are the most profound. For the equal distribution a 50% reduction in stack replacement costs yields a substantial 37.4% decrease in LCOH, while even a modest 10% increase leads to a 7.3% rise, underscoring the high sensitivity of the LCOH to replacement costs. Although electricity costs also affect the LCOH, their impact is comparatively moderate, with a ±50% variation resulting in only a ±9.8% change in LCOH. However, given the volatility of electricity markets, incorporating time-resolved electricity pricing in future models will be essential for capturing realistic cost dynamics and improving the robustness of techno-economic assessments.

### 5.5.3 Setup Sensitivity Analysis

In this study, a 1:1 ratio between the OWF capacity and electrolyser capacity is assumed, meaning that 400 kW of wind generation is coupled with 400 kW of electrolyser capacity. Figure 5-6 illustrates the impact of varying this ratio on the LCOH for the equal distribution strategy. The results indicate that reducing the ratio improves the LCOH, likely because the electrolyser operates less frequently in the high current density regime, where efficiency drops and degradation accelerates. However, when the ratio falls below 0.5, the LCOH begins to rise again, due to underutilization of the electrolyser, causing fixed costs to dominate. At higher ratios, the electrolyser runs more consistently with a higher capacity factor. However increased operation at high current densities accelerates degradation and raises the LCOH, due to the dominant effect of stack replacement costs.

Overall, these findings highlight the existence of an optimal wind-to-electrolyser capacity ratio that balances utilization and degradation, minimizing the LCOH by avoiding both excessive idle time and prolonged operation under high current density.

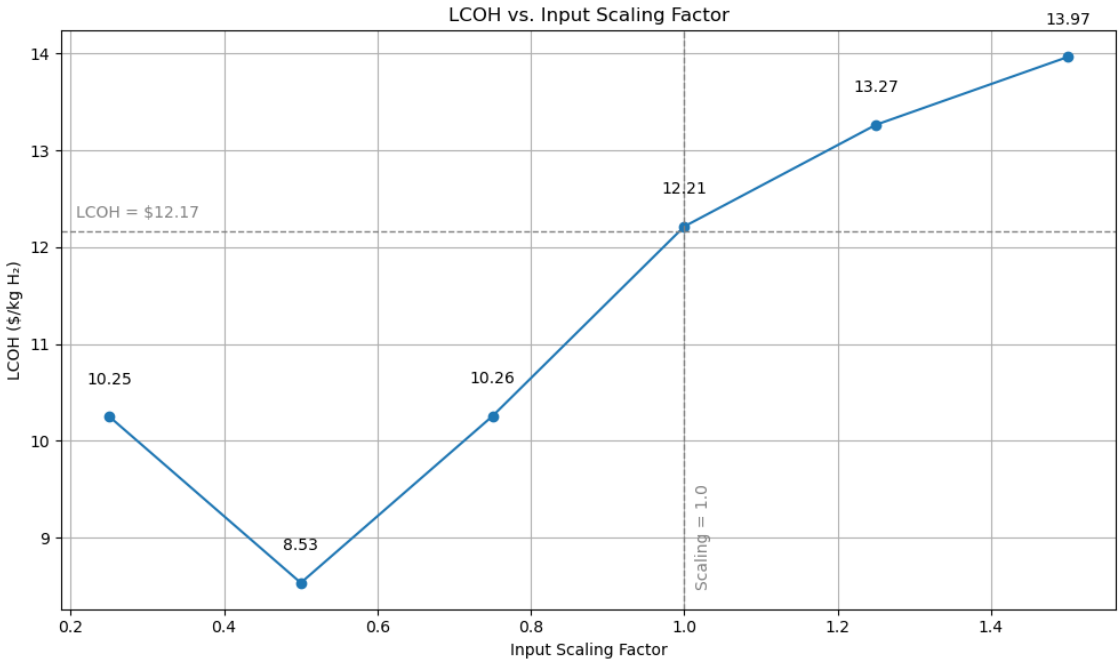


*Figure 5-6: Sensitivity analysis of the setup for equal distribution strategy*

**In short:** The sensitivity analysis reveals that the degradation relation is the most critical factor affecting the LCOH. Stack replacement costs significantly impact outcomes, while electricity price variations have a more moderate effect, but are likely to occur. Setup configurations exhibit a nonlinear impact: both over- and under-sizing the OWF capacity compared to the electrolyser capacity negatively impacts the LCOH.

## 5.6 Model Discussions and Limitations

This section critically reflects on the assumptions, design choices, and limitations of the operational strategy model. While the model offers valuable insights into the techno-economic performance of PEM electrolysis under variable offshore wind conditions, several limitations constrain its accuracy and generalizability.

**Timesteps Resolution Limitations**

The operational strategy model is based on hourly time intervals with instantaneous transitions between states. However, power output from offshore wind farms (OWFs) can fluctuate on sub-hourly timescales. These short-term variations are not captured in a model with hourly resolution, which limits its ability to reflect the dynamic behaviour of the system. Such fluctuations influence PEM electrolyser degradation through more frequent power- and on/off cycling. This represents a limitation of the current approach; a model with finer resolution would more accurately capture these dynamics and provide deeper insight into degradation.

**Steady-State Representation of a Dynamic System**

Although the underlying Simulink model simulates transient thermal and flow dynamics, the operational strategy model simplifies this to steady-state behaviour by using performance outputs at

discrete power inputs (0–100 kW). Consequently, thermal inertia, water management dynamics, and pressure build-up are not modelled.

As a result, cumulative effects such as heat build-up, delayed water saturation, or gas crossover phenomena are omitted in the operational strategy model. This simplification improves computational feasibility but may understate degradation or efficiency losses during prolonged dynamic operation.

**Degradation Uncertainties**

As previously discussed, the degradation behaviour of PEM electrolysers under variable power input is highly uncertain and remains an active area of research. This model relies on a degradation versus current density relationship derived from literature; however, degradation rates can vary significantly across different PEM systems. It is also possible that current commercial systems exhibit lower degradation rates than reported, with such data remaining confidential. This uncertainty in degradation behaviour introduces considerable variability in the LCOH, as demonstrated by the sensitivity analysis.

**Cost Assumption Simplifications**

The cost assumptions used in this study are based on literature averages and are not project specific. Several important economic aspects are excluded:

- Capital costs for offshore platforms and offshore hydrogen infrastructure
- Maintenance and downtime-related costs outside of stack replacements
- Grid connection, energy arbitrage, or market participation revenues

Electricity prices are assumed to be static at $0.04/kWh. This does not reflect market-based variability, which could be significant for offshore wind. Incorporating dynamic electricity pricing would improve the economic accuracy of future studies.

**Scenario Representativeness and Generalizability**

The model uses historical wind data from a 2 GW North Sea offshore wind farm for the year 2013, scaled down to 400 kW. This provides a realistic but narrow representation of wind conditions. Results may not generalize to other offshore locations or years.

Additionally, the 1:1 ratio between wind farm and electrolyser capacity may not reflect optimized system sizing. As shown in the sensitivity analysis, this ratio significantly influences degradation dynamics and LCOH. Thus, caution is advised when generalizing the results beyond the assumed scenario.

**In short:** While the operational strategy model provides valuable insights into PEM electrolyser performance under offshore wind conditions, its simplifications, such as narrow system boundaries, hourly resolution, steady-state assumptions, uncertain degradation behaviour, and static cost inputs, limit its generalizability and may underestimate the LCOH. To enhance accuracy and applicability, future models should adopt broader system integration, smaller timesteps, more comprehensive degradation modelling, and dynamic economic assumptions.

# 6 Conclusion

This thesis set out to answer the central research question:

*How does the operational strategy for managing intermittent offshore wind power supply in an offshore PEM electrolyser system affect hydrogen production, stack degradation and the LCOH?*

The research followed three main phases. First, a literature review established PEM electrolysis as the most suitable technology for offshore hydrogen production, examined degradation mechanisms under dynamic conditions, and analysed degradation data to establish a degradation relation. Subsequently, a Simulink model was developed to simulate PEM electrolyser stack performance under various power inputs. Finally, analysis of the operational strategies was performed in a Python model, which incorporated both the Simulink outputs and the degradation data.

Key findings reveal that:

- **Operational strategy is a critical lever:** The three operational strategies evaluated—equal, serial, and optimal efficiency power distribution—have a significant effect on system performance. Equal distribution achieved an LCOH of $12.17/kg with 68 stack replacements over 15 years due to degradation, while serial distribution resulted in a higher LCOH of $15.83/kg and required 90 stack replacements. This means that the choice of operational strategy can yield a 30% (!) reduction in LCOH and prevent up to 22 stack replacements, an impact that is both technically and economically significant. Notably, hydrogen production varied little between strategies; serial distribution delivered only 4% more hydrogen compared to equal distribution. The optimal efficiency distribution produced an LCOH nearly identical to equal distribution ($12.25/kg), with 69 stack replacements, similar hydrogen production and an efficiency just 0.3 percentage points higher.

- **High current density operation should be avoided:** The poorest performing strategy, serial distribution, operates stacks most frequently in the high current density range. According to the degradation relation adopted in this study (Schofield et al., 2024), high current density significantly accelerates degradation, leading to reduced performance and more frequent stack replacements. These drawbacks outweigh the gain in the hydrogen production rate at higher current densities. On the other hand, both equal and optimal efficiency distribution strategies are much more effective at limiting operation in the high current density range, with equal distribution performing best since it does not require a threshold for optimal efficiency. However, while both strategies effectively reduce high current density operation, they greatly differ in the number of power- and on/off cycles. Although the precise impact of these cycles on degradation is not well understood yet, it is clear that operational strategies significantly influence them.

- **Degradation is a critical uncertainty:** This research has made clear that our understanding of PEM electrolyser degradation, particularly under intermittent operation, is still very limited. There is no standardization in degradation testing, and reliable, long-term data reflecting real-world dynamic conditions are largely missing. The sector is confronted with fragmented datasets, inconsistent methodologies, and a lack of transparency from manufacturers. As a

result, even fundamental questions about degradation rates and mechanisms remain unanswered, and the field lacks the robust knowledge base needed to confidently predict or optimize system performance over time.

- **Industry implications are immediate:** As the hydrogen sector scales up, the absence of robust operational strategies and reliable degradation data poses a substantial risk to project viability. Without deliberate control of stack operation based on known degradation behaviour, projects may face unexpected downtimes, premature stack failures, and inflated costs. These challenges are already emerging in early offshore pilot projects. For industry stakeholders, this underscores the need to treat operational strategy as a core design parameter.

Based on these key findings the research question can be answered in the following manner:

*The operational strategy significantly affects the performance of offshore PEM electrolyser systems. Strategies that cause prolonged operation at high current densities cause higher stack degradation, requiring costly stack replacements and negatively affecting efficiency. Operational strategies that avoid high current density operation have lower stack degradation, higher efficiency and can reduce the LCOH by up to 30%.*

The conducted research makes the following contribution to the field:

- **Highlighting the need for standardized degradation research:** This work demonstrates the urgent necessity for harmonized degradation testing protocols and long-term field data. Without these, it remains impossible to accurately assess PEM electrolyser performance under real-world, fluctuating conditions or to develop reliable, cost-effective operational strategies.

- **Introducing a novel, time-resolved simulation framework**: This thesis presents a unique simulation approach that combines a dynamic Simulink-based PEM electrolyser model, a literature-based degradation relation, and a techno-economic operational strategy model using offshore wind input data. This framework makes it possible to assess the long-term performance of multi-stack PEM systems under realistic offshore wind conditions

- **Establishing operational strategy as a critical design factor:** The research demonstrates that operational strategy has a direct and measurable impact on both system cost and stack longevity. The developed simulation tool provides a practical foundation for evaluating operational strategies and optimizing future offshore hydrogen projects.

In summary, this thesis shows that operational strategy is a key determinant of performance in offshore renewable PEM electrolyser systems. Choosing the right strategy can lower the LCOH by 30% and reduce the number of stack replacements by up to 22 over a 15-year period, with only minor differences in hydrogen output. Strategies that avoid high current density operation are most effective at limiting degradation. However, the lack of standardized degradation data remains a major challenge and threatens future project viability. This underscores the urgent need for harmonized testing protocols and long-term field data to support reliable, cost-effective system design and operation.

# 7 Discussion and Recommendations

This study showed that operational strategy is a key factor in the performance and cost-efficiency of offshore renewable PEM electrolyser systems, revealing up to a 30% variation in LCOH and significant differences in degradation-related stack replacement. However, the findings are subject to limitations, as outlined in Sections 3.6 and 5.6. The following section presents a discussion of these findings and offers recommendations for future research.

**Discussion**

While the operational model provides valuable insights, it is built on several simplifying assumptions and limitations that must be acknowledged. These factors limit the accuracy of the simulation and reduce the extent to which the conclusions can be generalized to real-world scenarios:

- **Time Resolution:** The operational strategy model uses an hourly time step, with instantaneous changes in power input from hour to hour. This low resolution means that sub-hourly fluctuations in wind power are not captured, even though offshore wind farms (OWFs) can ramp up or down within minutes, leading to rapid changes in power output (Theuer et al., 2020). By relying on hourly intervals, the model fails to capture sub-hourly fluctuations that may cause power cycles which contribute to additional electrolyser degradation (Rakousky et al., 2017). On/off cycles are less likely to be influenced by the resolution as OWF's rarely shutdown and startup on a sub-hourly interval. The hourly model may be too optimistic in terms of stack durability, which can result in a higher LCOH.

- **Steady-State vs.. Transient Operation:** The operational strategy model uses steady-state performance data from the transient Simulink model, by using fixed hourly values from operating points (0–100 kW per stack). This simplification ignores transient effects like thermal inertia, pressure dynamics, and membrane hydration changes. The electrolyser is assumed to instantly reach the fixed value, overlooking delays in temperature response, voltage overshoot, and ramp-up inefficiencies (Buttler & Spliethoff, 2018). As a result, the model likely underestimates overpotential losses during dynamic operation. Therefore, the predicted degradation, hydrogen output and ultimately the LCOH, might be somewhat optimistic

- **Degradation Model Uncertainty:** PEM electrolyser degradation under intermittent power remains highly uncertain due to limited long-term data on PEM electrolysers operating with fluctuating renewables (Wang et al., 2022). This study applies the degradation model from Schofield et al. (2024), one of the few to examine usage-based degradation under dynamic operation. However, this research omits power- and on/off cycling due to lack of data, thus simplifying degradation. As a result, the number of stack replacement carry significant uncertainty. As noted by Martínez López et al. (2023), there is no agreed-upon degradation model for intermittent PEM operation, with studies showing conflicting results. This highlights the need for standardized testing. The findings of this research are therefore indicative and may shift with better degradation data.

- **Economic Assumptions:** The LCOH analysis uses simplified and fixed inputs. For example, a constant electricity price of $0.04/kWh is assumed whereas in reality, if the system were grid-connected, electricity costs could vary (Hydrogen Council & McKinsey, 2024). Furthermore, certain costs like offshore platform infrastructure, pipelines, and various operational expenses beyond stack replacement were ignored. These simplifications likely lead to an underestimation of the LCOH. On the other hand, the model assumes a fixed 400 kW electrolyser and current cost levels, while future larger-scale projects and ongoing technological advancements could significantly lower costs through economies of scale and innovation.

- **Scenario Specificity:** This study uses historical wind data from a North Sea location, scaled to a 400 kW system with a 1:1 wind-to-electrolyser capacity ratio. While this offers a base case, it represents only one possible configuration. Other sites may have different wind patterns or use hybrid inputs like solar, batteries or connections to the grid, which would affect how the electrolyser operates. Similarly, the chosen capacity ratio may not be optimal. Some studies suggest that oversizing the electrolyser can reduce the LCOH, depending on the trade-off between utilization and capital expenses (Oszcipok et al., 2018). As shown in the sensitivity analysis, this ratio has a noticeable impact on system behaviour. While the conclusions about strategy performance remain relevant, the specific results vary in different scenarios. Future work should investigate a broader set of locations, sizing ratios, and renewable mixes to test how robust different operational strategies really are.

In summary, these limitations mean the present model likely underestimates some negative effects (like cycling, degradation and transient inefficiencies) and simplifies economic reality. This could make this thesis' scenario look more favourable than a fully detailed real-world simulation might. Recognizing these gaps provides direction for future improvements to enhance model accuracy and relevance. Recommendations for future are therefore proposed below.

**Recommendations for Future Work**

To build on this work and address the limitations above, several recommendations are proposed for future research and system design:

- **Integrated Energy System Design:** To mitigate the impact of power intermittency on PEM electrolysers, future research should explore hybrid configurations that combine energy storage and broader grid integration. Coupling electrolysers with batteries or other storage can smooth short-term fluctuations, reduce harmful cycling, and extend system life. Even small buffers can prevent on/off cycles and improve operational stability. Additionally, connecting electrolysers to the grid or other renewable energy sources offers flexibility to draw supplemental power or respond to the market. Research into smart control strategies of such systems can explore the LCOH optimization based on forecasts of wind availability, electricity prices, and degradation.

- **Advanced Time-Resolved System Modelling:** Future work should incorporate transient behaviour and finer time steps to better capture the dynamic response of multi-stack PEM electrolyser systems. This could involve integrating power input, degradation, and economic factors into a unified Simulink model, simulating multiple stacks. Such modelling would enable quantification of effects like thermal cycling, pressure swings, and membrane stress

under realistic conditions, and if the data is available, their impact on degradation. Prior studies have developed dynamic PEM electrolyser models for this purpose (Sood et al., 2020) and extending them to multi-stack systems over long periods with degradation is a logical next step.

- **Advanced Control and Optimization strategies:** This study explored three fixed operational strategies. Future research should explore the development of real-time optimization-based approaches to minimize the LCOH. Instead of manually testing scenarios, optimization frameworks can identify cost-effective strategies under constraints like power availability and degradation limits.

- **Long-Term Degradation Testing**: Empirical data under variable loads is still limited. Long-duration experiments at relevant scale that use renewable profiles are needed to quantify degradation effects such as start-stop cycles and partial load idling (Martínez López et al., 2023)(Schofield et al., 2024). These results will help calibrate and validate degradation models used in future simulations.

- **Advanced Techno-Economic Analysis:** Future work should take a more integrated approach, combining detailed modelling of offshore PEM electrolyser systems with full economic evaluation over the system's lifetime. This means coupling technical models with financial ones. The advanced analysis should include dynamic electricity prices, cost of offshore infrastructure, BoP degradation and maintenance, cost of downtime, cost of potential integration with batteries or storage and operational planning. This will give a more realistic view of the operation and the LCOH. Adding lifecycle assessment would further broaden the analysis. This also allows researchers to compare trade-offs, such as investing in electricity storage vs. improving stack durability. Also, it would allow meaningful evaluation of project economics under different price scenarios.

I hope this thesis and future work serve as a spark in the great flame of green hydrogen, lighting the way for the energy transition.

# Bibliography


Abdin, Z., Webb, C. J., & Gray, E. MacA. (2015). Modelling and simulation of a proton exchange membrane (PEM) electrolyser cell. International Journal of Hydrogen Energy, 40(39), 13243–13257. https://doi.org/10.1016/j.ijhydene.2015.07.129

Abdol Rahim, A. H., Tijani, A. S., Kamarudin, S. K., & Hanapi, S. (2016). An overview of polymer electrolyte membrane electrolyzer for hydrogen production: Modeling and mass transport. Journal of Power Sources, 309, 56–65. https://doi.org/10.1016/j.jpowsour.2016.01.012

Acevedo, Y., Prosser, J., Huya-Kouadio, J., McNamara, K., & James, B. (2023). Hydrogen Production Cost with Alkaline Electrolysis. OSTI OAI (U.S. Department of Energy). https://doi.org/10.2172/2203367

Alia, Shaun. M., Reeves, K. S., Cullen, D. A., Yu, H., Kropf, A. J., Kariuki, N., Park, J. H., & Myers, D. J. (2024). Simulated Start-Stop and the Impact of Catalyst Layer Redox on Degradation and Performance Loss in Low-Temperature Electrolysis. Journal of the Electrochemical Society, 171(4), 044503. https://doi.org/10.1149/1945-7111/ad2bea

Alia, Shaun. M., Stariha, S., & Borup, R. L. (2019). Electrolyzer Durability at Low Catalyst Loading and with Dynamic Operation. Journal of the Electrochemical Society, 166(15), F1164–F1172. https://doi.org/10.1149/2.0231915jes

Alk Electrolyser Stack and Electrolyte System | Nel Hydrogen. (2024, August). Nel Hydrogen. https://nelhydrogen.com/resources/a485-series-alkaline-electrolyser-stack-and-electrolyte-system-module/

Becker, H., Murawski, J., Shinde, D. V., Stephens, I. E. L., Hinds, G., & Smith, G. (2023). Impact of impurities on water electrolysis: a review. Sustainable Energy & Fuels, 7(7), 1565–1603. https://doi.org/10.1039/d2se01517j

Bornemann, L., Lange, J., & Kaltschmitt, M. (2024). Optimizing temperature and pressure in PEM electrolyzers: A model-based approach to enhanced efficiency in integrated energy systems. Energy Conversion and Management, 325, 119338. https://doi.org/10.1016/j.enconman.2024.119338

Bristowe, G., & Smallbone, A. (2021). The Key Techno-Economic and Manufacturing Drivers for Reducing the Cost of Power-to-Gas and a Hydrogen-Enabled Energy System. Hydrogen, 2(3), 273–300. https://doi.org/10.3390/hydrogen2030015

Buttler, A., & Spliethoff, H. (2018). Current status of water electrolysis for energy storage, grid balancing and sector coupling via power-to-gas and power-to-liquids: a review. Renewable and Sustainable Energy Reviews, 82, 2440–2454. https://doi.org/10.1016/j.rser.2017.09.003

Cable installation vessels: costs and operating parameters? (2023, January 6). Thunder Said Energy. https://thundersaidenergy.com/downloads/cable-installation-vessels-costs-and-operating-parameters/

Carmo, M., Fritz, D. L., Mergel, J., & Stolten, D. (2013). A comprehensive review on PEM water electrolysis. International Journal of Hydrogen Energy, 38(12), 4901–4934. https://doi.org/10.1016/j.ijhydene.2013.01.151

C.Y. Biaku, Dale, N., Mann, M. D., Hossein Salehfar, Peters, A., & Han, T. (2008). A semiempirical study of the temperature dependence of the anode charge transfer coefficient of a 6kW PEM electrolyzer. 33(16), 4247–4254. https://doi.org/10.1016/j.ijhydene.2008.06.006

Cherevko, S., Geiger, S., Kasian, O., Mingers, A., & Mayrhofer, K. J. J. (2016). Oxygen evolution activity and stability of iridium in acidic media. Part 1 – Metallic iridium. Journal of Electroanalytical Chemistry, 773, 69–78. https://doi.org/10.1016/j.jelechem.2016.04.033

CHOI, P. (2004). A simple model for solid polymer electrolyte (SPE) water electrolysis. Solid State Ionics, 175(1-4), 535–539. https://doi.org/10.1016/j.ssi.2004.01.076

Collins, L. (2023). World's largest solid-oxide hydrogen electrolyser installed at Nasa facility in California. Hydrogeninsight.com. https://www.hydrogeninsight.com/electrolysers/world-s-largest-solid-oxide-hydrogen-electrolyser-installed-at-nasa-facility-in-california/2-1-1445358

Collins, L. (2024). "Global risk" | Hydrogen electrolysers could degrade faster than stated by manufacturers due to insufficient testing: BNEF. Hydrogeninsight.com. https://www.hydrogeninsight.com/electrolysers/global-risk-hydrogen-electrolysers-could-degrade-faster-than-stated-by-manufacturers-due-to-insufficient-testing-bnef/2-1-1733111

Dharini, T., Kuppusami, P., & Kirubaharan, A. M. K. (2023, January 1). Nanocomposite ceramic diffusion barrier coatings for nuclear vitrification furnace (R. K. Gupta et al., Eds.). ScienceDirect; Elsevier. https://www.sciencedirect.com/science/article/abs/pii/B9780323996594000206

Dong, B., Zhang, Z., Tang, Y., & Wang, X. (2023). Optimal operation of grid-connected electrolyzers integrated with renewable energy and battery storage. Applied Energy, 336, 120764. https://doi.org/10.1016/j.apenergy.2023.120764

Dong, Y., Ma, S., Han, Z., Bai, J., & Wang, Q. (2023). Research on the adaptability of proton exchange membrane electrolysis in green hydrogen–electric coupling system under multi-operating conditions. Energy Reports, 9, 4789–4798. https://doi.org/10.1016/j.egyr.2023.03.119

Du, N., Roy, C., Peach, R., Turnbull, M., Thiele, S., & Bock, C. (2022). Anion-Exchange Membrane Water Electrolyzers. Chemical Reviews, 122(13), 11830–11895. https://doi.org/10.1021/acs.chemrev.1c00854

Dwi, S., Nikmatin Sholichah, S., Susilowati, S., Sukirmiyadi, A., Mohd, N., & Hamzah Fansuri. (2023). Crystallography Analysis on LSCF and LSM-based Perovskite Oxides. Technium Romanian Journal of Applied Sciences and Technology, 16, 405–410. https://doi.org/10.47577/technium.v16i.10019

Electric Power Research Institute (EPRI). (2022). Water electrolyzer stack degradation: Insights from field data and implications for durability testing (Product ID 3002025148). EPRI. https://www.epri.com/research/products/000000003002025148

Electrolysis in the North Sea: our role and the role of green hydrogen. (2025). Gasunie. https://www.gasunie.nl/en/expertise/hydrogen/offshore-hydrogen/electrolysis-in-the-north-sea-our-role-and-the-role-of-green-hydrogen

Emam, A. S., Hamdan, M. O., Abu-Nabah, B. A., & Emad Elnajjar. (2024). A review on recent trends, challenges, and innovations in alkaline water electrolysis. International Journal of Hydrogen Energy, 64, 599–625. https://doi.org/10.1016/j.ijhydene.2024.03.238

Environmental and Energy Study Institute. (2021, July 22). Fossil Fuels. Eesi.org. https://www.eesi.org/topics/fossil-fuels/description

Espinosa-López, M., Darras, C., Poggi, P., Glises, R., Baucour, P., Rakotondrainibe, A., Besse, S., & Serre-Combe, P. (2018). Modelling and experimental validation of a 46 kW PEM high pressure water electrolyzer. Renewable Energy, 119, 160–173. https://doi.org/10.1016/j.renene.2017.11.081

Evaluation of the levelised cost of hydrogen based on proposed electrolyser projects in the Netherlands. (2024, May 30). 1848.nl. https://app.1848.nl/document/tkapi/504159

European Hydrogen Observatory. (2024). The European hydrogen market landscape. https://observatory.clean-hydrogen.europa.eu/sites/default/files/2024-11/The%20European%20hydrogen%20market%20landscape_November%202024.pdf

Falcão, D. S., & Pinto, A. M. F. R. (2020). A review on PEM electrolyzer modelling: Guidelines for beginners. Journal of Cleaner Production, 261, 121184. https://doi.org/10.1016/j.jclepro.2020.121184

Feng, Q., Yuan, X., Liu, G., Wei, B., Zhang, Z., Li, H., & Wang, H. (2017). A review of proton exchange membrane water electrolysis on degradation mechanisms and mitigation strategies. Journal of Power Sources, 366, 33–55. https://doi.org/10.1016/j.jpowsour.2017.09.006

Flis, G., & Wakim, G. (2023). Solid Oxide Electrolysis: A Technology Status Assessment. https://cdn.catf.us/wp-content/uploads/2023/11/15092028/solid-oxide-electrolysis-report.pdf

Frensch, S. H., Fouda-Onana, F., Serre, G., Thoby, D., Araya, S. S., & Kær, S. K. (2019). Influence of the operation mode on PEM water electrolysis degradation. International Journal of Hydrogen Energy, 44(57), 29889–29898. https://doi.org/10.1016/j.ijhydene.2019.09.169

Frensch, S. H., Serre, G., Fouda-Onana, F., Jensen, H. C., Christensen, M. L., Araya, S. S., & Kær, S. K. (2019). Impact of iron and hydrogen peroxide on membrane degradation for polymer electrolyte membrane water electrolysis: Computational and experimental investigation on fluoride emission. Journal of Power Sources, 420, 54–62. https://doi.org/10.1016/j.jpowsour.2019.02.076

FuelCell Energy. (2025). Solid Oxide Electrolysis | FuelCell Energy. https://www.fuelcellenergy.com/applications/solid-oxide-electrolysis

Gas for Climate. (n.d.). Gas for Climate 2050: A pathway to climate neutrality. Retrieved July 6, 2025, from https://gasforclimate2050.eu/

Glenk, G., & Reichelstein, S. (2019). Economics of converting renewable power to hydrogen. Nature Energy, 4(3), 216–222. https://doi.org/10.1038/s41560-019-0326-1

Gonçalves, J. M., Kumar, A., da Silva, M. I., Toma, H. E., Martins, P. R., Araki, K., Bertotti, M., & Angnes, L. (2021). Nanoporous Gold-Based Materials for Electrochemical Energy Storage and Conversion. Energy Technology, 9(5), 2000927. https://doi.org/10.1002/ente.202000927

Harrison, K. W., Remick, R., Martin, G. D., & Hoskin, A. (2010, January). Hydrogen production: Fundamentals and case study summaries (Conference Paper No. NREL/CP-550-47302). National Renewable Energy Laboratory. https://www.nrel.gov/docs/fy10osti/47302.pdf

Hernández-Gómez, Á., Ramirez, V., & Guilbert, D. (2020). Investigation of PEM electrolyzer modeling: Electrical domain, efficiency, and specific energy consumption. International Journal of Hydrogen Energy, 45(29), 14625–14639. https://doi.org/10.1016/j.ijhydene.2020.03.195

Hfto, D., & Gilbert, A. (2024). Campbell Howe (DOE Loan Program Office) Peer Reviewed by: Neha Rustagi. Strategic Analysis, Inc. https://www.hydrogen.energy.gov/docs/hydrogenprogramlibraries/pdfs/24005-clean-hydrogen-production-cost-pem-electrolyzer.pdf

Holladay, J. D., Hu, J., King, D. L., & Wang, Y. (2009). An overview of hydrogen production technologies. Catalysis Today, 139(4), 244–260. https://doi.org/10.1016/j.cattod.2008.08.039

Hongsirikarn, K., Goodwin, J. G., Greenway, S., & Creager, S. (2010). Effect of cations (Na+, Ca2+, Fe3+) on the conductivity of a Nafion membrane. Journal of Power Sources, 195(21), 7213–7220. https://doi.org/10.1016/j.jpowsour.2010.05.005

Hydrogen Council, & McKinsey & Company. (2024). Hydrogen Insights 2024: Global hydrogen flows and project pipeline analysis. Hydrogen Council.

Hydrogen Council, & McKinsey & Company. (2024). Hydrogen insights 2024. Hydrogen Council. https://hydrogencouncil.com/wp-content/uploads/2024/09/Hydrogen-Insights-2024.pdf

Hydrogen pipelines' CAPEX by type 2021. (n.d.). Statista. https://www.statista.com/statistics/1220856/capex-new-retrofitted-h2-pipelines-by-type/

Idealhy. (n.d.). idealhy.eu - Liquid Hydrogen Outline. https://www.idealhy.eu/index.php?page=lh2_outline

IEA. (2021). Global Hydrogen Review 2021 – Analysis. IEA. https://www.iea.org/reports/global-hydrogen-review-2021

IEA. (2023, July 10). Electrolysers - Energy System. IEA. https://www.iea.org/energy-system/low-emission-fuels/electrolysers

International Energy Agency. (2021). Global Hydrogen Review 2021. IEA. https://www.iea.org/reports/global-hydrogen-review-2021

International Renewable Energy Agency (IRENA). (2021). Green hydrogen supply: A guide to policy making. IRENA. https://h2chile.cl/wpcontent/uploads/2024/02/IRENA_Green_Hydrogen_Supply_2021.pdf

IRENA. (2020). GREEN HYDROGEN COST REDUCTION SCALING UP ELECTROLYSERS CLIMATE GOAL $H_2O_2$. https://www.irena.org/-/media/Files/IRENA/Agency/Publication/2020/Dec/IRENA_Green_hydrogen_cost_2020.pdf

Ji Eun Park, Sun Kil Kang, Oh, S.-H., Kim, J.-K., Myung Su Lim, Ahn, C.-Y., Cho, Y.-H., & Sung, Y.-E. (2019). High-performance anion-exchange membrane water electrolysis. 295, 99–106. https://doi.org/10.1016/j.electacta.2018.10.143

Kelly, M. J., Fafilek, G., Besenhard, J., Kronberger, H., & Nauer, G. (2005). Contaminant absorption and conductivity in polymer electrolyte membranes. Journal of Power Sources, 145(2), 249–252. https://doi.org/10.1016/j.jpowsour.2005.01.064

Knop, V. (2022). A World Of Energy - Alkaline electrolyser. Awoe.net. https://awoe.net/Water-Electrolysis-Alkaline-Technology.html

Koch, S., Disch, J., Kilian, S. K., Han, Y., Metzler, L., Tengattini, A., Helfen, L., Schulz, M., Breitwieser, M., & Vierrath, S. (2022). Water management in anion-exchange membrane water electrolyzers under dry cathode operation. RSC Advances, 12(32), 20778–20784. https://doi.org/10.1039/D2RA03846C

Lamagna, M., Groppi, D., & Nastasi, B. (2023). Reversible solid oxide cells applications to the building sector. International Journal of Hydrogen Energy. https://doi.org/10.1016/j.ijhydene.2023.03.387

Li, N., Araya, S. S., & Kær, S. K. (2021). Investigating low and high load cycling tests as accelerated stress tests for proton exchange membrane water electrolysis. Electrochimica Acta, 370, 137748. https://doi.org/10.1016/j.electacta.2021.137748

Li, W., Tian, H., Ma, L., Wang, Y., Liu, X., & Gao, X. (2022). Low-temperature water electrolysis: fundamentals, progress, and new strategies. Materials Advances, 3(14), 5598–5644. https://doi.org/10.1039/D2MA00185C

Liso, V., Savoia, G., Araya, S. S., Cinti, G., & Kær, S. K. (2018). Modelling and Experimental Analysis of a Polymer Electrolyte Membrane Water Electrolysis Cell at Different Operating Temperatures. Energies, 11(12), 3273. https://doi.org/10.3390/en11123273

Lu, X., Du, B., Zhou, S., Zhu, W., Li, Y., Yang, Y., Xie, C., Zhao, B., Zhang, L., Song, J., & Deng, Z. (2023). Optimization of power allocation for wind-hydrogen system multi-stack PEM water electrolyzer considering degradation conditions. International Journal of Hydrogen Energy, 48(15), 5850–5872. https://doi.org/10.1016/j.ijhydene.2022.11.092

Ma, S., Li, L., Kohama, R., Nakajima, H., & Ito, K. (2024). Effects of temperature and pressure on the limiting current density of PEM electrolysis cells based on a theoretical prediction model and experiments. International Journal of Hydrogen Energy, 71, 1428–1441. https://doi.org/10.1016/j.ijhydene.2024.05.345

Majumdar, A., Haas, M., Elliot, I., & Nazari, S. (2023). Control and control-oriented modeling of PEM water electrolyzers: A review. International Journal of Hydrogen Energy, 48(79), 30621–30641. https://doi.org/10.1016/j.ijhydene.2023.04.204

Martínez López, J. A., Gallet, B., Götz, M., Rihko-Struckmann, L., & Sundmacher, K. (2023). PEM electrolysis under variable renewable power: Effects on degradation and system design. Journal of Power Sources, 560, 232583. https://doi.org/10.1016/j.jpowsour.2022.232583

Mesbah, A., Streif, S., & Findeisen, R. (2017). Stochastic nonlinear model predictive control: A survey and perspective towards advanced applications. Annual Reviews in Control, 44, 221–236. https://doi.org/10.1016/j.arcontrol.2017.09.002

Millet, P., & Grigoriev, S. (2013). Water Electrolysis Technologies. Renewable Hydrogen Technologies, 19–41. https://doi.org/10.1016/b978-0-444-56352-1.00002-7

Mo, J., Kang, Z., Yang, G., Retterer, S. T., Cullen, D. A., Toops, T. J., Green, J. B., & Zhang, F.-Y. (2016). Thin liquid/gas diffusion layers for high-efficiency hydrogen production from water splitting. Applied Energy, 177, 817–822. https://doi.org/10.1016/j.apenergy.2016.05.154

Mustafa Ergin Şahin. (2024). An Overview of Different Water Electrolyzer Types for Hydrogen Production. Energies, 17(19), 4944–4944. https://doi.org/10.3390/en17194944

Nasser, M., Megahed, T. F., Ookawara, S., & Hassan, H. (2022). A review of water electrolysis–based systems for hydrogen production using hybrid/solar/wind energy systems. Environmental Science and Pollution Research, 29. https://doi.org/10.1007/s11356-022-23323-y

NortH2. (n.d.). Kickstarting the green hydrogen economy. Retrieved July 6, 2025, from https://www.north2.eu/

Offshore Energy Hubs: Blueprints with Offshore Electrolysis. (2021). North Sea Wind Power Hub. https://northseawindpowerhub.eu/knowledge/offshore-energy-hubs-blueprints-with-offshore-electrolysis

Ojong, E. T., Kwan, J. T. H., Nouri-Khorasani, A., Bonakdarpour, A., Wilkinson, D. P., & Smolinka, T. (2017). Development of an experimentally validated semi-empirical fully-coupled performance model of a PEM electrolysis cell with a 3-D structured porous transport layer. International Journal of Hydrogen Energy, 42(41), 25831–25847. https://doi.org/10.1016/j.ijhydene.2017.08.183

Onda, K., Murakami, T., Hikosaka, T., Kobayashi, M., Notu, R., & Ito, K. (2002). Performance Analysis of Polymer-Electrolyte Water Electrolysis Cell at a Small-Unit Test Cell and Performance Prediction of Large Stacked Cell. Journal of the Electrochemical Society, 149(8), A1069. https://doi.org/10.1149/1.1492287

PEM Electrolyser - MC Series. (2019, May 7). Nel Hydrogen. https://nelhydrogen.com/product/mc-series-electrolyser/

PEM Electrolysis System - MATLAB & Simulink. (2018). MathWorks. https://nl.mathworks.com/help/simscape/ug/pem-electrolysis-system.html

PEM vs. Alkaline: Re-examining market perceptions of electrolyzer technologies in an evolving landscape. (2024). Electric Hydrogen. https://eh2.com/wp-content/uploads/2025/01/Final_PEM_vs_Alkaline_December_2024_Whitepaper.pdf

PEM Water Electrolysis System (100 kW). (2024). FuelCellStore.com. https://www.fuelcellstore.com/pem-water-electrolysis-system-100kw

Pfennig, M., Schiffer, B., & Clees, T. (2024). Thermodynamical and electrochemical model of a PEM electrolyzer plant in the megawatt range with a literature analysis of the fitting parameters. International Journal of Hydrogen Energy. https://doi.org/10.1016/j.ijhydene.2024.04.335

Poshydon | Green Hydrogen Energy. (2024). Poshydon.com. https://poshydon.com/nl/home/

Products Overview - Enapter. (2025, June 21). Enapter. https://www.enapter.com/en/products/

Program Records | Hydrogen Program. (2025). Energy.gov. https://www.hydrogen.energy.gov/home/program-records

Rakousky, C., Reimer, U., Wippermann, K., Kuhri, S., Carmo, M., Lueke, W., & Stolten, D. (2017). Polymer electrolyte membrane water electrolysis: Restraining degradation in the presence of fluctuating power. Journal of Power Sources, 342, 38–47. https://doi.org/10.1016/j.jpowsour.2016.11.118

Reksten, A. H., Thomassen, M. S., Møller-Holst, S., & Sundseth, K. (2022). Projecting the future cost of PEM and alkaline water electrolysers; a CAPEX model including electrolyser plant size and technology development. International Journal of Hydrogen Energy, 47(90), 38106–38113. https://doi.org/10.1016/j.ijhydene.2022.08.306

Ren, P., Pei, P., Li, Y., Wu, Z., Chen, D., & Huang, S. (2020). Degradation mechanisms of proton exchange membrane fuel cell under typical automotive operating conditions. Progress in Energy and Combustion Science, 80, 100859. https://doi.org/10.1016/j.pecs.2020.100859

Saba, S. M., Müller, M., Robinius, M., & Stolten, D. (2018). The investment costs of electrolysis – A comparison of cost studies from the past 30 years. International Journal of Hydrogen Energy, 43(3), 1209–1223. https://doi.org/10.1016/j.ijhydene.2017.11.115

Sadeghi Alavijeh, A., Goulet, M.-A., Khorasany, R. M. H., Ghataurah, J., Lim, C., Lauritzen, M., Kjeang, E., Wang, G. G., & Rajapakse, R. K. N. D. (2014). Decay in Mechanical Properties of Catalyst Coated Membranes Subjected to Combined Chemical and Mechanical Membrane Degradation. Fuel Cells, 15(1), 204–213. https://doi.org/10.1002/fuce.201400040

Salehmin, M. N. I., Husaini, T., Goh, J., & Sulong, A. B. (2022). High-pressure PEM water electrolyser: A review on challenges and mitigation strategies towards green and low-cost hydrogen production. Energy Conversion and Management, 268, 115985. https://doi.org/10.1016/j.enconman.2022.115985

Sampangi, S. K., SUB, R., Reddy, S. D., Bhagawan, D., & Vurimindi, H. (2017). Synthesis of polysulfone and zirconium oxide coated asbestos composite separators for alkaline water electrolysis. Chemical Central. https://www.researchgate.net/publication/317418102

Sapountzi, F. M., Gracia, J. M., Weststrate, C. J., Fredriksson, H. O. A., & Niemantsverdriet, J. W. (2017). Electrocatalysts for the generation of hydrogen, oxygen and synthesis gas. Progress in Energy and Combustion Science, 58, 1–35. https://doi.org/10.1016/j.pecs.2016.09.001

Scheepers, F., Stähler, M., Stähler, A., Rauls, E., Müller, M., Carmo, M., & Lehnert, W. (2020). Improving the Efficiency of PEM Electrolyzers through Membrane-Specific Pressure Optimization. Energies, 13(3), 612. https://doi.org/10.3390/en13030612

Schofield, L., Paren, B., Macdonald, R., Shao-Horn, Y., & Mallapragada, D. (2024). Dynamic Optimization of Proton Exchange Membrane Water Electrolyzers Considering Usage-Based Degradation. ArXiv.org. https://arxiv.org/abs/2405.06766

Schofield, L., Paren, B., Macdonald, R., Shao-Horn, Y., & Mallapragada, D. (2024). Dynamic optimization of proton exchange membrane water electrolyzers considering usage-based degradation. AIChE Journal. https://doi.org/10.1002/aic.18635

Schofield, M., Lam, C. Q., Verma, A., Brealey, D., & Shah, N. (2024). Modelling PEM electrolyzer lifetime under dynamic operating conditions for renewable hydrogen production. Renewable Energy, 219, 1197–1212. https://doi.org/10.1016/j.renene.2023.11.030

Scott, K. (2019). Chapter 1 Introduction to Electrolysis, Electrolysers and Hydrogen Production. Royal Society of Chemistry. https://doi.org/10.1039/9781788016049-00001

Sezer, N., Sertac Bayhan, Ugur Fesli, & Sanfilippo, A. (2025). A comprehensive review of the state-of-the-art of proton exchange membrane water electrolysis. Materials Science for Energy Technologies, 8, 44–65. https://doi.org/10.1016/j.mset.2024.07.006

# List of Figures

Figure 1-1: Schematic overview of thesis models ..... 5
Figure 2-1: Pourbaix diagram of water (Gonçalves et al., 2021) ..... 9
Figure 2-2: Electrolysis technologies for hydrogen production (Mustafa Ergin Şahin, 2024) ..... 12
Figure 2-3: Alkaline electrolyser cell (IRENA, 2020) ..... 12
Figure 2-4: AEM electrolyser cell (IRENA, 2020) ..... 14
Figure 2-5: SOEC electrolyser cell (IRENA, 2020) ..... 15
Figure 2-6: PEM electrolyser cell (IRENA, 2020) ..... 16
Figure 2-7 PEM electrolyser BoP (IRENA, 2020) ..... 20
Figure 2-8: PEM-cell components (Sezer et al., 2025) ..... 25
Figure 2-9: Example of a PEM electrolyser polarization curve and its components (Ojong et al., 2017) ..... 32
Figure 2-10: PEM electrolyser model classification (Hernández-Gómez et al., 2020) ..... 33
Figure 2-11: Number of published PEM electrolyser model works (Hernández-Gómez et al., 2020) ..... 35
Figure 2-12 PEM electrolyser system cost breakdown (IRENA, 2020) ..... 36
Figure 3-1: PEM electrolyser Simulink Model (MATLAB, 2018) ..... 42
Figure 3-2: Simulated polarization curve ..... 48
Figure 3-3: Polarization curve as found by (Liso et al., 2018) ..... 49
Figure 3-4: Polarization curve as found by (8. (Sapountzi et al., 2017) ..... 49
Figure 3-5: Simulated $H_2$ production rate vs current density ..... 50
Figure 3-6: Simulated $H_2$ production rate vs power input ..... 50
Figure 3-7: Simulated efficiency vs current density ..... 51
Figure 3-8: Simulated voltage efficiency vs current density ..... 52
Figure 3-9: Simulated Faradaic efficiency vs current density ..... 52
Figure 3-10: Simulated total efficiency vs power input ..... 53
Figure 3-11: Experimental efficiency curve of PosHydon project (Poshydon, 2024) ..... 53
Figure 3-12: Not degraded and degraded simulated efficiency curves as found by (Lu et al., 2023) ..... 54
Figure 4-1: Plot of initial collected degradation data ..... 61
Figure 4-2: Degradation relation according to (Schofield et al., 2024) ..... 61
Figure 5-1: Schematic overview of Operational Strategy Model ..... 67
Figure 5-2: Upper and lower bound of the degradation relation ..... 73
Figure 5-3: Sensitivity analysis of degradation for equal distribution ..... 74
Figure 5-4: Sensitivity analysis of stack replacement costs ..... 76
Figure 5-5: Sensitivity analysis of electricity costs ..... 77
Figure 5-6: Sensitivity Analysis of the Setup for Equal Distribution Operation ..... 78

# List of Tables

Table 2-1: Electrolysis energy values ((Tsutsumi, n.d.). ..... 11
Table 2-2: PEM electrolyser half-cell reactions ..... 17
Table 2-3: PEM electrolyser materials ..... 17
Table 2-4: PEM electrolyser operating conditions ..... 19
Table 2-5 Overview of electrolyser technologies characteristics ..... 23
Table 2-6: PEM Components Functions and Materials ..... 26
Table 2-7: PEM electrolyser degradation mechanisms descriptions and consequences ..... 27
Table 2-8: Classification, probabilities and effects of PEM electrolyser degradation mechanisms (Wallnöfer-Ogris et al., 2024) ..... 29
Table 2-9: Influence of operating conditions of PEM electrolyser degradation (Wallnöfer-Ogris et al., 2024) ..... 31
Table 2-10: PEM Electrolyser CAPEX breakdown ..... 37
Table 3-1: Fixed and fitted model parameters ..... 47
Table 4-1: Data sample analysis results ..... 63
Table 5-1: Equal distribution; system results ..... 69
Table 5-2: Equal distribution; stack results ..... 69
Table 5-3: Serial distribution; system results ..... 70
Table 5-4: Serial distribution; stack results ..... 70
Table 5-5: Efficiency distribution; system results ..... 71
Table 5-6: Efficiency distribution; stack results ..... 71
Table 5-7: LCOH data from literature ..... 72
Table 5-8: Influence of degradation deviation on the LCOH ..... 74
Table 5-9: LCOH with power an on/off cycle degradation ..... 75
Table 5-10: Stack Replacement Cost Sensitivity ..... 76

# Appendix A – Alkaline Electrolysers

This appendix gives a more in-depth analysis of Alkaline electrolysers.

**Alkaline Electrolysers**

Alkaline electrolysis is the most mature and widely utilized technology for industrial hydrogen production. In 1939, the first large-scale Alkaline electrolyser plant went into operation and these days multi megawatt Alkaline electrolyser installations are not uncommon (Shiva Kumar & Lim, 2022). In 2023 the total installed capacity of Alkaline electrolysers worldwide was 840MW (IEA, 2023). Alkaline electrolysis is known for its relative simplicity and cost-effectiveness (Seddiq Sebbahi et al., 2024).

An Alkaline cell comprises of two electrodes, the Cathode and Anode, immersed in a liquid Alkaline electrolyte and separated by a diaphragm. A schematic review of an Alkaline cell can be seen in Figure A-1.

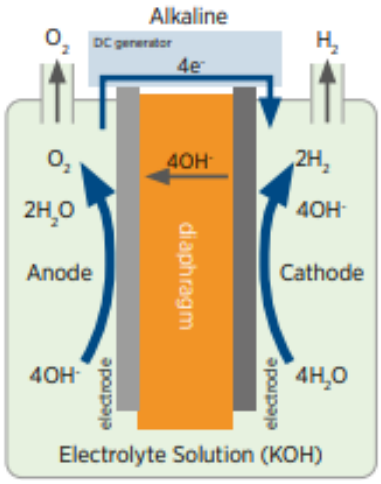


*Figure A-1: Alkaline electrolyser cell (IRENA, 2020)*

**Alkaline electrolysers - Electrochemical Reactions**

The electrochemical reactions of an Alkaline electrolysers consist of two individual half-cell reactions. The hydrogen evolution reaction (HER) at the Cathode and oxygen evolution reaction (OER) at the Anode. At Cathode water ($H_2O$) is reduced to hydrogen ($H^2$) and hydroxyl ions ($OH^-$), the hydroxyl ions are transferred under the influence of the electric circuit from the negative Cathode to the positive Anode side trough the diaphragm. At the Anode the hydroxyl ions ($OH^-$) are discharged to produce water ($H_2O$) and oxygen ($O_2$). The electrons ($e^-$) produced at this reaction travel via an external circuit to the Cathode (Knop, 2022).

The half-cell reaction of the Cathode is given by equation (A.1) and of the Anode by equation (A.2) One can recognise these reactions from the Alkaline region in the Pourbaix diagram in Figure A-1.

$$4H_2O\ (l) + 4e^-(aq) \rightarrow 2H_2(g) + 4OH^-(aq) \qquad (A.1)$$

$$4OH^-(aq) \rightarrow 2H_2O(g) + O^2(g) + 4e^-$$

*(A.2)*

The overall cell reaction is given by equation (A.3).

$$H_2O\ (l) \rightarrow H_2(g) + \frac{1}{2}O_2(g)$$

*(A.3)*

An overview of the Alkaline reactions can be found in Table A-1.

*Table A-1: Alkaline electrolyser half-cell reactions*

| Reaction | Equation |
|---|---|
| OER | $2OH^-(aq) \rightarrow 2H_2O(g) + 2O^2(g) + 2e^-$ |
| HER | $2H_2O\ (l) + 2e^-(aq) \rightarrow H_2(g) + 2OH^-(aq)$ |
| Total | $H_2O\ (l) \rightarrow H_2(g) + \frac{1}{2}O_2(g)$ |

**Alkaline electrolysers - Materials**

Alkaline electrolysers have a liquid electrolyte made out of a highly concentrated Alkaline solution of KOH/NaOH, typically around 5 mol/Liter (IEA, 2023)(Sampangi et al., 2017). The ionic charge carrier is a hydroxyl ion ($OH^-$). The separator diaphragm is usually asbestos/$ZrO_2$-based and has a porous structure to allow the hydroxyl ions to permeate from the Cathode to the Anode and separate the liquid and gases. The Anode and Cathode of an Alkaline electrolyser are often made of nickel (Ni) coated perforated stainless steel. Nickel functions as a catalyst and provides resistance to corrosion in the highly Alkaline environment of the electrolyser, which helps extend the lifespan of the electrodes. Nickel is a good conductor of electricity, which is essential for efficient electrolysis. The stainless-steel base provides mechanical strength and is cost-effective compared to for example a platinum base (Knop, 2022). The perforated design increases the surface area, enhancing the efficiency of the electrochemical reactions. An overview of the Alkaline materials can be found in Table A-2.

*Table A-2 Alkaline electrolyser materials*

| Component | Material |
|---|---|
| Electrolyte | KOH/NaOH solution (5M) |
| Anode | Nickel coated perforated stainless steel |
| Cathode | Nickel coated perforated stainless steel |
| Separator | Asbestos/ZrO2-based diaphragm |

**Alkaline electrolysers - Operating conditions**

At higher temperatures the electrochemical reactions are more favorable. However, due to the liquid electrolyte, Alkaline electrolysers are thermally limited by the boiling temperature of water. Also, the Ni-coated electrodes and porous diaphragms are reasonably durable up to about 90 $^0$C (Seddiq Sebbahi et al., 2024). Therefore, Alkaline electrolysers typically operate at temperatures between 70-90 $^0$C (IEA, 2023).

Alkaline electrolysers operate at low to moderate pressures, usually between 1 to 30 bars [2]. Typical Alkaline diaphragms are not tolerant of high-pressure differentials, and higher pressure increases the risk of gas-crossover where hydrogen mixes with oxygen creating a highly flammable gas. Also, the

liquid electrolyte increases the risk of leaks under higher pressure (Seddiq Sebbahi et al., 2024). Thicker diagrams can increase pressure tolerance but also increase resistant potential, reducing efficiency.

Alkaline electrolysers have a relatively low current density of around 0.2-0.8 A/cm$^2$ (IEA, 2023). Mainly because the HER and OER are intrinsically slower in an Alkaline electrolyte than an acidic electrolyte such as in PEM electrolysers (Millet & Grigoriev, 2013). The ionic conductivity of the hydroxyls ($OH^-$) is limited compared to other charge carriers such as protons ($H^+$). Also, as mentioned, thick diaphragms increase resistance. Furthermore, hydrogen and oxygen can form bubbles at the electrode. Due to the liquid electrolyte these bubbles are trapped easily. Bubbles block the active sites, limiting mass transfer and increasing the voltage losses (IRENA, 2020).

Alkaline electrolysers have a voltage range of 1.4-3 V (IEA, 2023). The catalysts used in Alkaline electrolysers are often non-precious metal catalysts (Ni/Fe). These catalysts are less active and thus require a higher overpotential. Together with the voltage losses mentioned before, the voltage range of Alkaline electrolysers is relatively high. At higher voltage the liquid electrolyte can heat up quickly requiring thermal management to reduce the risk of overheating (Zeng & Zhang, 2010).

The hydrogen purity of Alkaline electrolysers ranges from 99.9%-99.9998% (IEA, 2023). The diaphragm cannot completely block gases thus oxygen diffuses to the hydrogen side and vice versa. Also, hydrogen and oxygen bubbles formed at the electrode can drag small droplets of the liquid electrolyte into the output gas stream reducing the purity (Carmo et al., 2013).

The expected lifetime of Alkaline electrolysers is around 60.000 hours (IEA, 2023). The electrolysers mainly degrade due to corrosion at the Anode and the formation of $Ni(OH)_2$ which reduces catalyst activity. The diaphragm can degrade due to chemical attack or mechanical stress and the electrolyte can be contaminated by nickel, iron or other contaminants from the environment (Zeng & Zhang, 2010)(Carmo et al., 2013).

Alkaline electrolysers tend to have some operation flexibility but are not ideal for fast grid balancing (Carmo et al., 2013). The cold start of an Alkaline electrolyser ranges from 10-50 minutes mainly due to the large thermal mass of the liquid electrolyte. Both the ionic conductivity and electrode activity depend heavily on temperature (IEA, 2023). The safe ramp rates for Alkaline electrolyser are typically between 30 seconds to a few minutes and are also limited by thermal inertia. Furthermore, the HER and OER require time to reach new steady-state. Ramping up too fast can cause local overheating and pressure imbalances. Ramping-down must deal with residual heat and requires cooling (Li et al., 2022).

Alkaline systems have an efficiency between 43-66% (IEA, 2023) which is relatively low. Mainly due to the large overpotentials in the stack as mentioned before, the power consumption of BoP and the low current density. An overview of the Alkaline operating conditions can be found in Table A-3.

*Table A-3 Alkaline electrolyser operating conditions*

| Operating condition | Range |
|---|---|
| Temperature | 70-90 [$^0$C] |
| Pressure | 1-30 [bar] |
| Current Density | 0.2-0.8 [A/cm$^2$] |
| Voltage | 1.4-3 [V] |
| Purity | 99.9%-99.9998% |
| Lifetime | 60.000 [hours] |
| Cold start | 10-50 [minutes] |
| Ramp-up/down | 30 seconds – a few minutes |
| Efficiency | 43-66% |

**Alkaline electrolysers - Balance of plants**

Alkaline electrolysers require a complex balance of plants. A water purification system is needed to create highly purified water and avoid electrolyte contamination and thus cell degradation. Temperature and pressure are controlled through a thermal and pressure management system. After electrolysis the $H_2$ and $O_2$ streams are dried and purified trough gas separation and drying units where contaminated hydrogen, and oxygen are separated, and water vapor is removed. For the power supply a rectifier is needed to convert AC to DC and transformers to perform volt adjustments if needed. What makes Alkaline BoP unique is the electrolyte management system consisting of electrolyte tanks and pumps to regulate the liquid electrolyte circulation (IRENA, 2020). An overview of an Alkaline BoP can be seen in Figure A-.

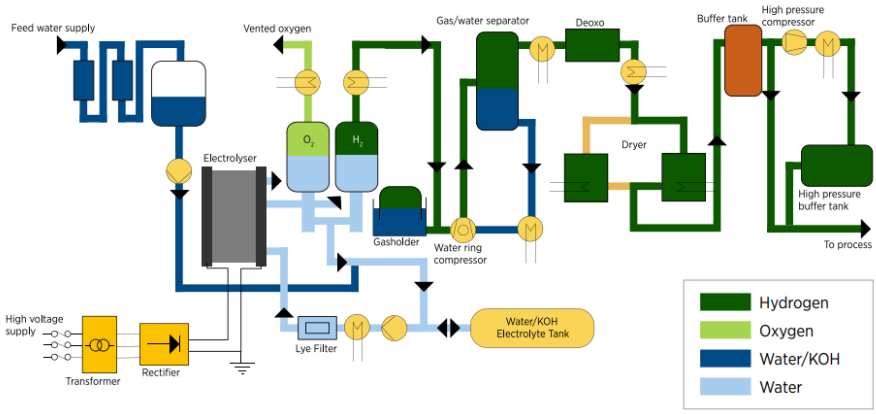


*Figure A-2 Alkaline electrolyser BoP (IRENA, 2020)*

**Alkaline electrolysers - Weight and dimensions**

Alkaline electrolysers are relatively heavy due to the large stack size, needed because of the low current density, and the relatively heavy liquid electrolyte. Also, the complex balance of plants makes that Alkaline systems have a large footprint. A 2.2MW Alkaline stack from NEL for example weighs 71.000 kg and has dimensions of approximately 14x4x4 meters (224m$^3$), this only includes the stack and electrolyte system, not the rest of the BoP (Nel Hydrogen, 2024).

**Alkaline electrolysers - CAPEX**

Although Alkaline technology is considered the most economical viable technology, Alkaline electrolysers are still expensive, especially compared to fossil fuel-based hydrogen production (Acevedo et al., 2023). Although data about stack or system costs is not widely available due to its

confidential nature, the International Renewable Energy Agency (IRENA, 2020) conducted thorough research on the capital costs of electrolyser systems. According to the International Renewable Energy Agency a minimum 10MW Alkaline systems costs 500-1000 USD/kW of which 45% for the stack components and 55% for the balance of plants. The power supply (i.e. rectifiers and transformers) make up for 50% of the BoP and the diaphragm and electrodes for 57% of the stack. Developments for cost reduction focus on increasing the current density, reducing diaphragm thickness and re-designing catalyst compositions and electrode architectures.

**Alkaline electrolysers - Challenges and technological developments**
The main challenges of Alkaline electrolysers are:

1. Limited current density and efficiency; Due to slower reaction kinetics in an Alkaline media and higher ohmic losses across the liquid electrolyte and diaphragm (Zeng & Zhang, 2010).
2. Gas crossover and hydrogen purity; Alkaline electrolysers have a relatively high gas-crossover, limiting its purity and increasing the risk of explosion due to the formation of a $H_2/O_2$ mixture (Li et al., 2022).
3. Limited dynamic operation and capabilities; The thermal inertia of the liquid electrolyte causes the Alkaline electrolyser to struggle ramping up and down quickly and perform cold starts or on/off cycles (Seddiq Sebbahi et al., 2024).

Recent research has focused on advancements in catalyst materials using non-precious metals to enhance efficiency and reduce the costs. Metal nitrides, such as titanium nitride (TiN) and molybdenum nitride (MoN) gained attention due to their impressive electrocatalytic properties, corrosion resistance and cost effectiveness showing competitive performance at lower cost (Emam et al., 2024). Zifron diaphragms could offer higher ionic conductivity, lower gas permeability and operation at higher current densities. Performance of Alkaline system is expected to increase in the future.

**In short:** Alkaline water electrolysis is the most mature and economically viable technology for industrial hydrogen production. However, it is hindered by key limitations such as low current density, slow electrochemical kinetics, and restricted dynamic flexibility. Its reliance on a bulky liquid electrolyte system and heavy balance of plant components results in large physical size and significant weight. These factors make Alkaline electrolysers less suitable for applications requiring rapid response or compact system design. Nevertheless, ongoing research into advanced materials and system optimization holds potential to overcome these drawbacks and enhance the competitiveness of Alkaline electrolysers in the evolving hydrogen economy.

# Appendix B – AEM Electrolysers

This appendix gives a more in-depth analysis of Anion Exchange electrolysers.

**Anion Exchange Membrane (AEM) Electrolysers**

Anion Exchange Membrane (AEM) electrolysers are an emerging water electrolysis technology that aims to combine the less harsh environment of Alkaline technologies with simplicity, higher current density and efficiency of PEM electrolysers. It allows the use of non-noble catalysts, titanium-free components, and, as with PEM electrolysers, operation under pressure (IRENA, 2020). The first journal publication about AEM electrolysers appeared in 2011 (Shiva Kumar & Lim, 2022). As the technology is in development and struggling with chemical and mechanical stability problems the total installed capacity worldwide is low. However, there are already some companies who are commercializing AEM electrolysers. The German company 'Enapter' for example, offers a 1MW AEM electrolyser (Enapter, 2025).

Just as with the Alkaline electrolysers, AEM electrolysers consist of an Anode and Cathode. The main difference is that an AEM electrolyser uses an anion exchange membrane. The membrane conducts hydroxyl ions (OH-) and serves as both the separator and the electrolyte. However, the electrolyte is often supported with a KOH solution like in Alkaline cells to improve conductivity (IRENA, 2020). A schematic view of an AEM electrolyser cell can be seen in Figure B-1.

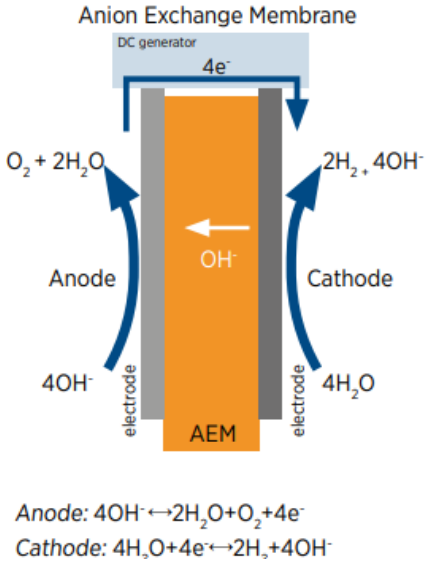


*Figure B-1: AEM electrolyser cell (IRENA, 2020)*

**AEM electrolysers - Electrochemical Reactions**

The electrochemical reactions of an AEM electrolyser cell consist of two individual half-cell reactions. At the Cathode a water molecule ($H_2O$) is reduced to generate hydrogen ($H_2$) and hydroxyl-ions ($OH^-$) by the addition of electrons according to the Hydrogen Evolution Reaction (HER) in equation (B.1).

The hydrogen is then removed from the Cathode and the hydroxyl-ions ($OH^-$) diffuse through the membrane towards the Anode. At the Anode the hydroxyl-ions ($OH^-$) recombine to form a water ($H_2O$) and oxygen ($O_2$) molecule according to the Oxygen Evolution Reaction in equation (B.2). One can recognise these reactions from the Alkaline region in the Pourbaix diagram in Figure 2-1. The overall reaction is the same as the Alkaline technology given by equation (A.3). An overview of the AEM electrolyser reactions can be found in Table .

$$4H_2O\ (l) + 4e^- \rightarrow 2H_2(g) + 4OH^- \quad (B.1)$$

$$4OH^- \rightarrow 2H_2O(l) + O_2(g) + 4e^- \quad (B.2)$$

*Table B-1: AEM electrolyser half-cell reactions*

| Reaction | Equation |
|---|---|
| OER | $4OH^- \rightarrow 2H_2O(l) + O_2(g) + 4e^-$ |
| HER | $4H_2O\ (l) + 4e^- \rightarrow 2H_2(g) + 4OH^-$ |
| Total | $H_2O\ (l) \rightarrow H_2(g) + \frac{1}{2}O_2(g)$ |

**AEM electrolysers - Materials**

AEM electrolysers are still in development and thus a variety of materials are being used and tested. Typical anion exchange membranes are quaternary ammonium ion exchange membranes such as Sustanion® (Shiva Kumar & Lim, 2022)( Xu et al., 2022), where the ammonium ($NH^{4+}$) groups are the active sites. The membrane enables the transport of hydroxyl-ions ($OH^-$) opposed to PEM membrane who enables proton ($H^+$) transport. For the Anode and Cathode, transition metal-based materials are used instead of expensive noble metals which is possible because of the milder Alkaline environment. For the Anode this could be Nickel alloy materials and for the Cathode NiFeCo alloy materials. Nickel provides resistance to corrosion in the Alkaline environment of the cell, which helps extend the lifespan of the electrodes. Nickel is a good conductor of electricity, which is essential for efficient electrolysis. The membrane is usually supported with a liquid electrolyte, which is a low concentrated Alkaline solution (1M KOH) instead of the high concentrated solution in Alkaline electrolysers (5M KOH) (Shiva Kumar & Lim, 2022)( Xu et al., 2022) ) An overview of the materials can be seen in Table B-2:.

*Table B-2: AEM electrolyser materials*

| Component | Material |
|---|---|
| Membrane (electrolyte and separator) | i.e. Sustanion® |
| Electrolyte support | 1M KOH |
| Anode | transition metal (i.e. Nickel alloys) |
| Cathode | transition metal (i.e. NiFeCo alloys) |

**AEM electrolyser - Operating conditions**

AEM electrolysers typically operate at temperatures between 40-60 $^0$C (Shiva Kumar & Lim, 2022) (IRENA, 2020). Higher temperatures are favorable for the hydroxyl ($OH^-$) mobility and membrane conductivity, however, at higher temperatures the membrane ammonium groups degrade, causing a loss in active sites of the membrane. Also, the increase in temperature can cause an increase in water absorption causing extensive swelling which can lead to delamination of the membrane (Du et al., 2022).

Due to their solid membrane AEM electrolysers are supposed to sustain pressure differentials similar to PEM electrolysers (Shiva Kumar & Lim, 2022) (IRENA, 2020). However, in reality AEM electrolysers typically operate at low pressure because the development of the membrane is expensive and immature (Du et al., 2022).

The current density of AEM electrolysers ranges between 0.2-2 A/cm$^2$ (Shiva Kumar & Lim, 2022) (IRENA, 2020). Just as with Alkaline electrolysers the conductivity of hydroxyl ions ($OH^-$) tends to be lower than for example protons ($H^+$), resulting in a lower current density than with PEM electrolysers. Due to the liquid electrolyte support, AEM electrolysers don't need to maintain a minimum current density to keep the membrane fully hydrated, allowing for low current density operation (Xu et al., 2022). Nonetheless, gas crossover always remains at risk (Du et al., 2022).

AEM electrolysers have a voltage range between 1.4-2.0 V (Shiva Kumar & Lim, 2022) (IRENA, 2020). The voltage losses in the cell are mainly caused by the activation potential of the HER and OER and the ohmic resistance of the membrane. Operation at higher voltages increase the risk of overheating and gas crossover.

The hydrogen purity of an AEM electrolyser is about 99.95% before drying. As mentioned, the AEM electrolyser membranes are less developed and allow for more crossover than PEM membranes. Especially under pressure differentials the liquid electrolyte support can be dragged into the hydrogen stream. After drying, the contaminations are removed from the hydrogen gas resulting in a 99.999% purity (Shiva Kumar & Lim, 2022).(IRENA, 2020)(Enapter, 2025).
.
AEM electrolysers are commercially available (Enapter, 2025) however the technology is not as mature. Different reports show instability of AEM electrolyser cells. (Du et al., 2022) reported stable a stable operation of 10.000 hours using a certain Sustanion® membrane whilst (IRENA, 2020) reported a lifetime of >5000 hours compared to a lifetime of >30.000 hours reported by (Shiva Kumar & Lim, 2022). There is no clear lifetime, but it is safe to say that AEM electrolyser's lifetime ranges between Alkaline/PEM and SOEC.

AEM electrolysers report a cold start of 20 minutes (IRENA, 2020)(Enapter, 2025), partially due to the thermal mass of liquid electrolyte support. Although there's no data available on the ramp up/down time of AEM electrolysers, one can consider that they have a lower thermal mass than Alkaline systems and higher than PEM electrolyser. Enapter reports ramp up/down times to be in the range of seconds-minutes (Enapter, 2025).

AEM electrolysers report a system efficiency between 48-57% (IRENA, 2020) although they are not tested on a large scale yet. The main sources of loss are similar to those of Alkaline and PEM systems i.e. ohmic and activation potentials and balance of plants. An overview of the PEM operating conditions can be found in Table B-3.

*Table B-3: AEM electrolyser operating conditions*

| Operating condition | Range |
|---|---|
| Temperature | 40-60 [$^0$C] |
| Pressure | <35 [bar] |
| Current Density | 0.2-2 [A/cm$^2$] |
| Voltage | 1.4-2.0 [V] |
| Purity | 99.95%-99.9999% |
| Lifetime | - [hours] |
| Cold start | 20 [minutes] |
| Ramp-up/down | _- |
| Efficiency | 48-57% |

**AEM electrolysers - Balance of plants**

Due to the low maturity of this technology, there is limited information on the BoP and its challenges. According to (IRENA, 2020) AEM electrolyser systems have a similar BoP as PEM systems. AEM systems also require a water purification system, temperature and pressure management, drying units and a transformer and rectifier. Other than PEM, AEM electrolysers don't have a gas separator as in certain setups water is only supplied to the Anode side, keeping the Cathode dry and thus minimizing the water crossover (Koch et al., 2022). In other setups where a liquid electrolyte support is used, the electrolyte infrastructures need to be included just like in the Alkaline electrolysers. An overview of an AEM electrolyser's BoP according to (IRENA, 2020) can be seen in Figure.

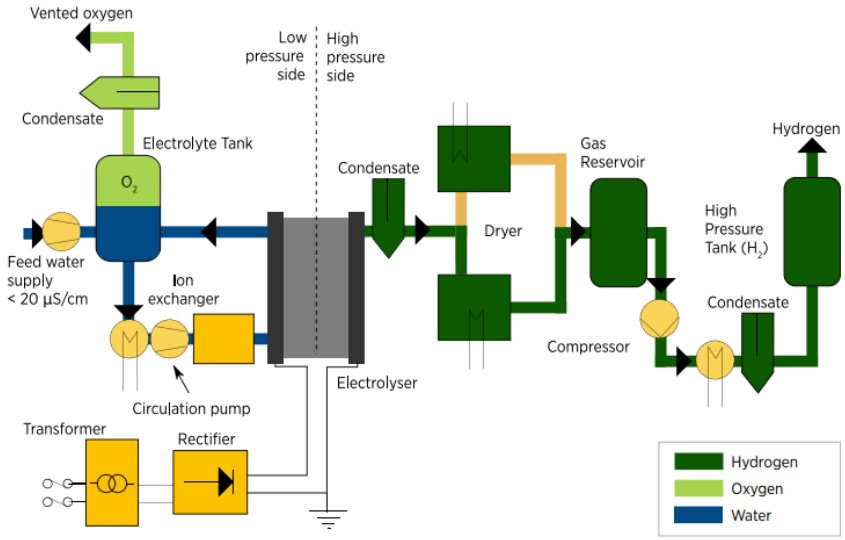


*Figure B-2: AEM electrolyser BoP (IRENA, 2020)*

**AEM electrolysers - Weight and dimensions**

Just like PEM electrolysers, AEM electrolyser systems tend to be quite compact. A 1MW AEM system by Enapter fits in container with the dimensions of 12x2.5x3m (90m$^3$) (Enapter, 2025). Although the limited manufacturers of AEM systems have not specified the weight on their datasheets yet, it can be expected to be quite like that of a PEM stack.

**AEM electrolysers - CAPEX**

There is limited data available on AEM stack or system costs due to its confidential nature. Also, in most studies systems boundaries are not specified (stack/BoP/system) making it hard to compare. Especially with SOEC and AEM electrolysers since there are only a few companies who commercialize these technologies. If the technology reaches a higher maturity level one can expect the stack costs to at least be lower than a PEM stack as the AEM stack uses less expensive metals, which was also the motivation for the development of AEM electrolyser (Xu et al., 2022).

**AEM electrolysers - Challenges and technological developments**

The main challenges of AEM electrolysers according to the IRENA are (IRENA, 2020):

1. Limited membrane durability and conductivity due to membrane degradation
2. Improving the kinetics for the HER and OER while maintaining long term stability and increasing current densities
3. Mechanical degradation of catalyst layers due to delamination and dissolution.

The low stability of the AEM cells is the main challenge of this technology. Just as with AWE and PEM electrolysers there are a lot of developments in terms om materials for the membrane and the catalysts. Research is focused on membrane materials with higher stability and conductivity and on the development of non-precious catalyst with enhanced stability and activity.

**In short:** Anion Exchange Membrane (AEM) electrolysers offer a strong potential at lower cost. AEM electrolysers are characterized by efficient hydrogen production due to their ability to operate with non-precious materials, compact design, and pressurized output. However, the technology is still in its early stages and faces significant challenges, particularly in terms of membrane stability, long-term durability, and performance consistency. While early commercial systems have emerged, AEM electrolysers are not yet mature enough for widespread deployment. Continued research and development are essential to improve materials and system design before AEM electrolysers can become a viable large-scale alternative

# Appendix C – SOEC Electrolysers

This appendix gives a more in-depth analysis Solid Oxide electrolysers.

**Solid Oxide Electrolysers (SOECs)**
Solid Oxide Electrolysis is an emerging high-temperature electrolysis technology that has gained attention for its efficiency and potential integration with industrial heat sources (Flis & Wakim, 2023). The development of the SOECs began in the 1970s by General Electric (Shiva Kumar & Lim, 2022). In April 2023 a 2.6MW SOEC was installed in a refinery in the Netherlands, just a few weeks later a 4MW SOEC was installed in a NASA research centre. Nonetheless, the capacity of SOECs is still less than 1% of the total electrolyser capacity worldwide (IEA, 2023). One of the advantages of SOECs is that their favourable kinetics allow the use of relatively cheap nickel electrodes. Furthermore, SOECs have the potential for reversibility, operating both as an electrolyser and fuel cell (IRENA, 2020).

A SOEC-cell comprises of two electrodes, the Anode and Cathode, separated by a dense ceramic oxide-ion ($O^{2-}$) conducting electrolyte (Wolf et al., 2023). Due to the high temperatures of the SOEC, water is consumed in the form of steam. A schematic view of a SOE-cell can be seen in **Fout! Verwijzingsbron niet gevonden.**.

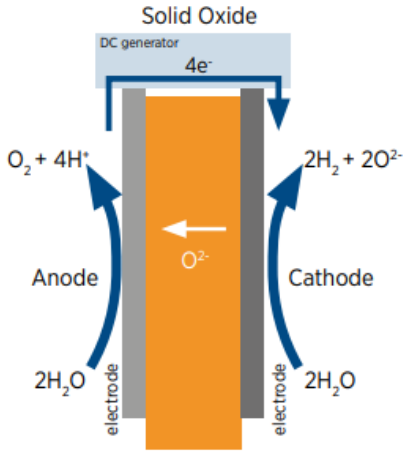


*Figure C-1: SOEC cell (IRENA, 2020)*

**SOEC's - Electrochemical Reactions**
The electrochemical reactions of a SOEC cell consist of two individual half-cell reactions. The process initiates at the Cathode with the HER, here the water molecule ($H_2O$) is reduced to hydrogen ($H^2$) and an oxide-ion ($O^{2-}$) by the addition of two electrons ($e^-$), according to equation (C.1). Wolf et al., 2023). The oxide-ion ($O^{2-}$) travels to the Anode through the ion-exchange membrane. At the Anode the oxide-ions ($O^{2-}$) are further reduced to produce oxygen ($O_2$) and electrons ($e^-$), according to the OER as equation (C.2). The electrons ($e^-$) travel through an external circuit towards the Cathode.

$$H_2O\ (g) + 2e^- \rightarrow H_2(g) + O^{2-} \qquad (C.1)$$

$$2O^{2-} \rightarrow O_2(g) + 4e^- \quad (C.2)$$

The overall reaction is according to (A.3 (A.3) . An overview of the reactions can be found Table C-1.

*Table C-1: SOEC half-cell reactions*

| Reaction | Equation |
|---|---|
| OER | $2O^{2-} \rightarrow O_2(g) + 4e^-$ |
| HER | $H_2O\ (g) + 2e^- \rightarrow H_2(g) + O^{2-}$ |
| Total | $H_2O\ (l) \rightarrow H_2(g) + \frac{1}{2}O_2(g)$ |

**SOECs- Materials**

The three main components of the SOEC cell are the Anode, Cathode and a ceramic membrane capable of conducting oxide-ions ($O^{2-}$). The membrane is typically made of yttria-stabilized zirconia (YSZ) (Shiva Kumar & Lim, 2022). YSZ is a ceramic in which a cubic crystal structure of zirconium dioxide is made stable by addition of yttrium-oxide. These oxides are commonly called "zirconia" ($ZrO^2$) and "yttria" ($Y^2O^3$), hence the name (Dharini et al., 2023). YSZ has a high ionic conductivity, can withstand high temperatures and shows good chemical stability (Shiva Kumar & Lim, 2022).

The Cathode is usually made from a ceramic metal composed of YSZ and nickel (Ni-YSZ). The porous structure of the Cathode maximizes surface area and allows for gas diffusion. Nickel is an effective catalyst for the HER at high temperatures and remains stable in the Cathode environment (Shiva Kumar & Lim, 2022).

The most widely used Anode material are perovskite materials such as LSCF and LSM. These are complex crystal structures of rare earth ions, transition metal ions and oxygen ions (Dwi et al., 2023). Perovskite materials have high ionic and electronic conductivity and can withstand high temperatures. An overview of the materials in a SOEC cell can be found in Table C-2.

*Table C-2: SOEC materials*

| Component | Material |
|---|---|
| Electrolyte (and separator) | YSZ |
| Anode | Ni-YSZ |
| Cathode | LSCF or LSM |

**SOECs - Operating conditions**

SOECs operate at high temperatures, between 700-850 $^0$C (IRENA, 2020). The ionic conductivity of the ceramic membrane increases with temperature, and a minimum temperature is needed for efficient operation. Also, higher temperatures thermally activate electrochemical processes such as the HER and OER by accelerating electrode kinetics and reducing overpotentials thus increasing efficiency (Wolf et al., 2023). Temperatures above 850 $^0$C can lead to degradation of the Cathode materials and thermal stresses in the ceramic membrane.

SOECs typically operate at atmospheric pressure (1 bar) (IRENA, 2020). Because of the higher temperature there is no need for pressure to improve the reaction kinetics. Also increased pressure requires specific sealants which need to be able to resist the high temperatures. These are expensive materials. Furthermore, the steam supply becomes much more complex at higher pressure. Some

SOEC systems do operate under pressure (1-30 bar) mainly for the ease of integration with downstream processes (Wolf et al., 2023). These pressurized SOECs are not common.

The current density of SOECs ranges from 0.3-1 A/cm$^2$ (IRENA, 2020), which is relatively low compared to PEM electrolysers. In SOECs higher current densities lead increased ohmic resistance, even in the hot ceramic. These voltage losses are generally higher in a SOEC then in for example PEM electrolyser because the membrane tends to be thicker. Also, the transport limitations of steam and the reactant through the porous ceramics becomes a limiting factor above 1 A/cm$^2$ (Shiva Kumar & Lim, 2022).

The operating voltage of a SOEC generally lies between 1.0-1.5V under standard conditions (IRENA, 2020), a relatively small range compared to other electrolysers. As mentioned in section 2.1.2 the standard cell voltage needed to overcome the Gibbs free energy is -1.299V, at standard conditions. Since SOEC operate at elevated temperatures the Gibbs free energy for water splitting is reduced, therefore SOEC's operation starts at 1.0V. At potentials above 1.5V the SOEC's risk of electrode degradation.

The purity of SOECs is generally about 99.9% (IRENA, 2020). The sealants in a SOEC cells must remain gas-tight at elevated temperatures and thermal cycles which induce microcracking that can lead to leakage. Also, the presence of residual steam in the hydrogen gas decreases its purity.

The approximated lifetime of a SOEC is 20.000 hours under constant power and well-defined operating conditions, i.e. not coupled to renewable energy sources (IRENA, 2020). The main degradation mechanism is the thermal cycling and associated mechanical stress, due to different thermal expansion coefficients within the cell's materials. Also, electrode degradation and failure of sealants influence the SOEC's lifetime.

SOECs have low operational flexibility. They operate at high temperatures and thus have a cold start over 600 minutes (IRENA, 2020). The ramp-up from hot idle to nominal power is about 10 minutes mostly due to the low thermal conductivity of the ceramics which can cause thermal hotspots when ramping up (Flis & Wakim, 2023).

SOECs tend to have a high efficiency due to the high temperatures which leads to thermodynamic advantages and reducing the electricity needed. For example, the reduction of the Gibbs free energy at elevated temperatures mentioned earlier. The reported electrical efficiency of SOECs is 66-82% (IRENA, 2020), where some others report electrical efficiencies reaching near 100% (Wolf et al., 2023). A requirement is that the SOEC is connect to a waste heat supply. An overview of the operating conditions can be found in Table C-3.

*Table C-3: SOEC operating conditions*

| Operating condition | Range |
|---|---|
| Temperature | 700-850 [$^0$C] |
| Pressure | 1 [bar] |
| Current Density | 0.3-1 [A/cm$^2$] |
| Voltage | 1.0-1.5 [V] |
| Purity | 99.9% |
| Lifetime | 20.000 [hours] |
| Cold start | 600 [minutes] |
| Ramp-up/down | 10 [minutes] |
| Efficiency | 66-75% |

**SOECs - Balance of plants**

SOEC systems require heat for the steam/air pre-heater and heating of the stack. Therefore, it is preferable to couple SOECs with heat-producing systems for a higher system efficiency (IRENA, 2020). As mentioned earlier, SOECs work with steam instead of liquid water, therefore the BoP of a SOEC requires an evaporator. Similar to a PEM and Alkaline electrolyser plant, SOECs need a transformer, rectifier and gas/water separator. As the SOEC usually operates at atmospheric pressure, an external pressurizer can be needed. An overview of a SOEC BoP can be seen in Figure C-2.

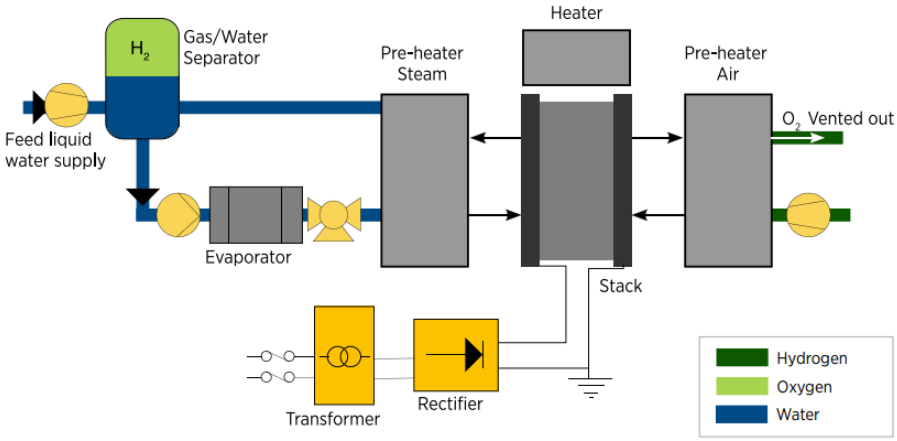


*Figure C-2: SOEC BoP (IRENA, 2020)*

**SOECs - Weight and dimensions**

SOECs are quite compact. Fuel Cell Energy reports a 1.1MW SOEC system with dimensions of 12x2.5x3m (90m$^3$). Although manufacturers do not have specified weights in their datasheets, it can be assumed that SOECs are heavier than PEM or Alkaline systems due to their ceramic components.

**SOECs - CAPEX**

Due to its confidential nature, there is no data available publicly for the CAPEX of SOEC systems.

**SOECs - Challenges and technological developments**

The main challenges of SOEC according to the IRENA are (IRENA, 2020):

1. Improving the kinetics for hydrogen and oxygen evolution and maintaining long-term stability.

2. Eliminating the thermal instability issues by an expansion coefficient mismatch between cell components.
3. Improve membrane conductivity.

The potential for SOECs lies in its higher efficiency, however, the extreme heat brings challenges when it comes to materials in SOEC. New materials, advances in manufacturing techniques, and growing interest of manufacturers cause the SOEC technology to mature rapidly (Koch et al., 2022).

**In short:** Solid Oxide Electrolysers (SOECs) are a promising high-efficiency hydrogen production technology that operates at high temperatures using steam instead of liquid water. Their ability to use low-cost materials like nickel and their potential for reversible operation, like a fuel cell, makes them attractive for industrial integration, especially where waste heat is available. However, SOECs are still in an early phase of development, with key challenges including thermal stress, slow start-up times, and limited operational flexibility. Although large-scale pilots have recently been installed, the technology requires further development in materials and system design to enable broader commercial use.

# Appendix D – Detailed PEM Components

This appendix elaborates on the PEM components.

The Bipolar plates, also known as endplates, serve several essential functions in a stack of cells. They establish electrical connections between neighbouring cells in series to form a stack and provide a rigid structure to support the electrodes and membrane. Bipolar plates also facilitate the mass transfer for the supply and removal of reactants ($H_2O$) and gaseous products ($H_2$ and $O_2$) through flow channels. These flow channels are crucial for ensuring even distribution of reactants across the catalyst layer. Additionally, bipolar plates play a significant role in the thermal management of the cells by incorporating fluid cooling channels to dissipate the heat created by overpotentials within the cell (Sezer et al., 2025). Bipolar plates are usually made of titanium due to its lightweight, mechanical strength, and corrosion resistance. Stainless-steel is considered as an alternative due to its low costs. At the Anode, the bipolar plate requires a coating with a high corrosion-resistant protective layer due to the harsh environment.

The Anode and Cathode base materials mentioned in Section 2.2.3 refer to the Porous Transportation Layer (PTL) also known as the current collector. The PTL facilitates electron transfers between the catalyst layer and the bipolar plates, as well as enabling the diffusion of water and product gases within the catalyst layer. Given the harsh operating conditions of PEM electrolysers, such as high temperatures, high potentials, high oxygen concentration, and acidic environments, the current collector must exhibit excellent electrical conductivity and corrosion resistance. Additionally, the current collector must provide sufficient mechanical support to the polymer membrane, particularly under pressurized operation. The porous microstructure of PTL's is essential to obtaining a decent performance. High porosity may promote easy gas removal in current collectors, but it can undesirably hinder electron transfer (Sezer et al., 2025). As mentioned in Section 2.2.3 the Anode PTL is usually made of porous titanium and the Cathode PTL of porous carbon black.

The Gaskets prevent leakage of hydrogen, oxygen and water. Furthermore, they ensure electrical insulation between components and maintain mechanical compression of the MEA. The gaskets are typically made of elastomers that are compatible with the chemicals within the cell and can withstand acidic, high-pressure and high-temperature environments.

# Appendix E – PEM Degradation Mechanisms

This Appendix provides a broad description of each of the degradation mechanisms.

## E.1 Membrane degradation and inhibition

The PEM membrane is a crucial component of the MEA. The PEM membrane can either degrade or be inhibited by impurities. This section outlines the different types of membrane degradation.

### Membrane degradation in general

In PEM electrolyser cells, the PFSA-membrane is a critical component that ensures proton conduction, electrical insulation, and gas separation between hydrogen and oxygen. Its stability is vital for long-term efficiency, safety, and durability. However, during operation, the membrane is subjected to multiple degradation mechanisms that interact and reinforce each other. These include chemical degradation by radical species, ionomer inhibition by contamination, and mechanical degradation by stress and deformation. Each of these pathways leads to the thinning, perforation, or loss of functional properties of the membrane, ultimately reducing proton conductivity, increasing gas crossover, and performance losses (Sun et al., 2014).

### Chemical membrane degradation

Chemical degradation of the perfluoro sulfonic acid (PFSA) ionomer is primarily driven by radical attacks, specifically by hydroxyl (OH•) and hydroperoxyl (OOH•) radicals generated from peroxide ($H_2O_2$) during cell operation. Peroxide ($H_2O_2$) is typically formed at the Cathode when the cell potential drops below 0.682 V in the presence of protons and dissolved oxygen due to gas crossover (Wallnöfer-Ogris et al., 2024), according to equation (E.1). Peroxide ($H_2O_2$) can also be formed at the Anode according to equation (E.2), even though it has a higher equilibrium potential then the half reaction at the Anode (OER), side reactions like these do occur at high potentials. Also, if the cell voltage drops during shutdown, the peroxide ($H_2O_2$) formation at the Anode can occur.

The peroxide ($H_2O_2$) can form hydroxyl radicals (OH•) according to equation (E.3), also known as the Fenton reaction (EPRI, 2022). Metal ions such as $Fe^{2+}$ (or $Cu^{2+}$) catalyse the formation of hydroxyl radicals through thermocatalytic reactions, increasing the rate of ionomer degradation similar to the better researched PEM fuel cells (Young et al., 2010) (Frensch et al., 2019). The hydroxyl (OH•) can react to less the aggressive and hydroperoxyl (OOH•), recombine or decompose to peroxide, water and oxygen or attack the membrane.

$$O_2 + 2H^+ + 2e^- \rightarrow H_2O_2 \qquad E^0 = 0.682V \tag{E.1}$$

$$H_2O \rightarrow H_2O_2 + 2H^+ + 2e^- \qquad E^0 = 1.776V \tag{E.2}$$

$$H_2O_2 + Fe^{2+} \rightarrow Fe^{3+} + OH\bullet + OH^- \tag{E.3}$$

The radicals attack vulnerable sites in the Nafion® polymer chain, particularly C–H bonds, initiating a irreversible chain-scission process that fragments the ionomer. The chemical structure of the Nafion® membrane can be seen in. This autocatalytic degradation results in the release of fluoride and sulphate anions, along with polymer fragments, leading to structural damage, membrane thinning and pinhole formation. Although small pinholes have limited impact on polarization behaviour, they significantly increase gas crossover, compromising hydrogen purity, reducing Faradaic efficiency, and posing safety risks. The loss of mechanical integrity caused by chemical degradation makes the membrane more susceptible to mechanical failure and the attack on the C-H bonds induces a loss of proton-conducting end groups, making the membrane less efficient.

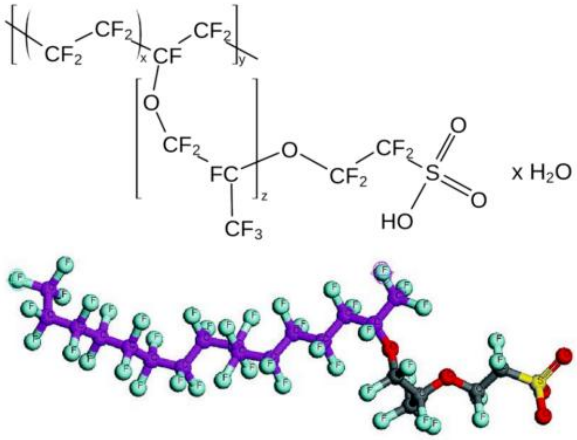


*Figure E-1: Chemical structure of Nafion® (Sezer et al., 2025)*

Additionally, degradation of the ionomer also influences the catalyst layers who are pressed against the membrane as in Figure E-1. Structural changes can affect wetting and bubble behaviour between the ionomer and the catalyst. Bubble nucleation, growth and detachment are affected and can lead to lead to larger gas bubbles and increased bubble coverage of catalyst sites, resulting in mass transport limitations and higher bubble-induced activation overpotentials (Yuan et al., 2023).

Membrane degradation in PEM electrolysers is not yet fully understood, but the here described mechanism and Fenton reaction has been suggested in the literature (EPRI, 2022) It is commonly agreed that metallic impurities accelerate membrane attack in the presence of $H_2O_2$.

**Mechanical membrane degradation**

Mechanical degradation in PEM electrolysers membranes is caused by physical stresses imposed on the membrane. These stresses arise from variations in temperature, differential pressures, hydration/dehydration cycles during operation and mechanical clamping stresses during production (Suermann et al., 2019).

The PEM electrolyser membrane together with the catalyst layers is clamped between the PTL's and bipolar plates, as can be seen in Figure E-1. The compressive force together with the gaskets insure gas-tightness and low interfacial stress. However, non-uniform pressure or over-compression can introduce residual stresses and cause plastic deformation or micro-cracks in the membrane (Wallnöfer-Ogris et al., 2024). During hydration cycles the membrane absorbs water and expands, where at dehydration it contracts, causing mechanical stress. Also, inhomogeneous distribution of the water supply can lead to local membrane swelling (Sun et al., 2015). During temperature changes the

mismatch between the thermal expansion coefficient of the components can cause thermos-mechanical stress. This effect is accelerated if combined with hydration stress (Suermann et al., 2019).

In PEM electrolysers the Cathode side often operates at a higher pressure than the Anode side due to hydrogen pressurization. The membrane experiences a pressure gradient which causes mechanical stress. The mechanical stresses induced on the membrane promotes crack and pinhole formation and delamination of the PTL's and catalyst layers, which facilitate gas crossover and thus accelerates chemical degradation as mentioned before. Chemical degradation, in turn, reduces membrane toughness, making it more brittle and susceptible to mechanical failure. Mechanical degradation thus acts synergistically with chemical processes, accelerating overall membrane failure and reducing system lifetime.

The irreversible mechanical degradation mechanisms of the membrane also influence the catalyst layers who are tightly pressed onto the membrane. Both temperature and pressure gradients can induce mechanical stress on the catalyst layers. Together with the clamping pressure this can lead to changes in the catalyst layer's structure affecting its function (Wallnöfer-Ogris et al., 2024).

**Ionomer membrane inhibition**

Ionomer inhibition occurs when the functional sulfonic acid groups of the ionomer are blocked by the adsorption or exchange of contaminant cations, which originate from both internal and external sources. Metallic cations (i.e. $Na^{()+}$, $Cu^{()+}$, etc.) are the most significant membrane poisoners, since the membrane shows a higher affinity for these cations than for protons. One study found that multivalent cations have an even higher affinity than monovalent cations (Kitiya Hongsirikarn et al., 2010). Common sources include residual impurities from membrane manufacturing and metal ions from system components, especially at the Anode side which operates under harsh conditions that promote the release of cations. Impurities can also be introduced through contaminated feed water (Wallnöfer-Ogris et al., 2024). Even at low concentrations in the feed water, these impurities are reported to accumulate within the ionomer, leading to performance degradation (Kelly et al., 2005). Ionomer inhibition decreases proton conductivity by reducing the active surface area leading to an increase in ohmic losses (Feng et al., 2017). Furthermore, the uneven delivery of protons can cause local heating and hotspots further increasing membrane and catalyst layer degradation.

Some cations influence the ionomer's hydration state by forming complex water-cation clusters, which in turn affect the membrane's water uptake capacity and proton conductivity. The altered hydration behaviour can destabilize membrane performance, particularly under varying load conditions. This inhibition mechanism reduces the electrochemical activity of the catalyst layer, lowers membrane conductivity, and can amplify other degradation pathways by altering local electrochemical and transport conditions (Wallnöfer-Ogris et al., 2024).

Research showed that ionomer membrane inhibition can be reversed. A 9-cell PEM electrolyser was tested for 7800 hours and measured an average degradation of 35.5 µV/h. However, after immersing the membrane in a 0.5M $H_2SO_4$ solution, almost all degradation was recovered. This research not only shows that ionomer inhibition is a reversible degradation mechanism, it also showed that the performance degradation of their stack was mainly caused by ionomer degradation (Sun et al., 2014).

**Consequence of membrane degradation**
Degradation of the membrane and the loss of active sites increases the membrane resistance and thus the ohmic voltage. Also, membrane degradation influences the cathodic activation voltage since chemical degradation usually takes place at the cathodic side of the membrane. These higher voltages reduce the electrolysers efficiency. Also, degradation of the membrane can cause membrane failures which then allows for gas crossover creating a highly explosive $H_2$ and $O_2$ mixture.

**Influence of operating factors on membrane degradation and inhibition**
Several operating factors influence the membrane degradation and inhibition. For example, low current density operation (<0.5 A/cm$^2$) is accompanied by high partial pressure of oxygen ($O_2$) on the Cathode side which leads to a high stability of the aggressive OH• radicals. Research found that membrane radical attack was the highest at 0.4 A/cm$^2$ (Wallnöfer-Ogris et al., 2024). At higher current densities the partial pressure of oxygen ($O_2$) reduced and the transformation rate of the OH• radicals to the less aggressive OOH• radicals increase. However, operation at higher current densities can induce side reactions which create other radicals and promote metal dissolution which can also induce radical formation.

Ramping up/down and on/off cycles increase ionomer degradation due to induced stresses and the possible formation of peroxide ($H_2O_2$) at low or high potentials. Also, cyclic operation can influence the wetting behaviour of the membrane, causing stresses due to absorption or drying.

The PEM ionomer transition temperature is generally around 120-140 °C. Constant temperature operation is usually below this point however elevated temperatures above 80 °C do influence the ionomer structure and increase degradation. Also, thermal cycling and transient hot spots can contribute to localized stress and damage and cyclic operation induce cyclic mechanical stresses due to pressure differentials.

**In short:** The key mechanisms that degrade the membrane in PEM electrolysers are chemical attack by radical species (e.g. OH•), mechanical stress from pressure and temperature cycling, and ionomer inhibition by contaminant cations. These processes reduce proton conductivity, increase gas crossover, and compromise efficiency and safety. Chemical and mechanical degradation reinforce each other, while ionomer poisoning, although sometimes reversible, lowers conductivity and accelerates failure. Operational factors such as current density, ramping, and thermal cycling further influence degradation, highlighting the critical role of operating conditions in PEM electrolyser performance and lifetime.

### E.2 Anode catalyst degradation (iridium)
The Anode operates at high potential conditions (>1.5V). The Anode catalyst is therefore made of iridium which is one of the most corrosive-resistant materials. Nevertheless, the cell still experiences iridium dissolution.

Because of the high oxidative conditions iridium oxide ($IrO_2$) is formed. Iridium oxide is more stable than iridium (Ir) and forms a protection layer initially, which is electrically conductive. However, at higher potentials even iridium oxide ($IrO_2$) is electrochemically dissolved, as can be confirmed by its Pourbaix diagram (Feng et al., 2017). A series of experiments found that losses of iridium mass

activity were more severely at higher potentials (>1.8V) although loss of mass activity already began at moderate potentials (1.5-1.6V).

Iridium catalyst degradation proceeds via both chemical and electrochemical mechanisms, with the oxygen evolution reaction (OER) playing a central role in accelerating these processes. The OER involves surface redox transformations between different oxidation states of iridium, which under certain conditions lead to the detachment or dissolution of iridium species (Wallnöfer-Ogris et al., 2024). Also, chlorine contamination from, for example, the feedwater can form iridium chlorine combinations and accelerate the detachment and dissolution of iridium and iridium oxide. Once dissolved, iridium ions can contribute to catalyst particle growth through mechanisms such as Ostwald ripening, reducing the electrochemically active surface area. Coalescence, which is the process of two or more particles merging, also takes place and reduces the active surface area of the catalyst layer (Feng et al., 2017).

Another degradation mechanism is surface poisoning or contamination, where impurities, such as titanium ions originating from upstream components like titanium porous transport layers or bipolar plates, adsorb onto the catalyst surface, blocking active sites and increasing interfacial resistances. This leads to a loss of ionomer–catalyst contact and electron conduction pathways, impairing the overall efficiency of proton transport and charge transfer within the electrode (Wallnöfer-Ogris et al., 2024)(Feng et al., 2017).

**Consequence of Anode catalyst degradation**

The cumulative consequence of these degradation processes is a progressive loss of electrochemically active surface area, leading to a permanent increase in activation overvoltage, structural changes in the electrode morphology, and higher mass transport and contact resistances. These factors together result in reduced electrolyser efficiency, higher energy consumption per unit hydrogen produced, and reduced stack lifetime. Since iridium is an extremely scarce and expensive noble metal, its degradation not only undermines performance but also significantly impacts the economic viability and sustainability of PEM electrolysers.

**Influence of operating factors on Anode catalyst degradation**

High current density and voltages are non-favourable as they encourage dissolution of the iridium catalysts. At low current densities and potentials, iridium redeposition can occur, which can be favourable if it doesn’t alter the structure of the catalyst layer. Intermitting operation and on/off cycles encourage the process of dissolution and redeposition and can cause coalescence (Wallnöfer-Ogris et al., 2024). Furthermore, frequent load fluctuations can increase gas bubbles which then induce stress on the catalyst layer, leading to detachment of the active layer (Sayed-Ahmed et al., 2024). Higher temperatures increase the rate of dissolution and the chemical reactions such as detachment and coalescence.

**In short:** The Anode Iridium catalyst degrades over time due to high voltages, aggressive oxidative conditions, and contamination. Iridium dissolves electrochemically, especially at voltages above 1.5 V, and surface reactions during the oxygen evolution reaction (OER) further accelerate this process. Additional degradation mechanisms include particle coalescence, Ostwald ripening, and surface poisoning by impurities, all of which reduce the active surface area and increase resistance. This leads to efficiency loss, higher energy consumption, and reduced system lifetime. Degradation is strongly influenced by current density, voltage, temperature, and dynamic operating conditions.

### E.3 Cathode catalyst degradation (platinum)

The platinum Cathode operates at low potential conditions that thermodynamically stabilize platinum and prevent its electrochemical dissolution since platinum is stable at potentials below 1.188V (Wallnöfer-Ogris et al., 2024). Just like at the Anode, chlorine contamination can accelerate platinum dissolution. However, the chemical dissolution of platinum under the influence of chlorine occurs at potentials above 0.75V and are therefore not relevant for the Cathode catalyst.

Platinum catalyst particles can be detached by degradation of the carbon catalyst support. This degradation can be chemically induced by carbon corrosion due to a decrease in the van der Waals forces between the carbon and platinum which occurs at lower potentials such as at the Cathode (Ren et al., 2020). The platinum degradation can also be mechanically induced driven by vibrations, stack compression, or local mechanical stresses causing detachment.

Platinum particle growth can occur within the cell. Platinum particle growth is the process where the nanoparticles in the catalyst layer become larger over time, reducing their service area-to volume ratio resulting in a performance loss (Yu et al., 2011). This process is usually irreversible. Ostwald ripening, sintering and migration might cause platinum particle growth, but they all require dissolved metal ions which preferentially occur at higher potentials. However, coalescence is possible without the primary platinum dissolution step and can occur even at low potentials, like the potential at the Cathode, reducing the active surface area (Wallnöfer-Ogris et al., 2024)(Yu et al., 2011).

Another degradation pathway is catalyst surface contamination or blocking by particles and impurities. Metal cations such as $Fe^{2+}$ or $Zn^{2+}$, originating from corrosion of upstream components or impurities in the feedwater, can migrate to the Cathode surface and accumulate, forming agglomerations or being reduced to metallic deposits. These deposits physically block the electrochemical surface area, reducing the number of available active sites for the hydrogen evolution reaction (Feng et al., 2017). Research found that just like at the membrane, the contamination can be largely reversed by using a 0.5-1M $H_2SO_4$ solution (Becker et al., 2023).

#### Consequence of Cathode catalyst degradation

The results of these degradation mechanisms is a progressive loss of electrochemically active surface area at the Cathode, leading to a measurable increase in activation overvoltage. This requires higher operating cell voltages to maintain the same hydrogen production rate, reducing the system’s efficiency and increasing energy consumption per kilogram of hydrogen produced.

**Influence of operating factors on Cathode catalyst degradation**
An increase in current density of the cell decreases the potential at the Cathode which increases detachment. Transient operation and on/off cycles increase particle growth and coalescence. Also, at higher temperatures, platinum particle growth reactions are more favourable (Wallnöfer-Ogris et al., 2024). Impurities can cause blocking, therefore high-purity water is preferred.

**In short:** Although platinum at the Cathode is thermodynamically stable at low potentials, it can still degrade through particle detachment, growth, and surface contamination. Mechanical stresses and carbon support corrosion can lead to detachment, while coalescence reduces the active surface area without the need of prior dissolution. Contaminants such as metal ions may block active sites but can often be removed. These processes increase activation overvoltage and energy consumption making the PEM electrolysers less efficient. Degradation is influenced by factors like current density, transient operation, temperature, and water purity.

### E.4 Carbon porous transport layer degradation
At the Cathode, the platinum catalyst is supported with a carbon black PTL. Carbon is stable at potentials below 0.207V. However, due to kinetic barriers in the electrochemical cell, carbon is still oxidized at potentials above ~0.9V (Wallnöfer-Ogris et al., 2024). The Cathode operates at low potentials which decreases when the current density increases, so the low potential at the Cathode protects the carbon. However, as mentioned earlier, the low potentials can cause the van der Waals forces to weaking causing carbon and platinum to delaminate.

The carbon support is however prone to chemical degradation due to chemical attacks by peroxide radicals just like at the membrane (Wallnöfer-Ogris et al., 2024). The attacks degrade the carbon fibres and cause structural defects.

Mechanical degradation of the carbon support is caused by pressure peaks (Wallnöfer-Ogris et al., 2024)(Feng et al., 2017). Carbon fibres can suffer appreciable breakage or displacement under compression, changing the overall structure morphology, affecting current and mass transport.

**Consequence of carbon PTL degradation**
The loss of contact between the platinum catalyst layer and the carbon PTL causes an irreversible lower catalytic activity which leads to a higher Cathode activation voltage. The structural defects of the leads to increased ohmic and mass transport resistance.
**Influence of operating factors on carbon PTL degradation**
The degradation of carbon PTL is influenced by chemical attacks with peroxide radicals just like at the membrane. As mentioned earlier, high current density/voltages, transient operation, high temperatures and the intake of impurities have significant influence on the formation of these radicals. Low potentials can cause the van der Waals forces within the carbon to weaken.

**In short:** At the Cathode, the carbon PTL supports the platinum catalyst and operates at low potentials that generally protect it from oxidation. However, the carbon can degrade through chemical attacks by peroxide radicals. These attacks damage the carbon structure, while mechanical stresses such as pressure peaks can deform or break the PTL. As a result, contact with the catalyst is lost, increasing activation voltage and resistance. Degradation is influenced by current density, voltage spikes, temperature, impurities, and transient operation.

### E.5 Bipolar plate degradation

Bipolar plates are often made of titanium which has excellent corrosive resistance, good mechanical strength and is lightweight. Bipolar plates need to be able to withstand in an oxidizing (Anode) and reducing (Cathode) environments. Bp's are one of the most significant components and own 48% of the stack costs (Feng et al., 2017).

Chemical degradation of the BPL does occur. According to the Pourbaix diagram for a titanium-water system, titanium is easily passivated in a high potential, humid and oxide rich environment like at the Cathode. An oxide layer ($TiO_2$) is formed that offers protection against passivation. However, the oxide layer ($TiO_2$) has low electrical conductivity and increases the resistance between the bipolar plates and porous transport layers making the electrolyser less efficient. Therefore, some electrolysers have bipolar plates covered with metals like gold, platinum or iridium.

BPs also suffer from hydrogen embrittlement. At the Cathode the bipolar plates are exposed to high-pressure hydrogen gas. Hydrogen atoms can migrate into the porous titanium and form hydrides ($TiH_2$) (Feng et al., 2017), especially at elevated temperatures (>80 $^oC$) and high-pressure hydrogen. These hydrides accumulate at the grain boundaries and make the titanium brittle and thus susceptible to cracking under mechanical or thermal stress. At lower temperatures the oxide film ($TiO_2$). However, the oxide film is less effective at low PH and low potentials and $F^-$ originated from the ionomer can attack the oxide film. This makes the degradation process highly complex and no systematic and scientific investigations have been done yet (Feng et al., 2017).

As mentioned earlier, the oxide layer ($TiO_2$) prevents titanium from passivation and corrosion. However, the oxide layer ($TiO_2$) can be attack by ions such as fluoride ($F^-$), resulting in the formation of $Ti\text{-}F^-$. According to (Feng et al., 2017) the peroxide radicals are also known to attack titanium, however, the radical attack on PEM BP's has not been reported yet.

**Consequence of BPs degradation**

The degradation of BPs influences the electrical and contact resistance. As mentioned earlier the formation of oxide layers protects against corrosion but also increases resistance due to low electrical conductivity. The BPs also facilitate reactant distribution. Degradation of the BPs has major consequences for mass transport.

**Influence of operating factors on BPs degradation**

High current density and transient operation promote the formation of an oxide layer and the dissolution of platinum, especially in the presence of ions. The presences of hydrogen and elevated temperatures (>80 $^OC$) increase hydrogen embrittlement.

**In short:** The degradation of bipolar plates in PEM electrolysers is primarily driven by the formation of titanium oxide ($TiO_2$) layers and hydrogen embrittlement. While the $TiO_2$ layer provides corrosion protection, its poor electrical conductivity increases contact resistance, reducing overall efficiency. Hydrogen embrittlement, especially under high-pressure and temperature conditions, leads to the formation of brittle hydrides that compromise mechanical integrity. Additionally, aggressive ions like fluoride and reactive radicals can damage the oxide layer, further accelerating degradation. Operating conditions such as high current densities and transient loads exacerbate these effects.

### E.6 Titanium porous transport layer degradation

At the Anode, het catalyst is usually supported with a porous titanium PTL. The degradation of the PTL is quite like that of the titanium BPLs. Just as with the BPLs, the $TiO_2$ layer that is formed on the PTLs can degrade under the presence of fluoride ($F^-$) ions and are therefore often covered with metals like gold, platinum or iridium. PTLs also experience hydrogen embrittlement and corrosion.

The bipolar plates, PTLs, catalysts and gasket are pressed together to prevent leakage and provide low contact resistance. Research found (Feng et al., 2017) that higher pressure decreases performance due to higher diffusion resistance even though the contact resistant decreases. The higher pressure also increases the chances of mechanical degradation. The pore structure is of high importance in PTLs, and deformation of the pore structure due to mechanical stresses has great influence on the mass transport.

#### Consequence of titanium PTL degradation

The PTL is crucial for gas/water mass transport and electrical conductivity between the catalyst and bipolar plates. Dissolution, corrosion or hydrogen embrittlement of the PTL increases its electrical resistance, which decrease cell performance. If the pore structure of the PTL is affected, mass transport overpotentials may increase, also decreasing cell performance.

#### Influence of operating factors on titanium PTLs degradation

Just like bipolar plates, high current density and transient operation promote the formation of an oxide layer and the dissolution of platinum, especially in the presence of ions. Also elevated temperatures (>80 $^{O}C$) promote hydrogen embrittlement in the PTLs. Possible mass transport overpotential become more evident at higher current densities which means higher current densities (Wallnöfer-Ogris et al., 2024).

**In short:** At the Anode, the titanium PTL can degrade through oxide layer instability, hydrogen embrittlement, and corrosion, similar to the titanium BPLs. Mechanical pressure and deformation of the porous structure can impair gas and water transport. These effects increase electrical and mass transport resistance, reducing cell performance. Degradation is accelerated by high current density, elevated temperatures, transient operation, and ion contamination.

### E.7 Degradation of gaskets and sealants.

Gaskets and sealants are usually made of PTFE or similar polymers. Below its melting point of 327°C (Wallnöfer-Ogris et al., 2024) the polymers experience negligible weight loss. However, like ionomer degradation, the PTFE can experience peroxide radical attacks on C-H bonds which weakens its structure. Also, an oxygen rich environment like at the Anode can cause chain breakage and the

formation of –COF or –COOH surface groups further weaking its structure. Mechanical stress from clamping and design flaws in the stack can locally stress, weak points and deformation in the gaskets and sealants.,

**Consequence of gasket and sealant degradation**
Degradation of the gasket and sealants can lead to leaks, which pose severe safety risks and reduces efficiency. Additionally, fragments of polymer or elastomer can redeposit in the pores of the catalyst layer or the PTL. Metal ions from polymer additives or fillers can inhibit proton-conducting sites of the ionomer or hinder the catalyst, both reducing efficiency.

**Influence of operating factors on gasket and sealant degradation**
Low, high and transient current density promote the radical formation as mentioned earlier. These radicals can attack the gaskets and sealants. Also elevated temperatures promote the radical formation. High, pressure and pressure cycle exhibit more force on the gaskets and sealants, increasing the risk of mechanical failure.

**In short:** Gaskets and sealants in PEM electrolysers can degrade chemically through radical attacks and oxidation, particularly in oxygen-rich Anode environments, and mechanically through pressure and clamping stresses. This can lead to gas leaks, safety risks, and performance loss due to blockage of catalyst layers or ionomer contamination by degraded materials. Degradation is accelerated by high or fluctuating current densities, elevated temperatures, and pressure cycling.

# Appendix F – PEM Electrolyser Model Classifications

This appendix gives a elaborate description of the classifications of PEM electrolyser models.

**Analytical**
Analytical PEM electrolyser modelling is theoretical and based on a lot of simplifications, assumptions and approximations. The model is less complex but does not give an accurate of mass transport for example. It also neglects some overvoltage's within the cell.

**Semi-Empirical**
Semi-empirical modelling is a combination of experimental and theoretical models. Experimental determined coefficients or curve-fitted parameters are used. Measurements from experimental work allows for comparisons with existing models. Similarly, this comparison can be performed with theoretically derived differential or algebraic equations and in the development of new models. However, these models are limited to specific operating conditions and the particular electrolyser design they were developed for.

**Mechanistic**
Mechanistic modelling is based on the laws of physics and electrochemistry. It provides a better understanding of the in-depth modelling phenomena related to the PEM electrolyser process. Where analytical models use simplified equations, mechanistic models use detailed physical and chemical mechanisms. The modelling comprises of differential and algebraic equations, which are derived based on the characteristic of the PEM electrolyser. The downside is that these models often result in long simulation times

**Steady State and Dynamic**
PEM electrolyser models can be broadly categorized into steady-state and dynamic models. In a steady-state model, all state variables remain constant over time, making it a foundational tool in the early stages of PEM system design. This modelling approach is favoured for its conceptual simplicity and computational efficiency. In contrast, a dynamic model captures the transient behaviour of the system, accounting for time-dependent variations in for example pressure and temperature. This approach is essential for analysing the system's response to fluctuations. Dynamic modelling is particularly valuable when a PEM system is integrated with intermittent renewable energy sources like wind or solar power, as it enables the assessment of system performance under fluctuating load demands. The primary objective of dynamic modelling is to characterize the system's temporal response and stability under varying operational scenarios, thereby supporting robust control and optimization strategies.

**Model Dimensions**
Another consideration in modelling PEM electrolysers is the treatment of spatial dimensionality, which determines how physical and electrochemical variables are resolved across the geometry of the system. The chosen dimensionality significantly impacts model accuracy, computational complexity, and applicability to specific research or design goals (Falcão & Pinto, 2020)( Onda et al., 2002).

0-D models treat the cell as a lumped system, where all quantities are spatially uniform and averaged over the cell volume. These models are suitable for control system development, real-time simulations, and initial feasibility studies, due to their simplicity and low computational requirements. However, they cannot resolve local variations in temperature, current density, or reactant concentrations, limiting their utility for detailed performance or degradation analysis.

1-D models introduce spatial resolution in the through-plane direction of the membrane electrode assembly (MEA). These models capture gradients of ionic and electronic potentials, reactant and product species concentrations, temperature, and membrane hydration through the layers of the cell: Anode gas diffusion layer (GDL), catalyst layers, the membrane, and Cathode GDL (Falcão & Pinto, 2020)( Abdol Rahim et al., 2016). They are commonly used to analyse the impact of material properties and thicknesses on performance, and to simulate water and proton transport within the cell.

2-D models add an in-plane spatial dimension, often along the flow field direction, enabling the simulation of channel-to-channel non-uniformities and flow maldistribution (Carmo et al., 2013). These models can resolve local effects such as dry-out, flooding, or thermal hotspots arising from non-uniform gas supply and heat removal, which are critical for accurate system design and lifetime predictions.

3-D models offer full spatial resolution across all axes and are typically implemented using computational fluid dynamics (CFD) frameworks. These models allow comprehensive analysis of multiphysic phenomena, including fluid flow, electrochemical kinetics, heat and mass transfer, and phase change (e.g., bubble formation in the liquid phase). While 3D models offer the highest fidelity, their computational demands limit their routine use to component-level studies, design optimization, and validation purposes.

Ultimately, the appropriate level of spatial dimensionality depends on the intended application of the model. For instance, 0D and 1D models are often sufficient for system-level simulations or dynamic operation studies, whereas 2D or 3D models are more suitable for resolving non-uniformities in cell behaviour or validating new component designs (Onda et al., 2002).

**Isothermal and Non-Isothermal**

PEM models also must consider whether the model is isothermal (assuming uniform temperature) or non-isothermal (accounting for temperature gradients and heat transport). This modelling choice has direct implications on the fidelity and applicability of simulations, especially under dynamic or high-current operating conditions (Falcão & Pinto, 2020)( Hernández-Gómez et al., 2020)( Abdol Rahim et al., 2016)

Isothermal models assume that the entire electrolyser, or at least the membrane-electrode assembly (MEA), operates at a uniform temperature. This simplifies the governing equations by removing the need to solve for the energy conservation equation or account for spatially varying thermophysical properties. Such models are widely used in early-stage system analysis, control-oriented modelling, and performance evaluation under near-steady conditions. While isothermal models are computationally efficient, they do not account for thermally coupled processes such as membrane dehydration or temperature-induced degradation. This can limit their accuracy when modelling

transient operation or spatially resolved designs, where local heating from ohmic and reaction losses becomes non-negligible.

Non-isothermal models include the thermal energy balance equation, allowing temperature to vary across the domain (typically in the through-plane or in-plane directions) (Wu et al., 2007). These models capture the effects of Joule heating, reaction heat, and phase, which influence local temperature, water content, ionic conductivity, and thus, the overall cell performance. Non-isothermal models allow for studying dynamic operation or start-up/shutdown conditions, evaluating thermal management strategies and investigating localized degradation mechanisms.

The trade-off is increased computational complexity and the need for more precise input data on thermal and thermodynamic properties of cell components.

**Single-Phase and Multi-Phase Models**

Another key decision in PEM modelling is whether to treat the reactants and products as a single homogeneous phase or to distinguish between liquid and gas phases explicitly. This choice impacts the model's ability to resolve water transport, gas evolution, membrane hydration, and component-level performance degradation under varying conditions (Hernández-Gómez et al., 2020)(Mo et al., 2016).

Single-phase models typically assume that all species are in either the gas phase or a homogeneous pseudo-phase. These models use simplified mass and energy balances that neglect the distinct behaviours of water in liquid and vapor form. While computationally efficient, essential phenomena such as liquid water transport, membrane hydration, and water condensation or evaporation are neglected. According to (Mo et al., 2016), these simplifications are only valid under operating conditions where either full humidification or negligible phase interaction can be assumed.

Multiphase models distinguish between liquid and gaseous species and explicitly simulate their respective transport mechanisms and phase interactions. Multiphase treatment is particularly important at high current densities or pressurized operation, where phase change phenomena significantly affect efficiency and durability (Falcão & Pinto, 2020). (Hernández-Gómez et al., 2020) argues that models neglecting phase interactions may underestimate degradation risks due to improper water management, especially under variable load conditions.

There are a lot of characteristics of PEM models. When building or selecting a model it is important to consider its application to choose a model with the right accuracy without making it too complex.

# Appendix G – SIMULINK Model Equations

The full Simulink model and corresponding MATLAB codes can be entered through the following link:

https://drive.google.com/drive/folders/1neqYywerm56OdVIBPD7oxWcaOx5uNQ5i?usp=drive_link

# Appendix H – Additional Simulink model output

This Appendix provides additional output results of the Simulink model.

**Pressure and Temperature**

The pressure graph shows that the stack reaches a constant pressure of 3MPa almost instantly at a current density of about 0.2 (A/cm$^2$). The temperature graphs rise with increasing current density due to higher heat generation from ohmic and activation losses. A brief dip around 0.3 A/cm² indicates activation of the thermal control system. Above 1.37 A/cm², the temperature stabilizes around 353 K as active cooling maintains a constant setpoint.

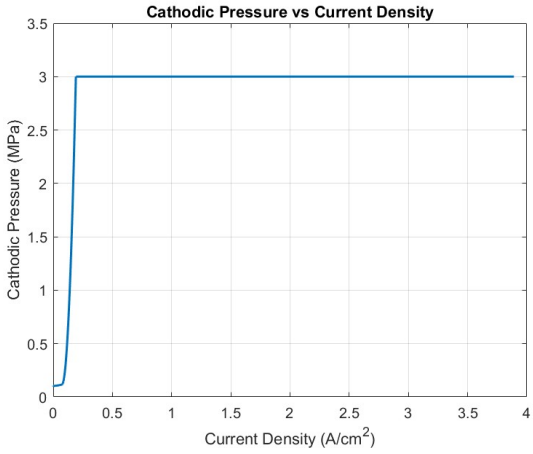


*Figure H-1: Cathodic pressure vs. current density*

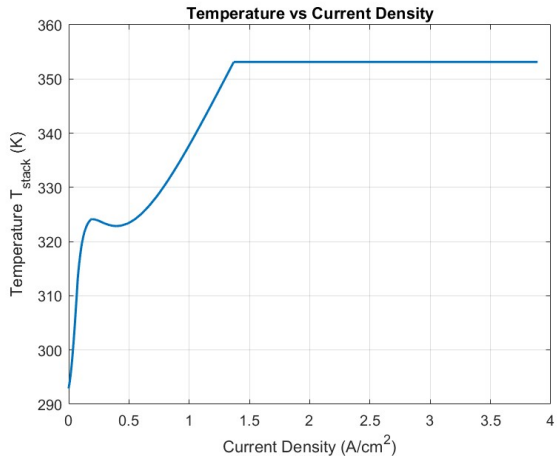


*Figure H-2: Temperature vs. current density*

**$H_2O$ and $O_2$ mass flows**

The following graphs show the $H_2O$ consumed and the $O_2$ produced by the reaction. These show a similar trend as the $H_2$ graphs which makes sense considering the chemical equation.

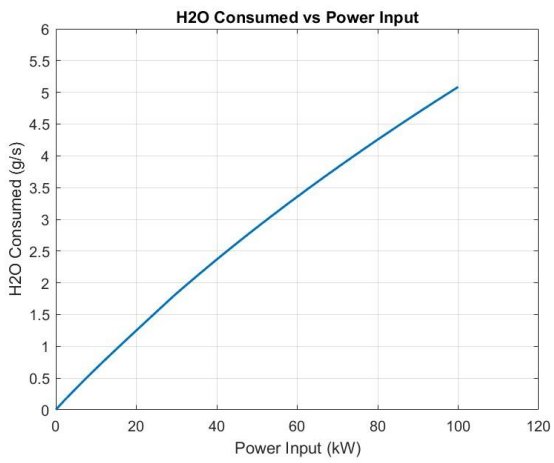


*Figure H-3: $H_2O$ consumed vs. current density*

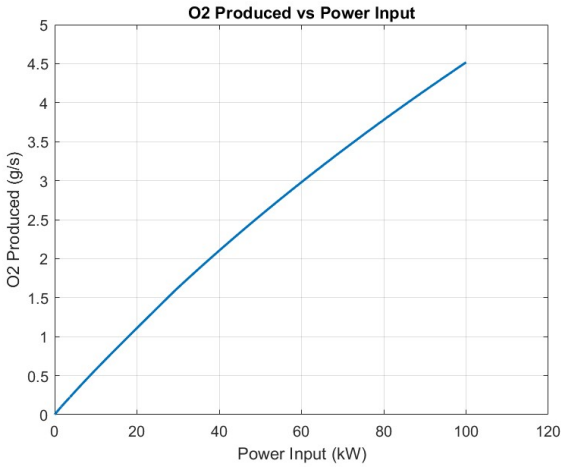


*Figure H-4: $O_2$ produced vs. current density*

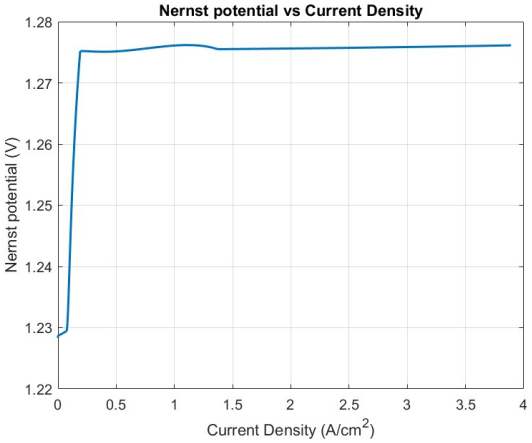


*Figure H-5: Nernst potential vs. current density*

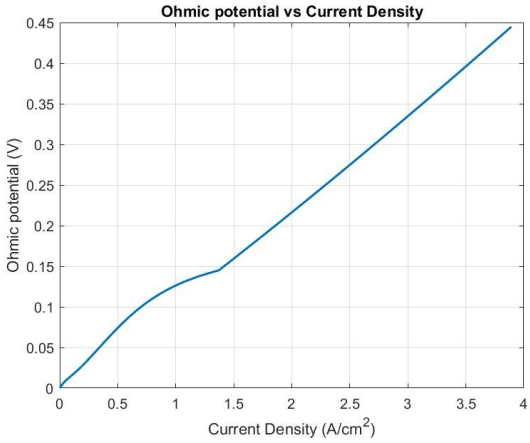


*Figure H-6: Ohmic potential vs. current density*

The graphs below show the Cathodic and Anodic activation potential. Both activation potentials rise steeply at low current densities and then gradually level off, following the behaviour predicted by the Tafel equation. This reflects kinetic limitations in the electrochemical reactions, which dominate at low currents. The Cathodic activation potential is noticeably higher than the anodic one. This is because the hydrogen evolution reaction (HER) at the Cathode has a lower exchange current density than the oxygen evolution reaction (OER) at the Anode, even on platinum catalysts. As a result, more overpotential is required to drive the same current density at the cathode

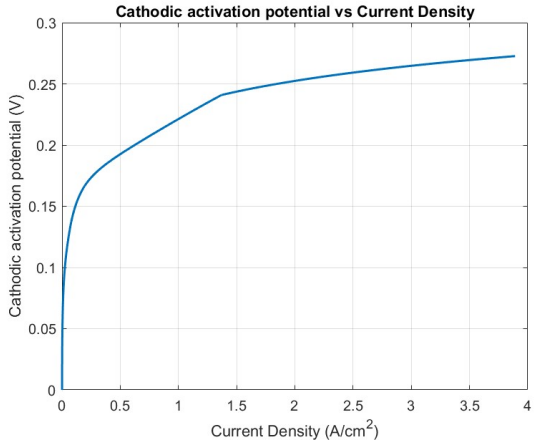


*Figure H-7: Cathodic activation potential vs. current density*

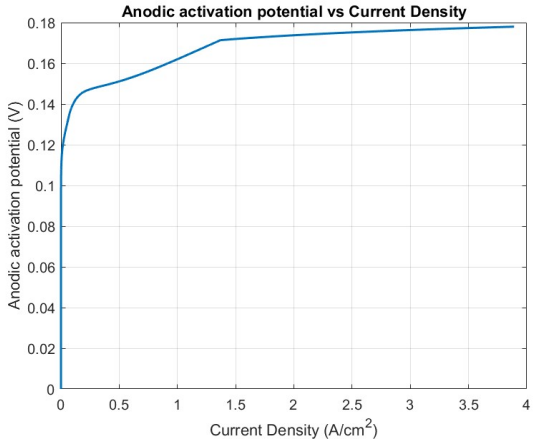


*Figure H-8: Anodic activation potential vs. current density*

**Output Excel**

The PEM electrolyser Simulink model creates an output Excel that defines the operating characteristics of the stack at every power input ranging from 0-100kW. The figure below shows a sample of this Excel. The full Excel can be found in the drive through the following link:

https://drive.google.com/drive/folders/1o9_PdVOzu3NMlfwkO4i2ZYUaDiCXvWOp?usp=drive_link

| | A | B | C | D | E | F | G | H |
|---|---|---|---|---|---|---|---|---|
| 1 | Power_kW | Cell_Voltage_V | Current_Density_A_per_cm2 | H2_Produced_g_per_ | O2_Produced_g_per_s | H2O_consumed_g_per_s | Efficiency_Percent | Degradation_uV_per_h_scofield |
| 2 | 0 | 1,233217491 | 0 | 0 | 0 | 0 | 0 | 30 |
| 3 | 1 | 1,345190881 | 0,053099156 | 0 | 0,061635114 | 0,069400915 | 0 | 30 |
| 4 | 2 | 1,38811961 | 0,102914099 | 0,004271155 | 0,119458062 | 0,134509344 | 25,23419819 | 30 |
| 5 | 3 | 1,416866408 | 0,151237433 | 0,011338536 | 0,175549616 | 0,197668231 | 45,16090963 | 30 |
| 6 | 4 | 1,429175125 | 0,199910897 | 0,018457123 | 0,232047586 | 0,261284741 | 55,14295275 | 30 |
| 7 | 5 | 1,44008221 | 0,247983967 | 0,025487902 | 0,287848646 | 0,324116532 | 60,89186411 | 30 |
| 8 | 6 | 1,449315806 | 0,295538504 | 0,032442844 | 0,343047815 | 0,386270597 | 64,54163768 | 30 |
| 9 | 7 | 1,458695237 | 0,342638155 | 0,039331258 | 0,397718973 | 0,447830123 | 67,02046748 | 30 |
| 10 | 8 | 1,467211984 | 0,389379405 | 0,046167256 | 0,451974116 | 0,508921217 | 68,8332672 | 30 |
| 11 | 9 | 1,474905814 | 0,435790707 | 0,052954998 | 0,50584627 | 0,569581067 | 70,16194331 | 30 |
| 12 | 10 | 1,482058653 | 0,481926985 | 0,059702517 | 0,559399189 | 0,62988146 | 71,16541042 | 30 |
| 13 | 11 | 1,488565755 | 0,527757566 | 0,066405327 | 0,612597268 | 0,689782304 | 71,88242328 | 30 |
| 14 | 12 | 1,49474119 | 0,573438375 | 0,073086233 | 0,665621498 | 0,749487395 | 72,47769392 | 30 |
| 15 | 13 | 1,500365873 | 0,618893927 | 0,079734194 | 0,718384261 | 0,808838074 | 72,91155918 | 30 |
| 16 | 14 | 1,505547796 | 0,664191321 | 0,086359025 | 0,77096344 | 0,868102039 | 73,24436331 | 30 |
| 17 | 15 | 1,51036791 | 0,709374111 | 0,092967095 | 0,823409592 | 0,927156216 | 73,50810319 | 30 |
| 18 | 16 | 1,514821055 | 0,754449408 | 0,099559443 | 0,875730971 | 0,986069899 | 73,71078056 | 30 |
| 19 | 17 | 1,518897029 | 0,799429713 | 0,106137899 | 0,927942088 | 1,044859428 | 73,86063385 | 30 |
| 20 | 18 | 1,522725752 | 0,844345881 | 0,112706975 | 0,980078758 | 1,103565129 | 73,97816684 | 30 |
| 21 | 19 | 1,526244412 | 0,889199707 | 0,119266933 | 1,032143064 | 1,162189349 | 74,06094695 | 30 |
| 22 | 20 | 1,529492427 | 0,934014956 | 0,125821249 | 1,084162592 | 1,220763149 | 74,1179297 | 30 |
| 23 | 21 | 1,532476995 | 0,978804869 | 0,13237186 | 1,136152709 | 1,279303833 | 74,15257905 | 30 |
| 24 | 22 | 1,535224104 | 1,023580018 | 0,138920311 | 1,188125691 | 1,337825222 | 74,1686695 | 31,43148162 |
| 25 | 23 | 1,539111941 | 1,067405482 | 0,145329869 | 1,238996319 | 1,395105365 | 74,15192876 | 34,18063388 |
| 26 | 24 | 1,544596805 | 1,109843141 | 0,151536458 | 1,288256047 | 1,45057164 | 74,09771322 | 36,95255394 |
| 27 | 25 | 1,550032076 | 1,152028639 | 0,157706168 | 1,337223077 | 1,505708339 | 74,03045497 | 39,81509953 |
| 28 | 26 | 1,555404809 | 1,193881272 | 0,163827196 | 1,385803734 | 1,560409981 | 73,94824243 | 42,76057476 |

*Figure H-9: Snippet of Simulink output Excel*

# Appendix I – PEM Electrolyser Degradation Dataset

The full degradation dataset can be accessed through the following link:

https://drive.google.com/drive/folders/1ub3shT2DT5yrsve2DxDFaANuDf1zitNs?usp=drive_link

# Appendix J – Correspondence on PEM Electrolyser Degradation

This appendix contains snippets of correspondence with industry experts. The following e-mail from Menno Landsmeer from the PosHYdon project showed that NEL did not provide them with degradation data and that it is something that they are currently researching in their pilot.

Thomas,

Er is niks mis met brutaal zijn. Helaas hebben wij nog geen leverancier omdat we nog niets gekocht hebben. We hopen degradatie informatie te halen uit het PosHYdon project waar we een Nel electrolyser hebben, maar dat zal pas over een jaar zijn. Ik zal eens vragen aan iemand binnen mijn netwerk of die je kan helpen, maar ga niet te veel hopen. Deze informatie houden de leveranciers angstvallig geheim.

**Menno Landsmeer**
**Lead H2 Development Engineer, NL**
Projects & Engineering

*Figure J-1: Correspondence with PosHydon project*

Rubio Omar from Siemens Energy confirmed the confidentiality of degradation data across vendors.

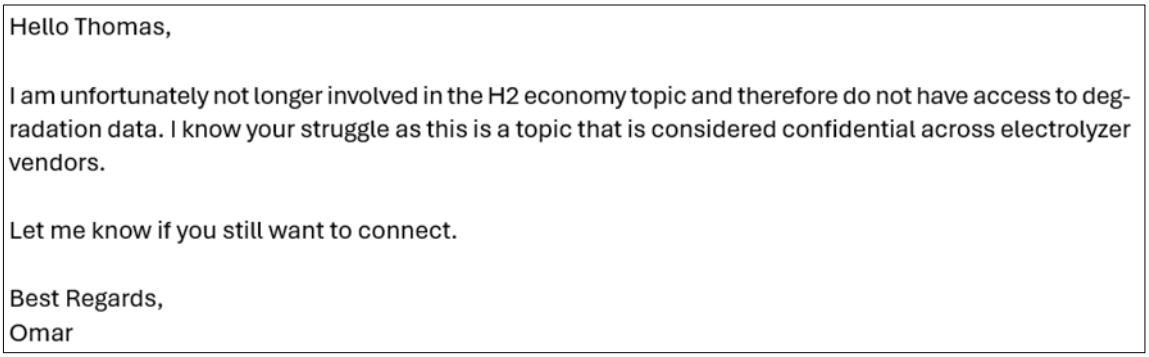

Hello Thomas,

I am unfortunately not longer involved in the H2 economy topic and therefore do not have access to degradation data. I know your struggle as this is a topic that is considered confidential across electrolyzer vendors.

Let me know if you still want to connect.

Best Regards,
Omar

*Figure J-2: Correspondence with Siemens Energy*

The correspondence with Atsushi Urakawa from the HyCentA confirmed the awareness under researchers on the topic of degradation and the need for standardized testing protocols. Atsushi also confirmed that few companies have a clear understanding of their degradation.

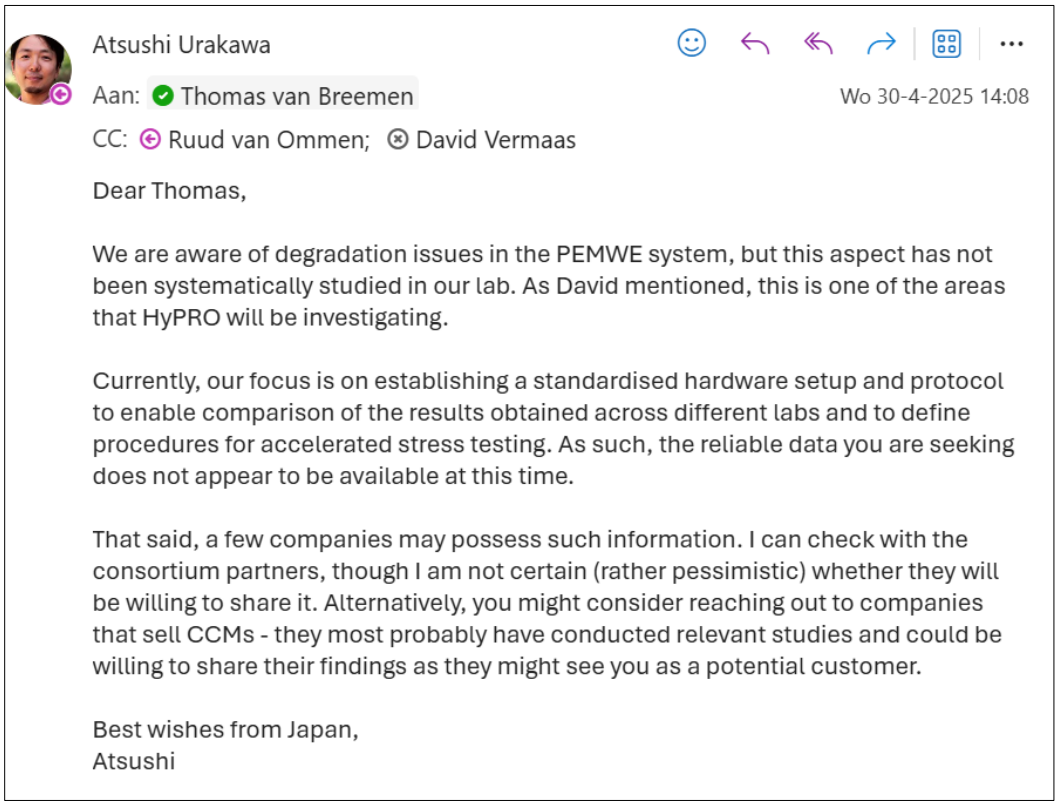

Atsushi Urakawa

Aan: Thomas van Breemen

Wo 30-4-2025 14:08

CC: Ruud van Ommen; David Vermaas

Dear Thomas,

We are aware of degradation issues in the PEMWE system, but this aspect has not been systematically studied in our lab. As David mentioned, this is one of the areas that HyPRO will be investigating.

Currently, our focus is on establishing a standardised hardware setup and protocol to enable comparison of the results obtained across different labs and to define procedures for accelerated stress testing. As such, the reliable data you are seeking does not appear to be available at this time.

That said, a few companies may possess such information. I can check with the consortium partners, though I am not certain (rather pessimistic) whether they will be willing to share it. Alternatively, you might consider reaching out to companies that sell CCMs - they most probably have conducted relevant studies and could be willing to share their findings as they might see you as a potential customer.

Best wishes from Japan,
Atsushi

*Figure J-3: Correspondence with HyCentA*

Assosiate professor David A. Vermaas confirmed the dependence of materials, loadings and operational conditions on PEM electrolyser degradation. Furthermore, he mentioned that according to him the degradation probably depends more on the fluctuations in current densities then o the average current density.

Hi Thomas,

That's a valid question, but I'm afraid that I can't judge very well which value is most reliable. I can imagine that there's a broad variety of degradation profiles, which will like depend on materials, loading and indeed operational conditions. It will probably depend more on the fluctuations in current densities rather than on the average current density. For example, companies are afraid about too large ripples in the DC voltage. If you need an order-of-magnitude estimate, then I would say that your curve below is maybe already a good estimate, acknowledging that the spread for different systems is large.

If you need more detailed information, I don't have much more concrete information than what you have plotted already for PEM specifically. I think this kind of information is more available in companies. The HyPRO consortium (where we're part of) have this information, but I'm not directly involved in the PEM task. Atsushi Urakawa is. Hope that helps.

Best, David

**David A. Vermaas**
Associate professor

**TU Delft / Transport Phenomena (TP)**

*Figure J-4: Correspondence with associate professor David A. Vermaas, TU Delft*

# Appendix K – Degradation Data sample plots

This appendix shows the scatterplot and trendline of the sampled degradation datasets based on their characteristics.

**The dataset sampled based on only experimental values:**

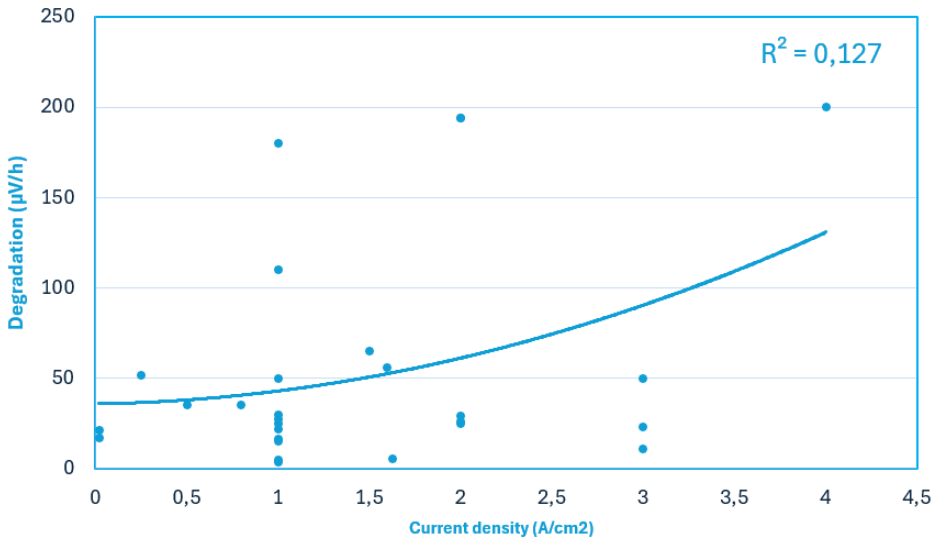


*Figure K-1: Degradation data filtered on experiments only*

**The dataset sampled based on cyclic experiments:**

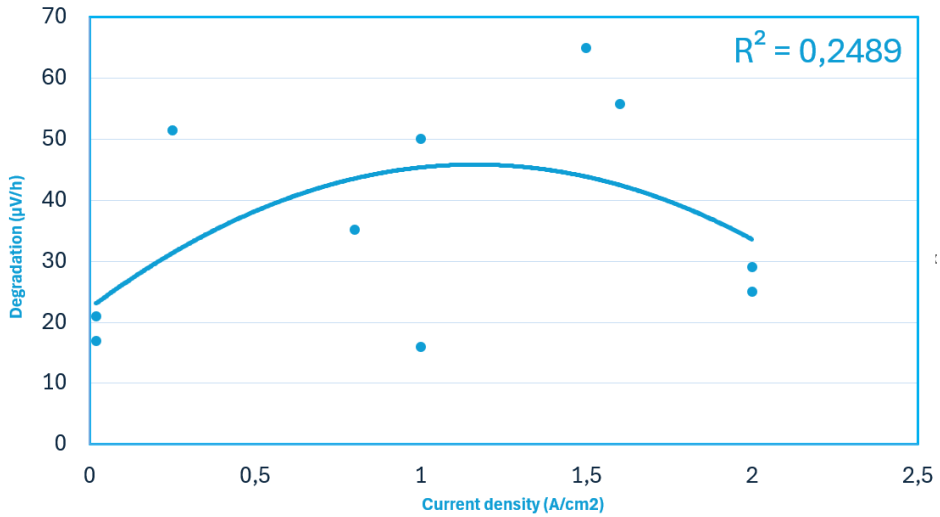


*Figure K-5: Degradation data filtered on cyclic loading experiments*

**The dataset sampled based on constant loading experiments:**

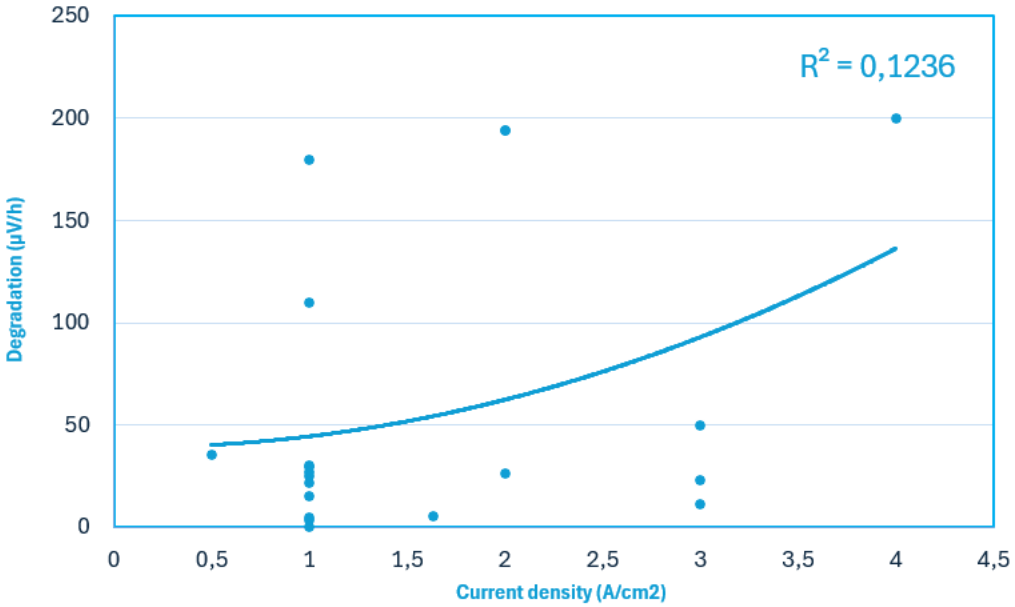


*Figure K-6: Degradation data filtered on constant loading experiments*

**The dataset sampled based on experiments and a realistic catalyst loading (>1.5 mg/cm$^2$):**

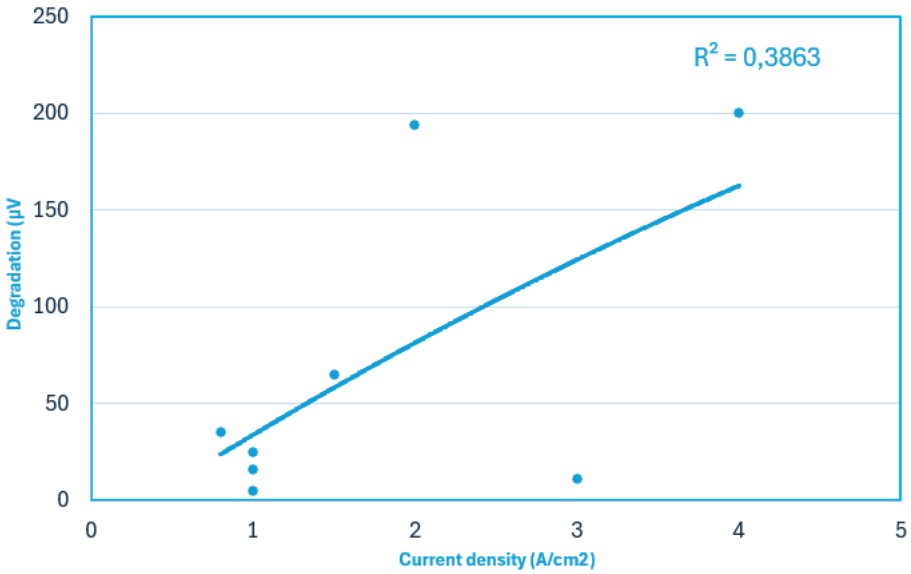


*Figure K-7: Degradation data filtered on realistic catalyst loading experiments*

# Appendix L – North Sea Wind Data

The figure shows an example of what the North Sea Wind Data looks like. Unfortunately, this data is confidential and can thus not be shared in the drive.

| Datetime (UTC) | Hourly load factor | output before wake loss (kW) | output with wake loss (kW) |
|---|---|---|---|
| 31.12.2012 00:00 | 0,88 | 353,44 | 300,42 |
| 01.01.2013 01:00 | 0,76 | 302,44 | 257,07 |
| 01.01.2013 02:00 | 0,67 | 269,72 | 229,26 |
| 01.01.2013 03:00 | 0,58 | 230,36 | 195,81 |
| 01.01.2013 04:00 | 0,45 | 180,52 | 153,44 |
| 01.01.2013 05:00 | 0,34 | 134,48 | 114,31 |
| 01.01.2013 06:00 | 0,35 | 141,88 | 120,60 |
| 01.01.2013 07:00 | 0,49 | 195,00 | 165,75 |
| 01.01.2013 08:00 | 0,67 | 269,36 | 228,96 |
| 01.01.2013 09:00 | 0,72 | 287,28 | 244,19 |
| 01.01.2013 10:00 | 0,72 | 287,88 | 244,70 |
| 01.01.2013 11:00 | 0,71 | 284,28 | 241,64 |
| 01.01.2013 12:00 | 0,82 | 326,16 | 277,24 |
| 01.01.2013 13:00 | 0,80 | 319,16 | 271,29 |
| 01.01.2013 14:00 | 0,84 | 334,80 | 284,58 |
| 01.01.2013 15:00 | 0,91 | 365,92 | 311,03 |

*Figure L-1: Snippet of 2013 North Sea wind data*

# Appendix M – Operational strategy Excel outputs.

This appendix gives a snippet of the output Excels of the operational strategy models.

**Equal distribution**

The figure below shows the output for the equal distribution strategy. One can see that all stacks receive the same amount of power and experience the same degradation.

| A | B | C | D | E | F | G | H | I | J | K | L |
|---|---|---|---|---|---|---|---|---|---|---|---|
| Hour | Available_Wind_P | Stack_1_kW | Stack_2_kW | Stack_3_kW | Stack_4_kW | Stack_1_deg | Stack_2_deg | Stack_3_deg | Stack_4_deg | Avg_Stack_Efficiency_ | Total_H2_Produce |
| 0 | 257,074 | 64,2685 | 64,2685 | 64,2685 | 64,2685 | 207,6007 | 207,6007 | 207,6007 | 207,6007 | 68,5854317 | 5384,255 |
| 1 | 229,262 | 57,3155 | 57,3155 | 57,3155 | 57,3155 | 170,7372 | 170,7372 | 170,7372 | 170,7372 | 69,6295203 | 4867,968 |
| 2 | 195,806 | 48,9515 | 48,9515 | 48,9515 | 48,9515 | 131,7974 | 131,7974 | 131,7974 | 131,7974 | 70,8445683 | 4257,833 |
| 3 | 153,442 | 38,3605 | 38,3605 | 38,3605 | 38,3605 | 84,51659 | 84,51659 | 84,51659 | 84,51659 | 72,4892076 | 3378,551 |
| 4 | 114,308 | 28,577 | 28,577 | 28,577 | 28,577 | 52,13104 | 52,13104 | 52,13104 | 52,13104 | 73,6578456 | 2620,05 |
| 5 | 120,598 | 30,1495 | 30,1495 | 30,1495 | 30,1495 | 55,41512 | 55,41512 | 55,41512 | 55,41512 | 73,5440442 | 2706,049 |
| 6 | 165,75 | 41,4375 | 41,4375 | 41,4375 | 41,4375 | 96,63283 | 96,63283 | 96,63283 | 96,63283 | 72,0519763 | 3622,968 |
| 7 | 228,956 | 57,239 | 57,239 | 57,239 | 57,239 | 170,7372 | 170,7372 | 170,7372 | 170,7372 | 69,6295203 | 4866,413 |
| 8 | 244,188 | 61,047 | 61,047 | 61,047 | 61,047 | 191,4971 | 191,4971 | 191,4971 | 191,4971 | 69,0299566 | 5162,409 |
| 9 | 244,698 | 61,1745 | 61,1745 | 61,1745 | 61,1745 | 191,4971 | 191,4971 | 191,4971 | 191,4971 | 69,0299566 | 5161,875 |
| 10 | 241,638 | 60,4095 | 60,4095 | 60,4095 | 60,4095 | 186,2408 | 186,2408 | 186,2408 | 186,2408 | 69,1789215 | 5087,884 |
| 11 | 277,236 | 69,309 | 69,309 | 69,309 | 69,309 | 235,3534 | 235,3534 | 235,3534 | 235,3534 | 67,8573369 | 5738,052 |
| 12 | 271,286 | 67,8215 | 67,8215 | 67,8215 | 67,8215 | 229,7213 | 229,7213 | 229,7213 | 229,7213 | 68,0014049 | 5666,409 |
| 13 | 284,58 | 71,145 | 71,145 | 71,145 | 71,145 | 246,7738 | 246,7738 | 246,7738 | 246,7738 | 67,5705546 | 5877,827 |
| 14 | 311,032 | 77,758 | 77,758 | 77,758 | 77,758 | 288,0883 | 288,0883 | 288,0883 | 288,0883 | 66,5883415 | 6362,311 |
| 15 | 320,28 | 80,07 | 80,07 | 80,07 | 80,07 | 300,2523 | 300,2523 | 300,2523 | 300,2523 | 66,314203 | 6497,426 |
| 16 | 323,646 | 80,9115 | 80,9115 | 80,9115 | 80,9115 | 306,3829 | 306,3829 | 306,3829 | 306,3829 | 66,1784949 | 6563,913 |
| 17 | 332,69 | 83,1725 | 83,1725 | 83,1725 | 83,1725 | 318,7769 | 318,7769 | 318,7769 | 318,7769 | 65,90866 | 6697,312 |
| 18 | 334,526 | 83,6315 | 83,6315 | 83,6315 | 83,6315 | 325,0384 | 325,0384 | 325,0384 | 325,0384 | 65,7745626 | 6763,095 |
| 19 | 337,28 | 84,32 | 84,32 | 84,32 | 84,32 | 325,0384 | 325,0384 | 325,0384 | 325,0384 | 65,7745626 | 6761,91 |
| 20 | 338,538 | 84,6345 | 84,6345 | 84,6345 | 84,6345 | 331,3193 | 331,3193 | 331,3193 | 331,3193 | 65,6417054 | 6827,199 |
| 21 | 338,334 | 84,5835 | 84,5835 | 84,5835 | 84,5835 | 331,3193 | 331,3193 | 331,3193 | 331,3193 | 65,6417054 | 6825,979 |
| 22 | 336,498 | 84,1245 | 84,1245 | 84,1245 | 84,1245 | 325,0384 | 325,0384 | 325,0384 | 325,0384 | 65,7745626 | 6758,31 |
| 23 | 328,44 | 82,11 | 82,11 | 82,11 | 82,11 | 312,5702 | 312,5702 | 312,5702 | 312,5702 | 66,042942 | 6623,307 |
| 24 | 305,32 | 76,33 | 76,33 | 76,33 | 76,33 | 276,0823 | 276,0823 | 276,0823 | 276,0823 | 66,8653453 | 6214,489 |

*Figure M-1: Equal distribution Excel output*

**Serial distribution**

The figure below shows the serial distribution. One can see that a stack is loaded until it reaches maximum capacity (100kW) before the next stack is activated. One can also see that at maximum capacity the stack experience significant degradation (ca. 430 µV/h).

| A | B | C | D | E | F | G | H | I | J | K | L |
|---|---|---|---|---|---|---|---|---|---|---|---|
| Hour | Available_Wind_Power_kW | Stack_1_kW | Stack_2_kW | Stack_3_kW | Stack_4_kW | Stack_1_deg | Stack_2_deg | Stack_3_deg | Stack_4_deg | Avg_Stack_Efficiency_Percent | Total_H2_Produced_g_per_hour |
| 0 | 257,074 | 100 | 100 | 57,074 | 0 | 429,7793 | 429,7793 | 170,7372 | 0 | 49,2723 | 5124,219 |
| 1 | 229,262 | 100 | 100 | 29,262 | 0 | 429,7793 | 429,7793 | 52,13104 | 0 | 50,27938 | 4561,346 |
| 2 | 195,806 | 100 | 95,806 | 0 | 0 | 429,7793 | 402,8058 | 0 | 0 | 31,98852 | 3841,8 |
| 3 | 153,442 | 100 | 53,442 | 0 | 0 | 429,7793 | 150,8171 | 0 | 0 | 33,49131 | 3093,01 |
| 4 | 114,308 | 100 | 14,308 | 0 | 0 | 429,7793 | 30 | 0 | 0 | 34,24355 | 2262,381 |
| 5 | 120,598 | 100 | 20,598 | 0 | 0 | 429,7793 | 30 | 0 | 0 | 34,4706 | 2427,437 |
| 6 | 165,75 | 100 | 65,75 | 0 | 0 | 429,7793 | 218,5685 | 0 | 0 | 33,0055 | 3331,886 |
| 7 | 228,956 | 100 | 100 | 28,956 | 0 | 429,7793 | 429,7793 | 52,13104 | 0 | 50,27938 | 4557,206 |
| 8 | 244,188 | 100 | 100 | 44,188 | 0 | 429,7793 | 429,7793 | 109,3365 | 0 | 49,76571 | 4867,255 |
| 9 | 244,698 | 100 | 100 | 44,698 | 0 | 429,7793 | 429,7793 | 113,7118 | 0 | 49,72803 | 4886,198 |
| 10 | 241,638 | 100 | 100 | 41,638 | 0 | 429,7793 | 429,7793 | 100,7966 | 0 | 49,84067 | 4825,299 |
| 11 | 277,236 | 100 | 100 | 77,236 | 0 | 429,7793 | 429,7793 | 282,055 | 0 | 48,54661 | 5473,192 |
| 12 | 271,286 | 100 | 100 | 71,286 | 0 | 429,7793 | 429,7793 | 246,7738 | 0 | 48,75755 | 5367,811 |
| 13 | 284,58 | 100 | 100 | 84,58 | 0 | 429,7793 | 429,7793 | 331,3193 | 0 | 48,27534 | 5606,091 |
| 14 | 311,032 | 100 | 100 | 100 | 11,032 | 429,7793 | 429,7793 | 429,7793 | 30 | 65,76798 | 6086,62 |
| 15 | 320,28 | 100 | 100 | 100 | 20,28 | 429,7793 | 429,7793 | 429,7793 | 30 | 66,32686 | 6299,102 |
| 16 | 323,646 | 100 | 100 | 100 | 23,646 | 429,7793 | 429,7793 | 429,7793 | 36,95255 | 66,3218 | 6390,287 |
| 17 | 332,69 | 100 | 100 | 100 | 32,69 | 429,7793 | 429,7793 | 429,7793 | 65,76569 | 66,09159 | 6584,06 |
| 18 | 334,526 | 100 | 100 | 100 | 34,526 | 429,7793 | 429,7793 | 429,7793 | 73,04804 | 66,02501 | 6624,69 |
| 19 | 337,28 | 100 | 100 | 100 | 37,28 | 429,7793 | 429,7793 | 429,7793 | 80,62647 | 65,95547 | 6664,853 |
| 20 | 338,538 | 100 | 100 | 100 | 38,538 | 429,7793 | 429,7793 | 429,7793 | 88,49118 | 65,88374 | 6704,562 |
| 21 | 338,334 | 100 | 100 | 100 | 38,334 | 429,7793 | 429,7793 | 429,7793 | 84,51659 | 65,91968 | 6682,64 |
| 22 | 336,498 | 100 | 100 | 100 | 36,498 | 429,7793 | 429,7793 | 429,7793 | 76,79436 | 65,99035 | 6639,938 |
| 23 | 328,44 | 100 | 100 | 100 | 28,44 | 429,7793 | 429,7793 | 429,7793 | 48,91982 | 66,2377 | 6468,618 |
| 24 | 305,32 | 100 | 100 | 100 | 5,32 | 429,7793 | 429,7793 | 429,7793 | 30 | 63,02034 | 5925,802 |

*Figure M-2: Serial distribution Excel output*

**Optimal efficiency distribution**

The figure below shows the optimal efficiency distribution. One can see that stacks only get activated if there's enough power input to operate them beyond the point of optimal efficiency. If not, the stack is inactive and doesn't produce hydrogen or experience degradation.

| Hour | Available_Wind_Power_kW | Stack_1_kW | Stack_2_kW | Stack_3_kW | Stack_4_kW | Stack_1_deg | Stack_2_deg | Stack_3_deg | Stack_4_deg | Avg_Stack_Efficiency_Percent | Total_H2_Produced_g_per_hour |
|---|---|---|---|---|---|---|---|---|---|---|---|
| 26 | 249,458 | 62,3645 | 62,3645 | 62,3645 | 62,3645 | 196,8231 | 196,8231 | 196,8231 | 196,8231 | 68,88107 | 5221,82 |
| 27 | 204,34 | 51,085 | 51,085 | 51,085 | 51,085 | 141,193 | 141,193 | 141,193 | 141,193 | 70,5398 | 4398,719 |
| 28 | 197,064 | 49,266 | 49,266 | 49,266 | 49,266 | 131,7974 | 131,7974 | 131,7974 | 131,7974 | 70,84457 | 4244,307 |
| 29 | 177,072 | 44,268 | 44,268 | 44,268 | 44,268 | 109,3365 | 109,3365 | 109,3365 | 109,3365 | 71,60319 | 3851,746 |
| 30 | 143,82 | 35,955 | 35,955 | 35,955 | 35,955 | 76,79436 | 76,79436 | 76,79436 | 76,79436 | 72,77189 | 3202,865 |
| 31 | 107,168 | 26,792 | 26,792 | 26,792 | 26,792 | 45,80103 | 45,80103 | 45,80103 | 45,80103 | 73,86102 | 2438,213 |
| 32 | 76,84 | 25,61333 | 25,61333 | 25,61333 | 0 | 42,76057 | 42,76057 | 42,76057 | 0 | 55,46118 | 1762,963 |
| 33 | 57,154 | 28,577 | 28,577 | 0 | 0 | 52,13104 | 52,13104 | 0 | 0 | 36,82892 | 1305,73 |
| 34 | 84,252 | 28,084 | 28,084 | 28,084 | 0 | 48,91982 | 48,91982 | 48,91982 | 0 | 55,32098 | 1893,638 |
| 35 | 78,336 | 26,112 | 26,112 | 26,112 | 0 | 42,76057 | 42,76057 | 42,76057 | 0 | 55,46118 | 1762,831 |
| 36 | 98,158 | 24,5395 | 24,5395 | 24,5395 | 24,5395 | 39,8151 | 39,8151 | 39,8151 | 39,8151 | 74,03045 | 2262,59 |
| 37 | 144,704 | 36,176 | 36,176 | 36,176 | 36,176 | 76,79436 | 76,79436 | 76,79436 | 76,79436 | 72,77189 | 3202,294 |
| 38 | 188,802 | 47,2005 | 47,2005 | 47,2005 | 47,2005 | 122,6325 | 122,6325 | 122,6325 | 122,6325 | 71,14905 | 4087,194 |
| 39 | 170,102 | 42,5255 | 42,5255 | 42,5255 | 42,5255 | 105,0425 | 105,0425 | 105,0425 | 105,0425 | 71,75382 | 3770,994 |
| 40 | 174,284 | 43,571 | 43,571 | 43,571 | 43,571 | 109,3365 | 109,3365 | 109,3365 | 109,3365 | 71,60319 | 3850,201 |
| 41 | 250,342 | 62,5855 | 62,5855 | 62,5855 | 62,5855 | 202,1773 | 202,1773 | 202,1773 | 202,1773 | 68,73322 | 5290,669 |
| 42 | 320,382 | 80,0955 | 80,0955 | 80,0955 | 80,0955 | 300,2523 | 300,2523 | 300,2523 | 300,2523 | 66,3142 | 6480,202 |
| 43 | 334,968 | 83,742 | 83,742 | 83,742 | 83,742 | 325,0384 | 325,0384 | 325,0384 | 325,0384 | 65,77456 | 6747,445 |
| 44 | 334,628 | 83,657 | 83,657 | 83,657 | 83,657 | 325,0384 | 325,0384 | 325,0384 | 325,0384 | 65,77456 | 6746,265 |
| 45 | 319,906 | 79,9765 | 79,9765 | 79,9765 | 79,9765 | 300,2523 | 300,2523 | 300,2523 | 300,2523 | 66,3142 | 6476,888 |
| 46 | 326,298 | 81,5745 | 81,5745 | 81,5745 | 81,5745 | 312,5702 | 312,5702 | 312,5702 | 312,5702 | 66,04294 | 6610,437 |

*Figure M-3: Optimal efficiency Excel output*

The full output datasets can be entered through the following link:

https://drive.google.com/drive/folders/1tArMLoUv0oICTs8h4vN4MPG1R885UA5e?usp=sharing

# Appendix N – Operational strategy Model Codes

The codes of the operational strategy model and sensitivity analysis can be entered through the following link:

https://drive.google.com/drive/folders/1x5VpaQ4GVLSsFthFabqIcLfY8SaEOnOb?usp=sharing

This page is left blank intentionally